Thermal and Mechanical Behavior of Railway Tracks

Ary Vinicius Nervis Frigeri

Thesis presented to the
School of Technology and Management of the **Polytechnic Institute of Bragança**
to fulfill the requirements to obtain the **Master of Science Degree in Construction Engineering**
as part of the **Double Degree Program** with the
Federal University of Technology - Paraná - Campus Guarapuava

Advisors
Professor PhD. Manuel J. C. Minhoto
Professor PhD. Paulo A. G. Piloto
Professor Msc. Dyorgge A. Silva

Bragança, 2021

ACKNOWLEDGMENTS

This academic work is a result of direct and indirect collaboration among many institutions and people.

Firstly, I thank the Federal University of Technology-Paraná (UTFPR), campus Guarapuava, and the Polytechnic Institute of Bragança (IPB) which provided me opportunities and the right tools to conduct this research. Beyond that, I am thankful for the double degree program between the graduation courses.

My advisors, Professor PhD. Manuel Minhoto, PhD. Paulo Piloto, and Msc. Dyorgge Alves for always willing to help me and clarify my questions. Professor PhD. Rodrigo Ribeiro for making possible the double degree program between the institutions. To all the Professors that have helped me during the graduation path.

To the Association of Municipalities of Terra Quente Transmontana (AMTQT) and Vale do Tua Regional Development Agency (ADRVT) for providing access to the facilities and the monitoring sites of this research. Also, the Portuguese Institute for Sea and Atmosphere (IPMA), for providing weather data that have been utilized in this work.

I thank my parents, Ivandra and Ari and my sister Alicia, for always being present to help me and to give support during all my years of study. Also for always helping me to overcome challenges and make decisions. Thank you also for understanding all comings and goings and the distance. Nothing would be possible without you.

I also thank Mariana Schulze for being by my side since the beginning of my graduation course, always helping and collaborating. Your support was essential during this time.

To all my friends that took part during this journey, always helping me to keep motivated, mainly during uncertain and turbulent times, in which company play a very important role.

AGRADECIMENTOS

Este trabalho acadêmico é fruto da colaboração de diversas instituições e pessoas, tanto de maneira direta como indireta.

Primeiramente agradeço às instituições de ensino, Universidade Tecnológica Federal do Paraná (UTFPR), campus Guarapuava e Instituto Politécnico de Bragança (IPB), que me propiciaram o acesso às oportunidades e ferramentas necessárias para conduzir este trabalho. Mais ainda por propiciarem o acordo de dupla diplomação entre os cursos.

Aos meus orientadores, Professor Dr. Manuel Minhoto, Dr. Paulo Piloto e Msc. Dyorgge Alves por auxiliarem e estarem sempre dispostos a sanar duvidas. Ao professor Dr. Rodrigo Ribeiro por efetivar e fazer possível o programa de dupla diplomação entre as instituições. A todos os professores que me auxiliaram durante a minha graduação.

Agradeço à Associação de Municípios da Terra Quente Transmontana (AMTQT) e à Agência de Desenvolvimento Regional do Vale do Tua por conceder acesso às instalações e aos locais de monitoramento desta pesquisa. Também, ao Instituto Português do Mar e Atmosfera (IPMA) por ceder dados utilizados ao longo desta pesquisa.

Agradeço aos meus pais, Ivandra e Ari e à minha irmã Alicia por sempre estarem dispostos a me ajudar e dar apoio durante todos os anos de graduação. Por sempre me ajudarem a superar os desafios e tomar decisões. Obrigado por compreenderem as idas e vindas e a distância. Sem vocês nada seria possível.

Agradeço a Mariana Schulze por estar ao meu lado desde o principio da graduação me auxiliando e sempre colaborando com minha formação. Seu apoio foi fundamental durante esta fase.

Aos amigos que fizeram parte desta caminhada, sempre auxiliando a manter a autoestima e positividade, principalmente em tempos turbulentos e incertos, no qual a companhia tem um papel muito importante. Obrigado, também, por sempre me auxiliarem a manter a motivação e perseverança para concluir esta etapa.

There are many hypotheses in science that are wrong. That is perfectly alright; it's the aperture to finding out what's right. Science is a self-correcting process [...] (SAGAN, Carl, 1980).

ABSTRACT

FRIGERI, A.V.N. Thermal and Mechanical Behavior of Railway Tracks. 2021. 119 f. Master Thesis – Polytechnic Institute of Bragança. Bragança, 2021.

Railways are infrastructures subject to open weather conditions and also to temperature changes during the day and over the season. Due to this change, internal stresses may appear, whether tensile or compressive depending on the stress-free temperature and the current measure. High compressive stress may lead the track to buckle, meanwhile tensile stress can cause brittle failure. Given the importance of the temperature on railways, many models have been developed to correlate weather conditions and rail temperatures, in order to avoid the occurrence of mechanical instabilities which cause major problems in the operation of railroads. The present work validates one model developed by CNU university by comparing it with finite element solutions and also with experimental data of a rail track in the city of Mirandela-Portugal. A python package was developed to solve the model and is available to download. The model shows a good correlation between measured and simulated rail temperatures. In addition, by utilizing weather information of other locations in Portugal, the maximum expected rail temperatures were determined. Furthermore, mechanical analyses were made to analyze the critical temperature to reach the buckling mode of instability without the effect of rolling loads and also the important parameters that affect this phenomenon. The simulations show that the quality of the ballast and the initial miss-alignment of the track are the most important.

Keywords: Railway. Thermal Buckling. Numerical Simulation. Finite Element Analysis.

RESUMO

FRIGERI, A.V.N. Thermal and Mechanical Behavior of Railway Tracks. 2021. 119 f. Tese de Mestrado – Instituto Politécnico de Bragança. Bragança, 2021.

Caminhos de ferro são estruturas expostas a uma grande variedade de condições climáticas e, concretamente a variações de temperatura durante o dia e ao longo das estações durante o ano. Devido a estas variações tensões internas ocorrem, podendo ser esforços de compressão ou tração, dependendo da temperatura neutral do perfil. A ocorrência de tensões de compressão elevadas pode causar encurvadura da via, enquanto que os esforços de tração podem ocasionar a fratura frágil. Devido a importância das temperaturas nas vias férreas, muitos modelos têm sido desenvolvidos para correlacionar condições climáticas com a temperatura da via tendo em vista o seu uso como ferramenta de prevenção de acidentes na operação. O presente trabalho utiliza um destes modelos, desenvolvido pela universidade CNU e valida-o utilizando soluções com o método dos elementos finitos e, também, com dados experimentais de uma via férrea localizada na cidade de Mirandela-Portugal. Foi ainda desenvolvido um software utilizando a linguagem Python para facilitar a solução do modelo, estando ainda disponível para download. O modelo demonstrou boa correlação entre as temperaturas simuladas e medidas. Além disso, utilizando informações meteorológicas de outras localidades em Portugal, as temperaturas máximas esperada das vias foram determinadas. Posteriormente, análises mecânicas de encurvadura foram realizadas para determinar em quais temperaturas uma via ferra pode sofrer encurvadura e, também, quais parâmetros que influenciam este fenômeno. As simulações mostram que a qualidade do balastro e as imperfeições iniciais da via são os mais importantes.

Palavras-chave: Caminhos de ferro. Ferrovias. Encurvadura Térmica. Simulações Numéricas. Análise de Elementos Finitos.

LIST OF FIGURES

LIST OF TABLES

LIST OF ABBREVIATIONS AND ACRONYMS

AREMA	American Railway Engineering and Maintenance-of-way Association
CNU	Chungnam National University
CP	Caminhos de Ferro Portugueses
CPCFP	Companhia Peninsular dos Caminhos de Ferro de Portugal
CRCFP	Companhia Real dos Caminhos de Ferro Portuguezes
CWR	Continuous Welded Rail
EU27	The 27 member countries of the European Union
FEA	Finite Element Analysis
FRA	Federal Railroad Admnistration
GB	Great Britain
IoT	Internet of Things
IP	Infraestruturas de Portugal
IPMA	Portuguese Institute for Sea and Atmosphere
REFER	Rede Ferroviária Nacional
SFT	Stress Free Temperature
STPT	Single Tie Push Test
US	United States of America

LIST OF SYMBOLS

T_{rail}	Rail temperature
T_{air}	Air temperature
T_{sky}	Atmospheric sky temperature
SR	Solar radiation
α_s	Solar absorptivity of rail
A_s	Area of rail surface exposed to the sun
A_c	Area of rail subject to convection
A_r	Area of the rail subject to radiation heat transfer
ϵ	Emissivity
h_{conv}	Convection coefficient
σ	Stefan-Boltzmann constant
ρ	Density of material
C	Specific heat of a material
V	Volume of a material
w_s	Wind speed
λ	Thermal conductivity of a material
α	Thermal expansion coefficient of a material
δ	Amplitude of imperfections

TABLE OF CONTENTS

1 INTRODUCTION

1.1 Framework

In the early days, rail transport was built to work with draft animals and utilized rocks or wood as a surface to the rolling stock. The limitation of this system was the load capacity since it was getting heavier. With the Industrial Revolution, cast iron was introduced as a support surface, lowering the friction force, and later on, the animal traction was replaced with the steam locomotive [1].

Great Britain was the pioneer using railways to transport goods and people in the context of the Industrial Revolution during the 19th century. Since its creation, railway transport has been improving in many aspects, namely rolling stock or rail tracks. These improvements led to higher efficiency of the modal, allowing great wagon compositions and high speed operations, reaching $350\,\mathrm{km\,h^{-1}}$ [2].

The first rail system utilized was the short rail, which was joined using bolts and allowed partially thermal expansion of the rail. However, too many joints along the tracks lead to problems on the rail and on the rolling stock, caused by the impact during the transition between segments and additionally the discomfort for the user, in case of passenger transportation. Therefore, a great technical effort was taken to remove the joint between segments. During the World War 2, welding techniques were developed and the Continuous Welded Rail was introduced (CWR). This method can reach up to 240 meters of continuous welded rail, much longer than before, 18 to 20 meters [1].

As mentioned, the joint method of the single segments of rail tracks allows partial deformation, thus the internal stresses are smaller. On the other hand, CWR's are constrained to their neighbors, which restrict axial thermal expansion, leading to a change of internal stresses state when the temperature changes. Compressive and tensile stresses must be considered when designing rail tracks since high compressive stress leads to buckling and tensile stresses cause brittle rupture [1]. Both processes can cause derailments, but buckling is more dangerous since causes miss-alignment of the track, meanwhile, rupture creates a short span and it may not lead to an accident with the train [3].

In addition, Wu *et al.* [4] mentions that the operation guideline in hot weather in Australia is to issue speed restrictions of 8 to 9 hours stretches when the weather forecasts air temperatures over $38\,^{\circ}\mathrm{C}$. This represents a great financial and mobility impact for companies and the population. This situation can be worsened due to climate changes and extreme weather events.

According to Van [3], CWR's must be installed under a certain temperature, which the internal stresses are zero, so called stress free temperature (SFT), approximately 25 °C. Bonnett [1] points that the ideal SFT is the median between the highest and the coldest ever recorded on the rail track's region.

Based on these info, this research work gathers rail temperature data of a segment of track localized in the city of Mirandela - Portugal, validate and analyze models of temperature prediction along the day. This model can help designing and maintaining railways and minimize the risk of buckling accidents, by issuing lower speed during critical temperatures events.

In addition, this work makes use of Finite Element Analysis (FEA) in order to determine the critical temperature in which static buckling (without considering vertical loads) phenomenon can occur. Many parameters are analyzed such as lateral and longitudinal ballast resistance, gauge, profile, and torsional resistance of the fastening.

1.2 Research Objectives

The objectives of this work are classified in general and specific and they are described in the following sections.

1.2.1 *General Objectives*

This research aims to validate a temperature prediction model in the city of Mirandela - Portugal, utilizing physical and statistical techniques based on collected sample data.

1.2.2 *Specific Objectives*

The specifics objectives are:

- Review of existent literature;
- Collect data in a track in the city of Mirandela - Portugal
- Data analysis;
- Identify maximum, minimum and average temperatures;
- Validate a model to predict rail temperatures with experimental data;
- Validate a thermal model utilizing FEA;
- Perform mechanical simulations to determine buckling; temperatures, also using FEA.

1.3 Structure of the Document

The present work consists of five chapters: Introduction, Literature Review, Methodology, Results and Conclusions. The introduction discusses the technical framework of the work and its main goals.

Next, the literature review summarizes the many aspects related to railways, including historical and political facts of the development of rail transport. In addition, the technical aspects, working principles and components of railways tracks are also discussed. Furthermore, many rail temperature prediction models are presented, including statistical and physical ones. Lastly, a review of thermal buckling o railway tracks is presented.

Following, the methodology discusses the instrumentation of the track and the weather collection instruments. Following, the material properties utilized during the work. In addition, the thermal and mechanical simulations are detailed.

Lastly, the results and the conclusion are presented, as well as the suggestion for future works.

2 LITERATURE REVIEW

2.1 History of Railway

According to Branco [5], during the Roman Empire, grooves on the limestone were found, which were used to guide wheeled wagon, pulled by animals, mainly used to transport raw material from mines. Furthermore, Lewis [6] states that the basic concept behind the railway is: a prepared track which so guides the vehicles running on it that they cannot leave the track. This example can be found on the *Diolkos*, a track that connects the Corinthian and Saronic gulf. The author also states that the same concept was applied within a wooden rail but left few traces due to material decomposition.

Metal Mining moved the economy during the Roman Empire and a trace of the Roman rails can be found in the north of Portugal, in an ancient gold mine, located in the city of *Trêsminas, Trás-os-Montes*. V-shaped sections were found carved on rocks in a way into the mine. This rail is approximately 150 meters long and has a gauge of 1.2 m. During the late Middle Ages, rails appear in the same precise context: metal mines, differing from *Trêsminas* in one aspect: they were wooden rails [6].

During medieval times, the traditional way to travel was by foot or horseback and the transports were used mainly to move goods. Before the eighteenth century, most roads were simply a mud track or at best reinforced with a broken stone foundation. When heavier loads were transported, using wheeled wagons, it was found that the heavier the load, the more damage on the road surface and foundations. This proved the needs of good road surface and foundation to move heavier goods and to avoid constant maintenance [1].

Branco [5] points out that the use of wooden rails as a surface for rolling stock dates to the 16th century in Germany. They were used, as mentioned, in mines. Lewis [6] confirms, stating that the best-known documented example of wooden rail appears in manuscripts dated around 1480, describing a mechanism that engages a parallel slot that forms the rails.

Approaching the Industrial Revolution, a big step was taken, by changing the wood surface to iron plates. This further evolved to iron profiles and the introduction of flanged wheels in the rolling stock was possible [1].

According to Branco [5], in 1776, wooden rails were substituted to iron profiles, which offers more durability. From this moment on, the term "Railway" began to be used to describe the new transportation system.

As the wrought iron became stronger, it was possible to stand heavy steam locomotives and to remove longitudinal timber supports. In 1825 in England, the Stockton and Darlington Railway was constructed with these characteristics, using iron rails mounted on iron chairs, supported by stones laid on the ground at 3 feet (approx. 91 cm) interval. With these facts, the concept of modern railways was established. Since the Industrial Revolution, the railways began to spread around the world [1].

On the other side of the Atlantic, the United states of America (US) began to develop its network in 1828. It reached 9500 km twenty years later. Boosted by the gold extraction and the exploration of the countryside, by the end of the 19th century, the network length reached around 300 000 km. An important landmark to the US railway network was the transcontinental rail, finished in 1869, connecting the pacific coast to the existing network on the east side of the country [7].

Scaggiante [8] mentions that, in the United States the name *railroads* is used, in contrast with *railway* as usual in Great Britain (GB). The purpose was to inspire a national identity. Google Ngram tool confirms this fact, as shown in figure 2.1. By searching the words railway and railroad, it is possible to see the frequency it appears in the literature during the time. It's also possible to search in different databases, in this case, *eng-2019*, *eng-us-2019*, *eng-gb-2019*, respectively: English books from any country, English books published in the US, English books published in GB.

The railways appear in the continental part of Europe in the year 1832, in France. Two years later, Belgium and Germany and until 1839 in Italy, in the old Austrian Empire and Netherlands. All these rails were based on British knowledge, since they had acquired experience in this new field of engineering. This is reflected in many technical aspects, such as gauge, signs, and directions. It may vary from one country to another. This fact later implied that the international connections were possible, developing the European network [8].

An important fact to mention is that, while the US and Great Britain let the private companies develop the network by themselves, the continental European countries participated actively on the development and established in 1907, with the Bern conference, all the technical standards related to railroads. The governments also realized that this transportation system was important to the countries development and then participated actively in route planning, considering many aspects, such as economic, social, and military [9] [8].

The railroads played a great role during war times, mainly during World War I and II. They were used to move goods, supplies, stocks and troops in USA, Europe and Asia. Hallberg [7] points out that in the US, from 1941 to 1945, railroads transported approximately 43,7 million service men and women. Imperial War Museums [10] mentioned that two technologies were

Figure 2.1 – Usage of the words Railway and Railroad during time. Mentions relative to the corpora database.

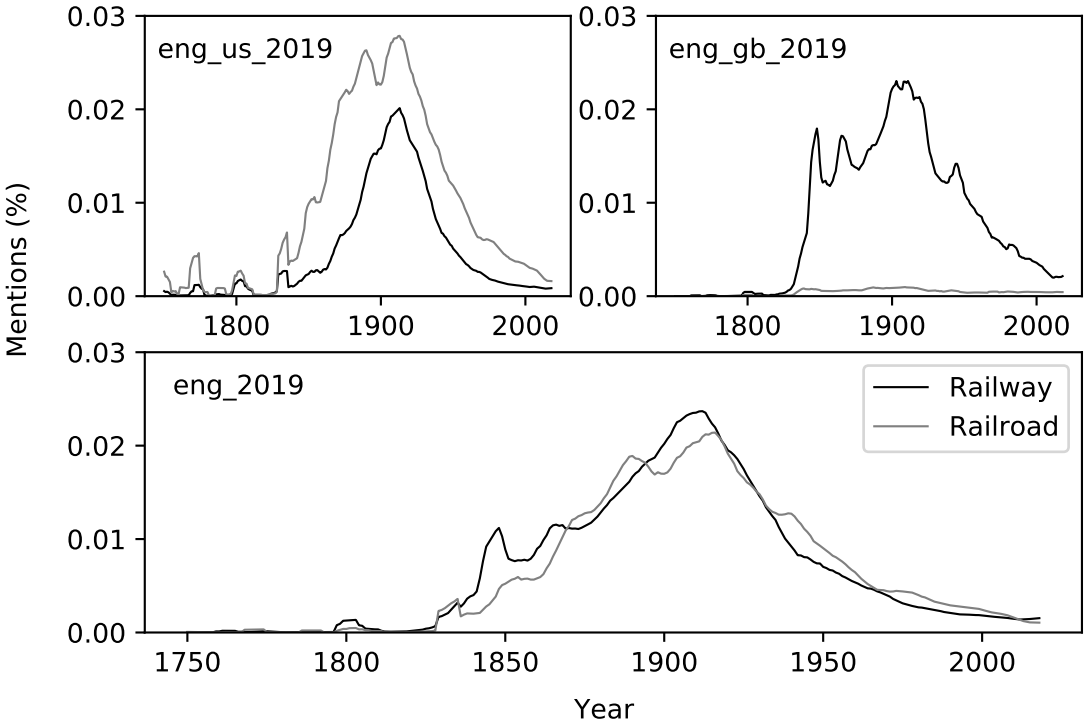

Source: Adapted from Google Ngram viewer.

crucial in shaping the World War I: railways and artillery. Railways provided enormous logistic capacity to move and maintain huge armies in the field for long periods.

Despite the huge impact of the WWII to the world, some improvements were made to the rail transport. Steam locomotives were substituted by diesel engines and also a development focused on passengers transport, to level up the comfort and increase the operational speed of the trains. By the end of the World War II, railroads were responsible for almost 70% of intercity freight and passenger transportation in the US [7].

This excitement with rail transport came to an end in the US, with government investing in others means of transportation, such as waterways and mainly highways. Because of this fact railways declined and by 1970, more than 20% of the rail industry was bankrupt in the US [7].

Branco [5] also points that rail development is divided in many steps: expansion, decline and restructuring. Although the specific point in time may be different, in most countries, the decline of railways is directly related to the expansion of highways.

2.2 21th Century

In the European Union, within the 27 member states (EU27) and United Kingdom, the length of the lines in use in 2017 was around 215 000 km, in which 54% electrified. This accounting for both passenger and freight lines. In the year 1995 the total lines in use was around 230 000 km. In summary, the length of lines has sunk $6{,}5\%$ [11]. Figure 2.2 shows the European network.

Figure 2.2 – European railway network.

Source: Adapted from openrailwaymap [12].

Regarding the freight transport, in 1995, in the EU, railways transported 388 billions ton kilometer (tkm), rising to 406 billion in 2000 and stabilized with low yearly growth rate of $0.2\,\%$. By the year 2017, reached 421 billions tkm. With respect to passenger transport, in the year 1995, EU achieved 343 billion passenger kilometer (pkm) with an average yearly growth rate of $1.3\,\%$. By 2017, the railway was responsible of 470 billion pkm in the EU27 and United Kingdom [11].

Another metric to analyze is the modal shares, shown in table 2.1. Which passenger shares, represent the percentage of pkm and freight shares represents the percentage of tkm. The modal share for both passenger and freight are bellow EU expectations and is mainly caused by overall lack of competitiveness and insufficient investments [13].

Since this study is focused in Portugal, which is one EU member state, it is important to

Table 2.1 – EU28 modal split in %.

	Passenger					Freight			
Year	**Passenger cars**	**Bus**	**Railway**	**Air**	**Others**	**Road**	**Rail**	**Sea**	**Others**
1995	73.3	9.7	6.4	6.5	4.1	45.3	13.6	32.7	8.4
2000	72.9	9.2	6.4	7.8	3.7	46.5	12.5	32.9	8.1
2005	72.7	8.7	6.2	8.5	3.8	48.6	11.5	32.2	7.7
2010	72.9	8.3	6.5	8.4	3.8	49.4	11.4	31.2	8.1
2015	71.6	8.0	6.8	9.7	3.8	49.0	11.8	31.6	7.6
2017	70.9	7.4	6.8	11.2	3.8	50.1	11.3	31.5	7.1

Source: Adapted from [11], [14].

mention the goals of the Union regarding its transportation matrix, especially regarding railways. Even though the transport has become cleaner, it increased in volume, what means that remains a major source of noise and pollution. The EU intends to reduce at least 60 % of green house gases by 2050 with respect to transportation sector. It is necessary to develop evenly across west and east European countries, in order to reach a fully connected and efficient railway network to achieve the reduction goals [15].

Furthermore, the White Paper [15] established ten goals for a competitive and resource efficient transportation system in which is important to mention the following:

- 30 % of road freight over 300 km should shift to other modes such as rail or waterborne transport by 2030, and more than 50 % by 2050, facilitated by efficient and green freight corridors. To meet this goal will also require appropriate infrastructure to be developed;
- By 2050, complete a European high-speed rail network. Triple the length of the existing high-speed rail network by 2030 and maintain a dense railway network in all Member States. By 2050 the majority of medium-distance passenger transport should go by rail;
- A fully functional and EU-wide multimodal TEN-T 'core network' by 2030, with a high quality and capacity network by 2050 and a corresponding set of information services;
- By 2050, connect all core network airports to the rail network, preferably high-speed; ensure that all core seaports are sufficiently connected to the rail freight and, where possible, inland waterway system.

In the US, in 2017, the total length of the railway network was around 202 700 km, also for passenger and freight purpose. Figure 2.3 shows the railway network in North America. The country experienced an average yearly growth in the tkm indicator of 28 %: from 1500 billion tkm in 1990 to 2530 billions in 2005. After this period, stabilized around 2500 billions. Since 2014, the indicator has dropped about 7 % yearly. Meanwhile, with respect to the passenger transport, the US improved from 26 billion to 39 billion pkm between 1995 and 2017.

Table 2.2 – US modal split in %.

	Passenger					Freight			
Year	**Passenger Cars**	**Bus**	**Railway**	**Air**	**Others**	**Road**	**Rail**	**Inland Water**	**Pipelines**
1995	-	-	-	-	-	43.0	27.2	7.6	22.2
2000	81.8	6.5	0.4	10.7	0.5	44.7	29.7	6.9	18.6
2005	82.6	5.3	0.4	11.2	0.5	45.6	32.2	6.1	16.1
2010	82.9	5.5	0.4	10.6	0.6	45.8	31.1	5.6	17.4
2015	81.6	6.0	0.4	11.3	0.7	40.6	35.3	6.4	17.8
2016	81.5	5.9	0.4	11.4	0.6	42.1	33.0	6.3	18.6

Source: Adapted from [11].

The US modal shares are shown in table 2.2. It is clear that the railway plays a much bigger role in freight than in passenger transport. The US rail freight share has grown, whilst for the EU it has slightly decreased in the same period. In the other side, for the passenger transport, the European Union uses it more than in the US: 470 billion against 39 billion pkm and a share of 6.8 % in comparison to 0.4 % for the year 2017 [11].

Figure 2.3 – North America railway network.

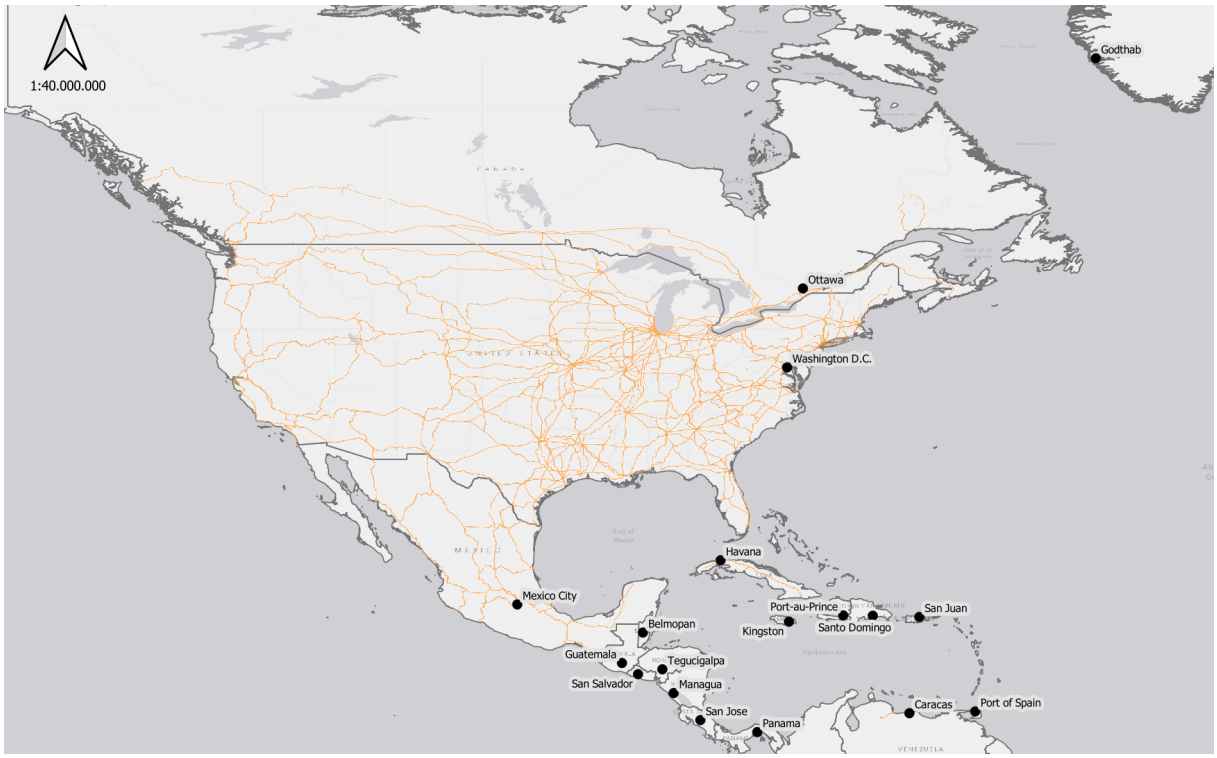

Source: Adapted from openrailwaymap [12].

2.3 Rail Transport in Portugal

The development of the railways in Portugal faced numerous difficulties such as: government bureaucracy, inexperience in construction and financial support. Also, politicians and intellectuals did not have a common opinion regarding the benefits of railway transport. Furthermore, the idea of railway transport bothered the already established terrestrial transportation companies at that time. However, the King of Portugal, D. Pedro V and his minister, Fontes Pereira de Melo, were committed to the development of railways in Portugal [16].

In 1844, a state company, named *Compania das Obras Públicas de Portugal* was founded. It was in charge of a railway connecting Lisbon to Spain. This project could not take place and the company was extinguished. A year later, the government established a set of conditions and rights regarding the construction of this project, such as: tax exemption, land use rights, the right to establish prices to transport passenger and goods for the first 10 years and others. With these acts, it was expected companies to take over the project [16].

In 1852 a decree law was approved, which opened a call for companies to construct a rail segment of around 50 km connecting Lisbon and Carregado. A company named *Companhia Peninsular dos Caminhos de Ferro de Portugal (CPCFP)* assumed the project. Soon after all contractual bureaucracy, the company started the railway construction. Finally in 1856, the first segment, from Lisbon to Carregado was launched [16].

Despite the first achievement of opening this segment, the company was going through financial difficulties and could not continue the project. During 1857 and 1859 new negotiations were announced and another company was chosen to continue the construction: *Companhia Real dos Caminhos de Ferro Portuguezes (CRCFP)*. The company leader was D. José de Salamanca and was the only person that met the requirements to take over the project and he also had the financial aid from Spain and France. By the time he has already experienced in these sort of project: he also led the construction of railways in Spain. From this time, Portugal had finally a reliable company developing the railway network. The government also assigned other companies the right to explore the sub regions inside the country, which were responsible to connect to the main lines. Any person or company that had enough funds to build the project could require the rights to explore the line. During the 99 years of exploration of the *Companhia Real dos Caminhos de Ferro Portuguezes* and with the other companies, Portugal developed its railway network as D. Pedro e Fontes Pereira de Melo expected to the country [16].

Is import to mention that in Portugal the routes of the railways were defined mainly under the technical aspects, not taking in account its social and economic relevance. Also, by that time, the country had a lack of geographical, geological and demographic information, affecting the

route planning. Portugal could have been an exception to what Scaggiante [8] mentioned about continental European governments participating actively to the railway route planning. The construction and development of the Portuguese railway were made utilizing in majority foreign work force. Workers came from Great Britain, Spain, France, Belgium, Italy and others. They shared their experience with Portuguese workers and soon after, with the shared knowledge, Portuguese engineers started their contribution to the railway development of their country [16].

The railway in Portugal had a great impact in the economic and social development. The rail freight transport began one year after the opening of the first line in 1856. The access by road to the main harbors in Portugal was deteriorated and as far as the rail network developed, further connecting the main cities, the roads could not follow the same growth and the freight transport utilizing rail was rapidly accepted and used. As soon as the lines started to path inside the country, some zones claimed for rail lines to enable financial and social development of the region. An important fact to that was the wine production zone between Porto e Barca d'Alva. The rail transport offered a safer and faster mode, compared to the road transport. Moreover, the people in Portugal were now able to move quicker through the country and to explore new places. The railways provided more mobility to the population. Furthermore, the potential use of railway to the tourism market was highly explored. Companies began to organize travel groups and offers. [16].

Every new segment built or a promise of construction was covered by the local and national newspaper. The railways became a landmark in the country's history. Some important cities connections are described, followed by its completion year:

- Carregado - 1856;
- Elvas - 1863;
- Coimbra - 1864;
- Beja - 1864;
- Entroncamento - 1872;
- Braga - 1875;
- Porto - 1877;
- Valença (connection with Spanish network) - 1882;
- Régua (connection with Spanish network) - 1887;
- Mirandela - 1887;
- Figueira da Foz - 1888
- Faro - 1889;
- Guarda - 1893;
- Bragança - 1906.

Figure 2.4 shows the list above in a map. The "in use" status means railways for passenger and freight operations. Meanwhile "not in use" can describe abandoned, disused or razed rail tracks, according to the data source. The city of Mirandela, in the north of Portugal, belongs to the Tua line, which is named after the Tua river. It was a common practice to name lines after the water stream they follow. Furthermore, this line is the object of this research.

Figure 2.4 – Railways in Portugal.

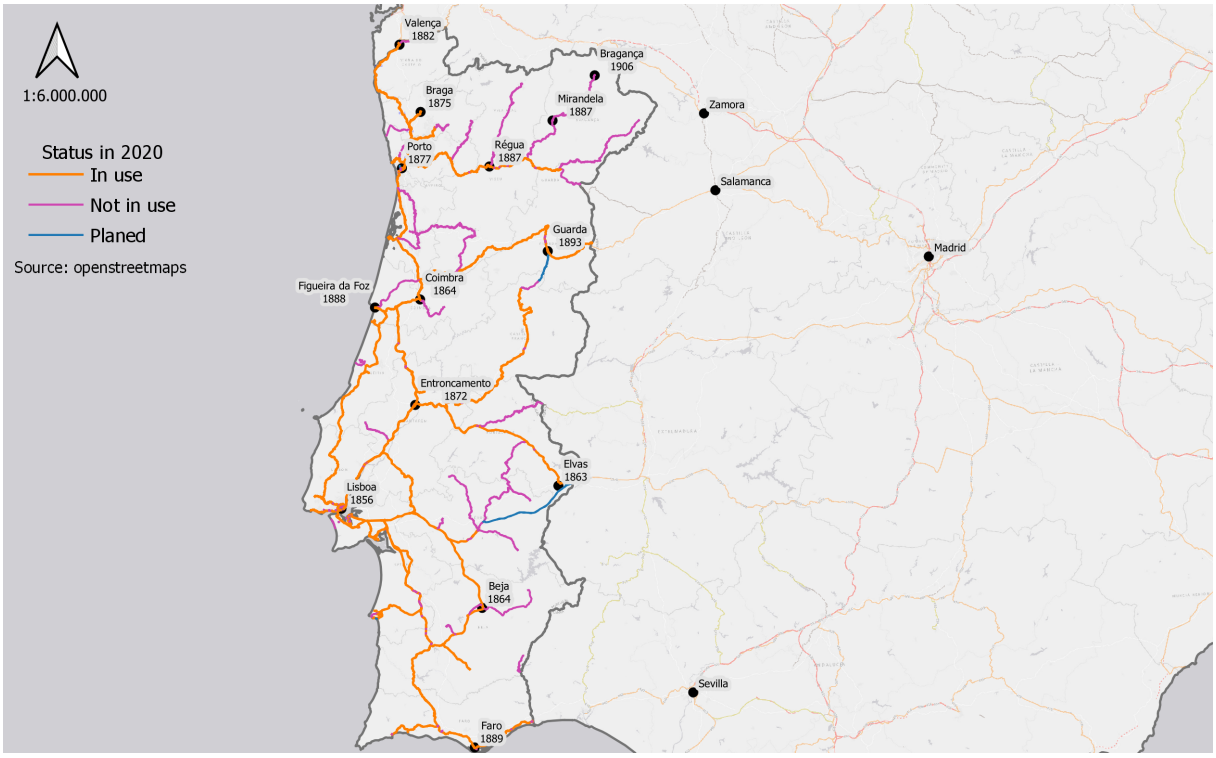

Source: Adapted from Openstreetmap [17].

During the 20th century the Portuguese government incorporated all the rail companies. In 1927 the state incorporated regional corporations and established a rent agreement with the CRCFP, so that the company could control and run all the national rails. In 1947 the company was given the control of other state railways and changed the name to *Caminhos de Ferro Portugueses (CP)*. Later in 1975, due to the expansion of roadway after the WWII, financial and political crises, the company was incorporated to the Portuguese state. Another major change happened in 1997, when a company named *Rede Ferroviária Nacional (REFER)* was founded and started controlling all the infrastructure, leaving the logistics and operations to CP. Nowadays the company *Infraestruturas de Portugal (IP)* is in charge of the railway infrastructure [16], [18].

In 2018 the total line length of Portugal was 3620 km, in which only 2546 km (70%) was in operation, and from the operational lines, 1639 km (64.4%) are electrified. The main network consists of 1175 km of tracks and the others are complementary and secondary tracks. Also counts as infrastructure bridges, tunnels and level crossings. By the end of 2018, bridges summed

up to 1836, tunnels 90 and crossings 839. The railway sector had in use 370 locomotives and 3072 wagons for freight transport and 999 vehicles for passengers [19].

Table 2.3 – Portugal - performance by mode.

	Passenger - billions pkm				Freight - billions tkm		
Year	**Railway**	**Metropolitan railway**	**Roadway**	**Air**	**Railway**	**Roadway**	**Air**
2015	3957	1009	6575	31611	2688	32525	320
2016	4146	1061	7612	29513	2774	34684	341
2017	4391	1121	7413	37119	2751	34073	478
2018	4487	1177	7926	40780	2863	32676	475

Source: Adapted from [19].

Table 2.3 shows that the railway mode continues to increase since 2015 both for passenger and freight operations. According to the Statistics National Institute [19], the growth on passenger performance is due to the improvement on the suburban movements, in contrast with decreasing movement in long course and international movements within the rail sector. The international freight operations keeps increasing since 2016. In particular 2,2 millions tons were transported from or to Spain [19].

Lopes [20] stated that Portugal highly depends on road freight transport to all the EU, except Spain. This can lead in the future to the isolation of Portugal from the rest of member states. Portugal (and Spain) struggles with interoperability with the European network. In these countries the adopted rail gauge was different from the others European countries. The Iberian gauge measures 1668 mm, meanwhile the European gauge, also known as UIC, measures 1434 mm. Due to this fact, trains leaving from Portugal can not cross the Franco-Spanish border. This lead to huge economical impact and decrease the financial attractiveness of Portuguese harbours.

In order to overcome the Interoperability issue and aligned with the European White Paper goals [15], the government released in 2015 the Strategic Plan of Transport and Infrastructure for the horizon 2014-2020 (PETI3+). In attendance to the plan, the company IP revealed a set of actions called *Ferrovia 2020* and some of the major investments and modifications are:

- Assure conditions to the rail interoperability with the European network by electrifying lines, installing electronic signalization and installing mechanisms to match (third rails) the Iberian and UIC gauges and progressively change main corridor gauges;
- Increase the railway sector competitiveness by reducing the travel times, travel costs and increasing the capacity of the network;
- Improve the international connections by creating better network conditions from and to the national harbours;

- The investment amount expected reaches circa 2000 million EUR.

The company expects the conclusion of the project by 2023 and by October 2020 78% of the investment is already finished or under construction. Furthermore, the government stated the desire of connecting all districts capital cities and continue the progress reached within the program *Ferrovia 2020* [21] [22]. Summarizing, Portugal has a great potential to keep growing in the railway sector with government support and with the European Union cooperation. These actions will assure a stronger economy and a more connected European mobility zone.

2.4 Technical Aspects of Railways

The role of railways is to promote a safe, economic, reliable and comfortable operations of trains to promote the transport of passenger and goods. The railway is a set of components interacting each other in a complex manner under many circumstances, such as, open weather conditions and different loads from the rolling stock. To assure secure operations and project lifespan, understanding the behavior of these elements in an essential task [23].

Each structural component should behave as expected, in order to the whole system to work together. The energy from the rolling stock is mainly transferred to the lower components by compression, from the rails, through the sleepers, ballast and then to the soil. The elements are divided in two groups: superstructure and substructure. Figure 2.5 shows the division and its sub-elements. The superstructure consists of rails, fasteners and sleepers. The elements beneath, ballast, sub-ballast, roadbed and natural soil stratum are part of the substructure. All these components will be explained in this section [23].

According to the American Railway Engineering and Maintenance-of-way Association [24] (AREMA), track superstructure is defined as the assembly of rail, cross ties (sleepers in British English), other track materials and special track materials which are the components of a conventionally constructed track system. The track substructure consists of layers of granular materials that are installed for the purpose of:

- Permitting drainage within the track substructure;
- Anchorage of the track superstructure in the three dimensions of space;
- Distribution of loads and transfer of the track superstructure loads to the underlying roadbed;
- Facilitating fine adjustment of track superstructure alignment, grade and cross level without system reconstruction;
- Shielding the materials of the roadbed from climatic forces.

Figure 2.5 – Railway cross section.

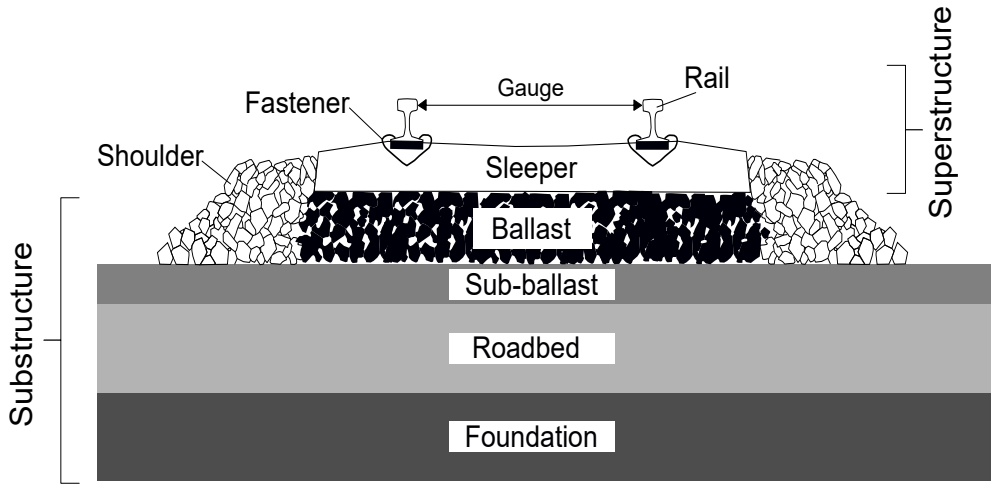

Source: Adapted from Fortunato [23] and AREMA [24].

In the early days of the development and improvement of the railway technologies, engineers focused their attention on the superstructure, neglecting attention on the substructure. The performance of the railway was associated only with the superstructure elements. Later on, it was realized that the substructure play an important role in economic aspects, due to the cost of conservation and maintenance, being as important as the other structures [23]. Also Bonnett [1] stated that the early railways engineers did not realise the importance of ballast beneath elements and many materials that were used for this purpose today would be completely unsuitable. Usually they were cheap and easily available locally materials, such as ashes, chalk and clay.

To facilitate the understanding of the technical aspects of railways, the components will be explained following the flow of stress dissipation through the structural elements, hence: rails, sleepers, ballast, sub-ballast and natural soil.

For this purpose, it is necessary to explain how loads appear: Rolling stocks. These are moving components that run on hard wheels on hard rails, supported and guided by the rails. The rolling stock also transmits vertical, horizontal and longitudinal forces to the track and track's supports, either by direct bearing on rail top, laterally through the flange or longitudinal by friction. Example of rolling stocks are: locomotives, freight wagons, passenger coaches/wagons, metro cars, trams, inspection and maintenance trolleys [1].

2.4.1 *Rails*

All modern railways use steel rails, as mentioned in section 2.1, since it has well known behavior and properties such as strength, fatigue, endurance and corrosion resistance. The rails act like supported beams, loaded by concentrated forces from the rolling stock wheels and transferring them to the sleepers without permanent deformations, namely, plastic deformation. Furthermore, it has a role of guiding the stocks' wheels along the track alignment [1], [23], [25].

The profile has been constantly improved since the appearance of railways. One of the first designs used is called bull head or double-headed rail (fig. 2.6a). It was expected that when the upper section was worn out, it could be reversed, although it did not work as planed and the design was abandoned. The most used nowadays is the *Vignole* section (or flat bottom), named after the Australian engineer who designed it. There are three named parts on the profile sketch: head, web and base or also called foot. (fig. 2.6b). Many variations on the design were made to follow the increasing loads from the rolling stock. Hence, to accomplish a great increase of section inertia, the height of the profile has constantly risen. Also is a best practice to name the rail profiles by its weight per unit length. For example, UIC54, UIC60 weighting $54.43\,\mathrm{kg\,m^{-1}}$ and $60.34\,\mathrm{kg\,m^{-1}}$ respectively [26].

Many organisations developed documents to standardize the production and assure quality in the rail network. In Europe, the European Standard EN 13674 covers all types of rail sections and also the steel requirements for the production, testing and acceptance of the segments. In the USA, the American Railway Engineering and Maintenance-of-Way Association (AREMA) is responsible for railway related standards.

Figure 2.6 – Railway profiles.

(a) Bull head or double-head

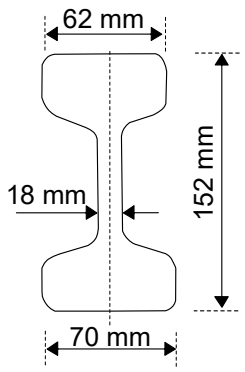

(b) Vignole or flat-bottom

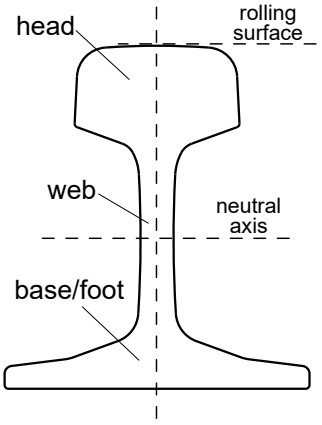

Source: Adapted from [26].

Constructive, geometric and material characteristics of rails play an essential role on the global behavior of the track structures because they affect how the sleepers receive and transfer the loads to the elements bellow. For example, higher profiles means greater inertia and this property allows the load to be dissipated by more sleepers, increasing force distribution area and reducing the stress on the layers bellow. Furthermore, geometric imperfections on the rail or on the wheels can lead to misalignment of the track and permanent damage of sleepers and beneath layers [23].

During the development of railway transport, many changes have occurred regarding the rail's steel manufacturing process and chemical composition, changing significantly its mechanical properties. In the past, ingot casting was used, in contrast with continuous casting technique that has been used for some years guaranteeing a continuous quality production control. Both oxygen or electric arc furnaces are used to produce steel. Furthermore, the maximum tensile strength in 1882 was 490 MPa in compassion with a range of 690 MPa to 1180 MPa nowadays. Despite the great increase of the mechanical strength, further improvement is not desirable, due to the reduction of ductility and the possibility of brittle failure of the material. Tables 2.4 and 2.5 show the chemical and mechanical properties of some rail grades [26].

In addition, according to Profillidis [26], the rail steel quality may be distinguished in two categories:

- Normal steel quality, with an ultimate tensile strength of 690-880 MPa;
- Hard steel quality, used mainly on curves and level crossings, with an ultimate tensile strength of 880 MPa to 1180 MPa.

Table 2.4 – Chemical properties according to EN 13674:1 for the various rail steel grades.

Grade	C(%)	Si(%)	Mn(%)	P_{max}(%)	S_{max}(%)	Cr(%)
R200	0.38-0.62	0.13-0.60	0.65-1.25	0.040	0.040	$\leq$ 0.15
R220	0.48-0.62	0.18-0.62	0.95-1.30	0.030	0.030	$\leq$ 0.15
R260	0.60-0.82	0.13-0.60	0.65-1.25	0.030	0.030	$\leq$ 0.15
R260Mn	0.53-0.77	0.13-0.62	1.25-1.75	0.030	0.030	$\leq$ 0.15
R320Cr	0.58-0.82	0.48-1.12	0.75-1.25	0.025	0.030	0.75-1.25
R350HT	0.72-0.80	0.15-0.58	0.70-1.20	0.020	0.025	$\leq$ 0.15
R400HT	0.88-1.07	0.18-0.62	0.95-1.35	0.025	0.025	$\leq$ 30

2.4.2 *Track Gauges*

The definition of track gauge is: the distance between the inner sides of the heads of the two rails, measured 14 mm bellow the rolling surface (fig. 2.6) [26]. Since railways developed in England, the first tracks were constructed with a gauge of 1435 mm and later most countries

Table 2.5 – Mechanical properties according to EN 13674:1 for the various rail steel grades.

Grade	Min. Tensile strength (MPa)	Elongation(%)	Hardness(HB)
R200	680	14	200-240
R220	770	12	220-260
R260	880	10	260-300
R260Mn	880	10	260-300
R320Cr	1080	9	320-360
R350HT	1175	9	350-390
R400HT	1280	9	440-440

adopted the dimension. Nowadays it is called "Standard gauge" or "UIC gauge". However, there are others values that are in use in different locations, and therefore gauges are divided in classes: standard, metric, broad and narrow gauges [26], [27].

- Standard: 1435 mm;
- Metric: 1000 mm;
- Broad: 1520 mm, 1524 mm, 1668 mm, 1676 mm and 1600 mm;
- Narrow: 914 mm and 760 mm.

According to Profillidis [26], 57.5 % of railways are constructed with standard, 26.5 % with broad, 15.5 % metric and 0.5 % with narrow gauge, in respect with 1 028 723 km of railways laid world wide. In Europe, the standard gauge is mostly used, however, some countries use different ones, making it harder to fully connect the entire continent. Table 2.6 shows some countries and its gauges values. In Portugal and Spain, as mentioned in section 2.3, the Iberian gauge is most used, measuring 1668 mm, thus classified as a broad gauge. Also, many secondary lines use metric gauges [27].

Table 2.6 – Gauges in some European countries.

Country	Gauge
DE	1435 mm
ES	1000 mm, 1435 mm and 1668 mm
FR	1000 mm and 1435 mm
PT	1000 mm and 1668 mm
UK	1435 mm and 1600 mm

Source: Adapted from [11].

The gauge affects many characteristics of the rail and it is fundamental to the whole network to function properly. Narrow (here not specifically addressing the class of narrow gauges) gauges means lower radius of curvature, less earthwork and cheaper rolling stocks. Meanwhile wider ones offer more load capacity and higher speeds. The choice should consider always technical

and economic aspects.

2.4.3 *Sleepers*

Sleepers (also called *ties* in North America) are the elements positioned between the rail and the ballast (see fig. 2.5). During the early days of railways, as mentioned in section 2.1, longitudinal supports were used to place the rails. Nowadays these are mounted on the sleepers, spaced in a regular interval, usually 60 cm, to support the rails and to promote a better stress distribution to the ballast. Moreover, sleepers must fulfill the following functions:

- Appropriate transfer and distribution of loads from the rails to the ballast;
- Constant rail spacing, specified by the track gauge;
- Constrain the track's vertical and horizontal displacements.

Sleepers should offer satisfactory mechanical resistance in both vertical and horizontal direction and the most used materials to produce them are wood and concrete [23].

Timber sleepers were the first technology to be implemented. It offers a good adaptability for non standard situation, proper insulation for electrified lines, great resilience and ease of handling. However, due to high cost, short lifespan and scarcity, lead to change in technology. Since 1950 prestressed-concrete sleepers began to be used for the purpose. Although, timber elements can still be used when concrete is not suitable [1], [23], [26].

In summary, timber sleepers have great advantage in the load distribution to the ballast, due to the flexibility of the material, and it is a preferred choice in cases where the ballast has poor mechanical properties. The disadvantages is related to variability of lifetime, depending on the wood properties and chemical treatment, varying from 25 to 50 years [26].

A important fact to mention when it comes to timber and concrete sleepers is the lateral resistance offered by these elements. This parameter affects speeds and axle loads that can be supported by the track and also for buckling analysis. The lateral resistance highly depends on the sleeper type and fastening method. Concrete sleepers offer high resistance due to its weight, when compared to timber ones [23].

The stress distribution on concrete sleepers is complex, therefore, many studies were done and the subject is still under development. Two types of concrete sleepers are used: mono-block and twin-block (fig. 2.7). Both have advantage and disadvantage between them and over with timber sleepers.

In general, concrete sleepers have a lifetime of 50 years and perform in a good manner when it comes to maintain the track gauge in appropriate levels for safe operations of trains. Both use elastic fastening methods and absorbing materials between rail and sleeper to reduce dynamic loading and also to distributing static loads. Mono-block accounts (fig. 2.7a) for 80 % of concrete sleepers and compared to the twin-block, has advantage on the load distribution to the ballast but less lateral resistance.

Regarding twin-blocks (fig. 2.7b), they have similar mechanical behavior as mono-blocks maintaining the track gauges, but when laid over poor ballast, their properties are modified. When it comes to load distribution, this type of sleepers have downsides compared to mono-block and timber ones. The small placement area creates a concentrated stress on the ballast. In terms of maintenance, the reinforcement bar on the central area of the sleeper needs special attention, otherwise it can lead to hazards on the track. The great feature of the twin-block system is its high transverse resistance due to great weight. It is suitable for high speed operations.

The choice of sleeper's material should be evaluated for every track, considering economic and technical aspects, such as, cost of manufacturing, fastenings types (see section 2.4.4), lifetime and maintenance costs [26].

Figure 2.7 – Example of concrete sleepers.

(a) Mono-block

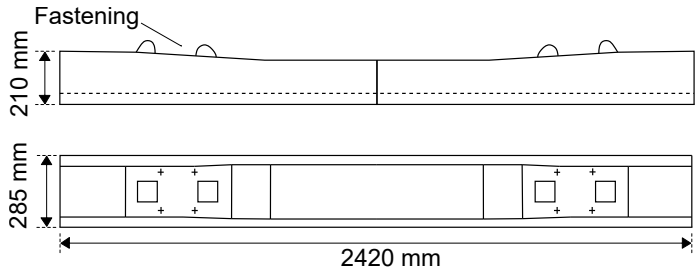

(b) Twin-block

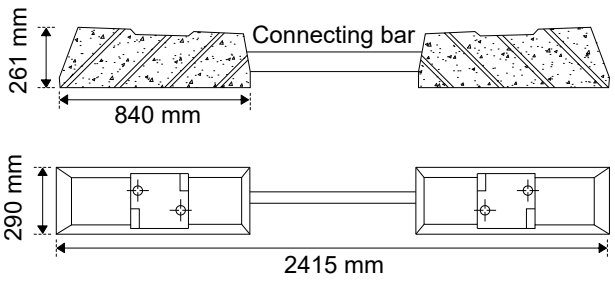

Source: Adapted from [26].

2.4.4 *Fastenings*

Fastenings are the elements ensuring the connection between rail and sleeper. There are two distinct types: rigid and elastic. Both should provide, according to Profillidis [26], these characteristics:

- Keep track gauge as close as possible to its nominal value;
- Keep the inclination of the rail on the sleeper constant;
- Transfer loads from the rail to the sleeper;
- Attenuate and dampen vibrations caused by train traffic;
- Easy installation and maintenance;
- Electrical insulation;
- Reasonable cost;
- Lifetime compatible to that of the sleeper.

Moreover, fasteners should withstand vertical, longitudinal, lateral, torsional and vibration loads transmitted from the rolling stock. It has also function to resist the stresses caused by temperature changes on the rail [23].

Rigid fastenings are achieved with bolts or nails and are used only with timber or steel sleepers (fig. 2.8). Due to its installation characteristics, when trains ride over the rail, small plastic deformations (e.g permanent deformation) occurs on sleeper, leading to the occurrence of gaps between rail and fastener. In a long term, the gaps grow causing gradual slackening of the fastening, affecting the safety and may be the origin of derailment. A seating plate is used (preferable) to place the rail in an uniform surface, instead of directly on the wood. Furthermore, this type of fastening does not handle well high frequency vibrations caused by the rolling stock and these effects contribute to the widening of gaps and slackening of fastenings [26].

Elastic fastenings are mandatory by use of concrete sleepers. Many technologies were developed, such as, *Vossloh*, *Nabla* and *Pandrol* (fig. 2.9). Each features its own properties, pros and cons, but all cover their function of damping vibration caused by dynamic loading, reducing the friction between rail and sleeper and promoting electric insulation. They also should retain their elastic characteristics for a long time after installation and remain tighten to the rail and sleepers [23], [26].

Figure 2.8 – Rigid fastening.

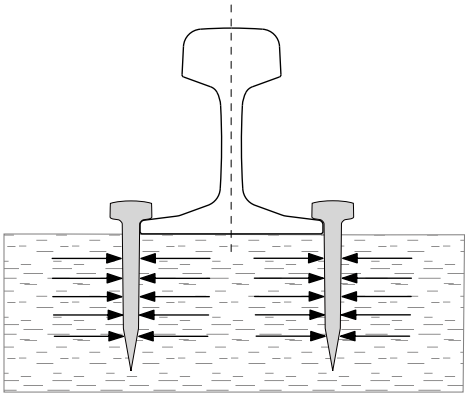

Source: Adapted from [26].

Figure 2.9 – Elastic Pandrol fastening.

Source: Marcus Wong Wongm on *Pandrol* [28].

2.4.5 *Ballast*

Ballast is a layer of crushed stone on which the sleeper rest. It also fills the space between sleepers as well as at some distance beyond the sleeper ends, called ballast shoulder (fig. 2.5). Usually, the layer has a thickness in the range of 20 cm to 40 cm and offers high vertical compressive strength. On the other hand, the lateral resistance is poor due the way the material works, relying only on the friction between gravel particles [25], [26].

As mentioned in section 2.4, the importance of the substructure layers were underestimated during the early days of railways. However, by the beginning of XX century, experimental results led to an agreement on the importance of the ballast. Nowadays rail companies pay great attention on the behavior, performance and quality of this element [23].

The functions of the ballast are, according to Profillidis [26]:

- Further distributing stresses transmitted by the sleepers through the foundation soil;
- Attenuating the greatest part of train vibrations;
- Resisting track shifting (transverse and longitudinal);
- Facilitating rainwater drainage;
- Allowing track geometry to be rather easily restored with use of track maintenance equipment.

Some aspects of the ballast work in opposite ways, for instance, to achieve a good load bearing characteristics and track stability, the ballast needs to be well graded and compact, which in turn, however, makes the rainwater drainage less efficient, increasing the drainage time. Furthermore maintenance would be more difficult due to high compaction factor of the ballast [23], [26]. Therefore a balance of the various functions is required to achieve the expected results. Fortunato [23] states that the ballast should be formed from granular materials of great dimensions (not less than 63 mm), creating a permeable layer and facilitating the maintenance. However, some authors state that in presence of small particles, the ballasts becomes more stable and easier to compact.

The behavior of the ballasts highly depends on its mechanical and hydraulic characteristics. In addition, the superstructure (rail and sleeper), traffic load from rolling stock and maintenance periodicity play an important role on the behavior of the layer. Thus, it is quite a difficult task to establish rigorous standards on the general behavior of the ballast [23].

2.4.6 *Jointed Tracks*

So far, many components were shown to ensure the track's position and dissipation of stresses through the layers. Now changing from the cross section point of view, to the top view of a railway, other component is necessary to provide continuity to the rails: Rail Joints. A track which uses joints elements along its paths is classified as a Jointed Track. This was the first type of railway tracks and they make use of fishplates (fig. 2.10) to proper join the rail bars.

Rail segments are manufactured in rods of 18 meters and then welded in groups of two or three, making a single rail with total length of 36 or 54 meters in which once more are jointed to other rail using fishplates. This element uses bolts and nuts in pre-bored holes at the end of rail bars, to keep the rail straight vertically and horizontally. Important to mention that, for each rail profile, an appropriate model of fishplate has to be used. Also, a gap between both aligned rails (expansion joint) is intentionally left, in order to allow the thermal expansion of the rails due to change in temperature of the steel. This is the main characteristic of jointed

Figure 2.10 – Fishplate joint.

tracks [26].

On the one hand, the gap allows thermal elongations, which prevent the rail from high internal compressive stresses, on the other hand has some downsides: wear on the rolling stock's wheels and on the joint region. Significant reduction of passenger comfort due to noise and a high cost of maintenance to keep the fishplates in good conditions [1], [26].

Therefore, removing rail joints meant a significant leap forward and a reduction of sizeable annual workload. This improvement was achieved by the end of the Second World War, which took the development and use of welding techniques further and made possible joining long segments of rails and grounding the Continuous Welded Rail (CWR) [1].

2.4.7 *Continuous Welded Rail*

Continuous Welded Rail (CWR) are achieved by welding discrete pieces of rails. Depending on the country, the manufacturing process produces rods with lengths of 18 m, 24 m, 30 m and 36 m in the UK, 60 m in Germany and up to 108 m in Austria, for example. The first welding process occurs in welding shops and is a controlled procedure. In Portugal, for instance, the rails are welded up to 144 meters from 18 m bars, meanwhile in UK, up to 240 meters. The last process is to weld in field once more the pieces to one single structural segment of rail [1], [26], [27].

Before fully adopting the CWR as main technology on railway tracks, some technical aspects had to be solved, in order to ensure the safety and stability of the operations. Fully understanding the welded joints under dynamic loads and fatigue were fundamental to this technology, as well as the invention of elastic fastenings (see section 2.4.4), which match the mechanical behavior of CWR.

The main advantages of CWR are, according to Leite [27]:

- Less deterioration of track components;
- Less vibration and oscillation of rolling stock.

Without gaps, the CWR is constrained with no room for thermal elongation, which induces thermal stresses along the rail. This fact raised concerns regarding structural instabilities on CWR tracks. This concern was well addressed with mechanical studies of ballast resistance, combined with a track weight increase [26].

Furthermore, many models regarding temperature prediction of railways using statistical or physical models were developed, as well as numerical and analytical ones to predict thermal buckling. These topics will be discussed in the following sections.

2.5 Rail Temperatures

Railways are usually structures exposed to open weather conditions, such as rain, snow, humidity, wind and solar radiation, with a seasonal variation. These conditions affect the mechanical behavior of the rails and may lead to buckling or tensile failure events. A particular phenomenon is discussed in this section: Temperature changes on rails upon weather conditions.

Although, is necessary to mention some impacts of weather on the rail network. Rain affects earthworks, by causing floods or long dry periods causing tracks to settle. Snow causes drifting of the rolling stock, poor visibility and poor adhesion, which may lead to malfunction of break systems. Wind may cause tree falls along the lines and can also affect the vehicle stability. Lightning can damage equipment, e.g. signalling and also cause line side fires [29].

High temperatures may cause thermal buckling on the rail and due to this fact speed restrictions are often issued to reduce the probability of derailments if the track fails. In the opposite spectrum of temperatures, low ones may lead to a tensile failure due to contraction [29]. Both types of tracks (jointed and CWR) are prone to these effects, however, due to mechanical constraints, CWR's are more likely to be affected.

Originally, as discussed in section 2.4.6, rail tracks included joints to allow thermal expansion. However, this type of track is being phased out because of its high maintenance cost compared to the welded rails alternative. In CWR's there is no room for expansion [29].

The analysis of thermal buckling have been on research since the introduction of CWR. The behaviour of tracks under high temperatures are now well understood, due to analytical models combined with advancing computing technologies, specifically, Finite Element Analysis (see section 2.6). However, the current goal is to be able to predict when critical temperatures will

take place, thus predicting the instability before it happens [4].

Thus, models were developed using field and laboratory measurements, physical relationships and computational solvers, trying to quantify the change in temperature under various weather conditions. They are divided in two categories: empirical methods and physical models [4]. The main characteristic of empirical models is that the method uses field collected data in order to find a correlation equation to predict rail temperatures. Meanwhile, physical models, as named, use heat conduction equations and material properties in addition with weather data to predict the rail temperatures. Details will be discussed in sections 2.5.1 and 2.5.2.

In addition, the rail temperature is different along the section and surface, thus a representative point or location to measure the temperature is necessary in order to correctly use in buckling models. Some studies were conducted to determine where is the suitable point of the rail section to measure the temperature, Hong *et al.* [30] and Marmash *et al.* [31].

Hong *et al.* [30] conducted experiments, collecting temperature data of a KS-50N rail section with 500 mm long of 16 points over the rail surface and inside the section, using K-Type thermocouples. Besides that, during the experiment, the ends of the section were insulated, in order to simulate an infinite rail segment. After collecting 10 months of data (from August 2016 to May 2017) and simulating using FEA, they suggest a representative measurement point to be used in buckling studies. For the section in case, the point is located at 74 mm from the bottom section. Their results are shown on figure 2.11.

Figure 2.11 – Point of measurement.

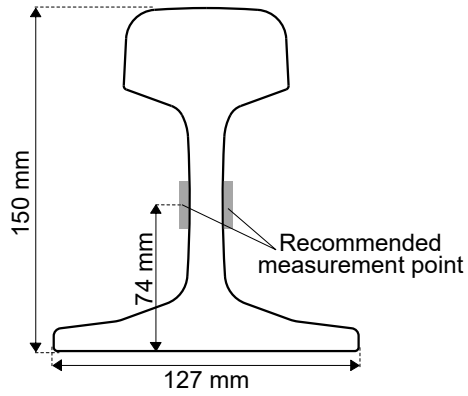

Source: Adapted from [30].

Marmash *et al.* [31] results are in accordance with Hong, regarding the surface temperature corresponding to bulk rail temperature. Also, the author states that measuring the temperature on the base, as common practice in UK, can lead to a large underestimation of the bulk temperature. Another result is that a difference around 2 °C is found between the cool and hot side of web.

2.5.1 *Empirical Models*

As stated before, empirical models depends on field collected data in order to develop a good approximation to rail temperature. This implies that from one location to another the relation may not be valid, since the micro climate can vary. Important models were developed by Hunt [32], Esveld [33] and Munro [34] as cited in Wu *et al.* [4] and Chapman *et al.* [29].

- Hunt's model

The easiest and most plausible approach is to correlate the air and rail temperatures. However, the rail temperature can also change due to wind, solar radiation and humidity [29]. Hunt developed two equations which relate these variables: eq. 2.1 is used for sunny days and eq. 2.2 used for cloudy days [4].

$$T_{rail} = 1.5 \cdot T_{air} \tag{2.1}$$

$$T_{rail} = T_{air} + 17 \tag{2.2}$$

- Esveld's model

Another model is suggested by Esveld [33], correlating air and rail temperature, for both sunny and cloudy days, valid for specific range of temperatures. The correlations are shown on figure 2.12.

Chapman *et al.* [29] conducted experiments on two test sites (Winterbourne and Leominster), in the UK, collecting weather and rail temperature data for a period of 12 months (from June 2003 to June 2004). The rail temperature was collected using K-type thermocouples. In Winterborne site, a segment of rail was built to mimic the real line, and thermocouples were installed on the base, web and head of the section. Meanwhile in Leominster, since it was a live line, the measurements were taken from the section's base.

The main purpose of Chapman study was to develop a physical model (see section 2.5.2), but first discussed the effectiveness of Hunt and Esveld models. Figure 2.13 shows the collected data and Hunt and Esveld correlation models.

There are large differences in the accuracy of the techniques used. Equations 2.1 and 2.2 only provide an approximation of rail temperature and this may be caused by other weather variables like wind, humidity and solar radiation. Regarding Esveld correlation, seems to perform well

Figure 2.12 – Esveld correlation.

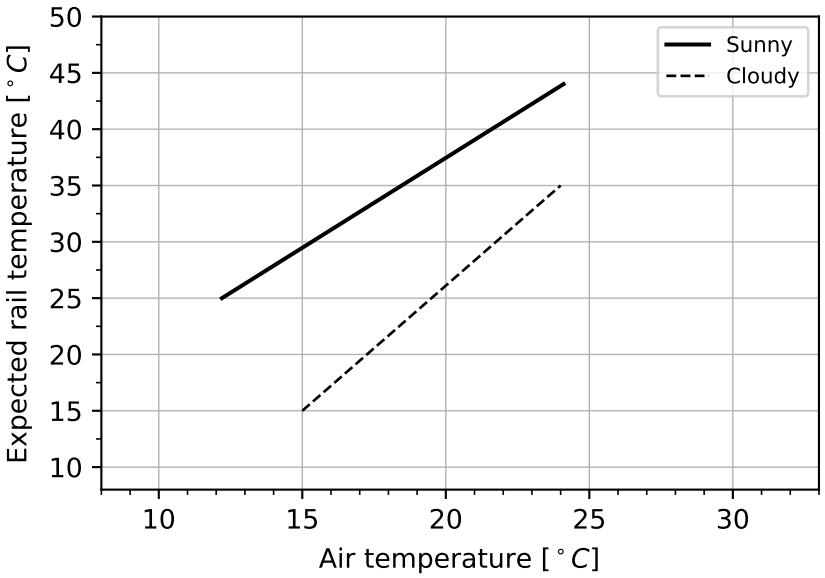

Source: Adapted from Esveld [33, p.383].

Figure 2.13 – Chapman's collected data.

(a) Winterbourne site

(b) Leonminster site

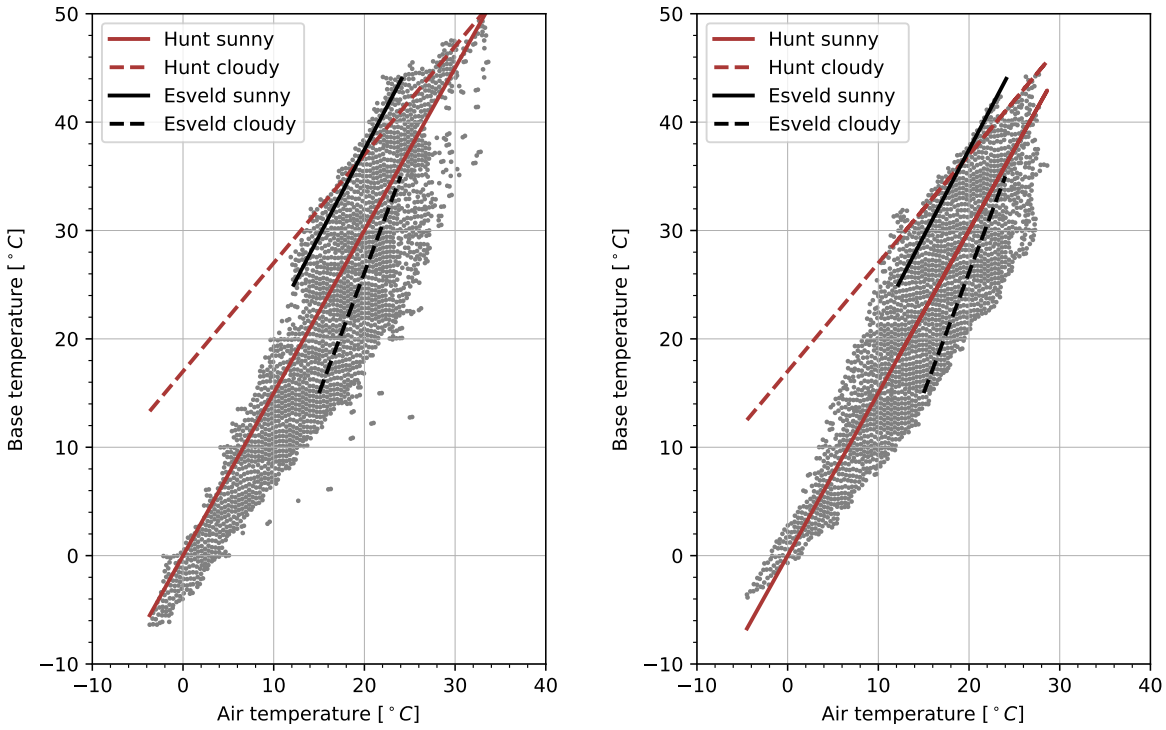

Source: Adapted from [29].

concerning high temperatures. However, figure 2.13 shows that (excepting the bottom side) the correlation is non-linear and a look-up chart would be a more useful empirical approach than linear-equations [29].

- Munro's model

The previous models were developed using data collected in the UK, although experiments were also made in Australia by Munro [34]. The author instrumented six sites around regional Victoria with weather stations and *in situ* stress monitoring product (Rail Stress Modules) from July 2008 to February 2010. Munro then used data from automatic weather stations near the rail sites, as well as the rail temperatures to fit equations 2.3 and 2.4, and correlate rail temperatures and weather variables [4].

$$T_{rail} = a \cdot T_{air} \tag{2.3}$$

$$T_{rail} = a \cdot T_{air} + b \cdot S + c \cdot W_n + d \cdot H \tag{2.4}$$

The values are defined at a given time instant, where:

T_{air} = Air temperature (°C)
T_{rail} = Rail temperature (°C)
S = Solar radiation (MJ m^{-2})
W_n = Wind intensity (km h^{-1})
H = Relative Humidity ($\%$)
a,b,c,d = Experimentally determined coefficients

According to Munro's findings, there is no significant correlation with rail elevation and temperatures, although deep investigation is required by increasing sample size. In addition, rails with N-S orientation showed higher temperatures than E-W ones. The relative humidity has minimal effects on the regression accuracy. Sleeper's material affects the rail temperature. Rails on wood sleepers are 7-15 $\%$ hotter than rails on concrete sleepers. Furthermore, wind effects are highly non-linear. Finally, Munro's model performed with a correlation factor in the range of 0.796 to 0.918 [4].

Despite the great correlations found within the empirical models, they are suitable to provide an idea of track conditions [29]. They highly depend on previous field collected data and are difficult to extrapolate to other locations. Although with new approaches, such as Machine

Learning and Neural Network techniques, this can be further investigated and may return better results.

2.5.2 *Physical Models*

Physical modeling is based on heat conduction, energy balance, material and environmental properties to predict and simulate rail temperatures, it means if all variables are known, it is possible to apply the model, regardless the location. Although to predict rail temperatures, is very important to have accurate weather forecast models in order to output the best performance of predictions. Furthermore, according to Chapman *et al.* [29], this type of model should output better results than statistical ones . In this section, three important models will be explored, developed respectively by: Chapman *et al.* [29], Zhang *et al.* [35] and Hong *et al.* [36]. The latter is the one utilized to perform simulations in this work.

- Chapman's model

An useful approach for physical models is to use existent models used for other applications and make specific modifications and adaptations. Within the transportation subject, road surface temperature models were developed and have been on research for a while. Chapman *et al.* [29] adapted a model developed by Thornes [37], which predicts ice formation on road surfaces. It uses a "0-dimension" energy balance approach, to predict an equilibrium surface temperature by balancing conductive, convective and radiative contribution of heat to a surface [29].

Chapman *et al.* [29] simplified the rail geometry by discounting negligible inclinations and fillets. Furthermore, divided the section into four parts, in which equations are assigned following their boundary condition. The simplified geometry is shown in figure 2.14

In addition, three surface heat equations are assigned (eq. 2.5), respectively, the rail head (H), web surface exposed to the sun (W_{sun}) and for the web surface in shadow (W_{shade}). Where RN is the net radiation flux, H is the sensible heat flux, LE is the latent heat flux and QS the thermal conduction. To calculate these parameters, the author used a mix of empirical and analytical equations described in [37]. The distinction between surfaces is essential, since they will have different properties varying during the day. For example, the web surface will have a reduced sky-view factor of 0.5, changing the radiative emissions of the rail section. In addition, the surfaces are linked to the inside of the rail (TMI_1,TMI_2,TMI_3 and TS) with a conduction

Figure 2.14 – Chapman's simplified rail geometry.

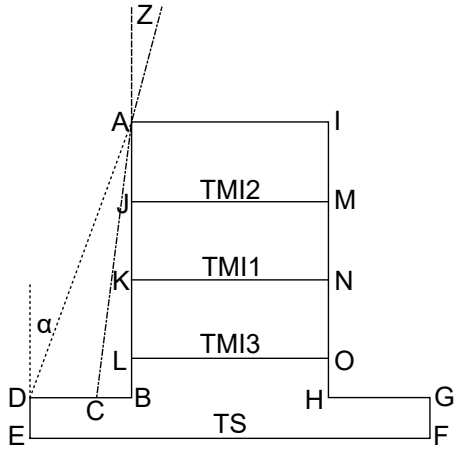

Source: Adapted from [29].

process, satisfied by equation 2.6 [29].

$$\begin{aligned} \pm RN_H \pm H_H \pm LE_H \pm QS_H &= 0 \\ \pm RN_{W_{sun}} \pm H_{W_{sun}} \pm LE_{W_{sun}} \pm QS_{W_{sun}} &= 0 \\ \pm RN_{W_{shade}} \pm H_{W_{shade}} \pm LE_{W_{shade}} \pm QS_{W_{shade}} &= 0 \end{aligned} \tag{2.5}$$

$$\frac{\partial T}{\partial t} = K_s \left(\frac{\partial^2 T}{\partial x^2} + \frac{\partial^2 T}{\partial y^2} \right) \tag{2.6}$$

$$\partial Q = V \cdot C_s \frac{\partial T_s}{\partial t} \tag{2.7}$$

In order to solve the model for the foot temperature, assumptions were needed, firstly, the foot is adiabatic and there is no heat conduction from underneath the base. If the foot surface receives directly sun radiation, its temperature should be equal to the head's surface temperature. Using the equation 2.7, where, ∂Q is the net heat storage, V is volume of the foot, C_f the heat capacity of the material and $\frac{\partial T_f}{\partial t}$ is the change of temperature during time, it is possible to solve for the foot temperature. The model was used to predict rail temperatures up to 24 hours ahead using forecast meteorological input data at hourly intervals.

Before exploring the overall results of Chapman's models, it is convenient to discuss the sensitivity of the model. Tests were conducted with the model utilizing hypothetical data for the longest and shortest day of the year. Relative humidity, wind speed, precipitation, cloud cover and cloud height were kept constant. Meanwhile, rail and air temperatures vary along the day in accordance with real data. Main findings are shown in table 2.7.

Table 2.7 – Chapman's model sensitivity result.

Parameter	**Influence**
Latitude	Is not a dominant parameter in relation to maximum temperatures on the longest day. The greatest impact occurs on the shortest day, decreasing the predicted rail temperature towards higher latitudes.
Rail orientation	Affects the timing of the maximum rail temperature. Slightly higher temperatures occur in the N-W/S-E (similar result to Munro's findings (see section 2.5.1). This is explained by the fact that the time in which the rail at this orientation will receive direct beam radiation will coincide with timing of the maximum air temperatures for the day.
Air temperature	Increasing or decreasing the air temperature, will always cause the rail temperature to go higher or to drop, respectively.
Relative humidity	An increase (decrease) in relative humidity results in a small increase (decrease) in forecasted rail temperatures
Wind speed	The effects of wind are greatest during summer, by decreasing rail temperatures. Lowest temperatures tend to occur at low wind speeds. The wind speed affects the convection coefficient and will affect the rail temperature.
Precipitation	When the rail is wet, there is a significant rail temperature decrease during the day.

Source: Adapted from [29].

The model performance is calculated by running a simulation over 200 days with field collected data, between June 2003 and May 2004, for Winterbourne site. The model achieved overall RMSE of 2.5 °C and an overall bias of 0.2 °C. Regarding maximum temperatures, the RMSE and bias are, respectively, 2.53 °C and −0.36 °C. The mean lag-time (delay in predicting maximum temperatures) of 44 minutes was recorded. Despite geometric simplifications and assumptions, this model predicts maximum and minimum temperatures accurately. However, modeling a more detailed section could improve the accuracy [29].

In conclusion, the model used a "simple" 1-dimensional equation, and proved to be a "practical engineering" solution. However, it can predict specific locations, and since rails are very long structures, a 3-dimensional would be a better modeling approach, but also way more complex. Furthermore, the study used the foot temperature as bulk temperature, although it is not the most representative to be used in buckling studies (see section 2.5), which the author also mentions. Finally, Chapman suggests that a continuous rail and weather monitoring is a recommended solution to mitigate the local effects of rail temperatures, imposing restriction locally, rather than general ones [29].

- Zhang's model

The next model to discuss is described by Zhang *et al.* [35] and Kesler *et al.* [38]. The model

makes use of an energy balance equation (later detailed), material and geometric properties, and the key factor for temperature prediction, a weather forecast service. This service enables the model to predict rail temperatures up to 9 hours ahead with accuracy. The study was conducted in the US. The rail temperatures, differently from Chapman's models, were collected on the web surface. The author also made use of test rail segment, which was instrumented with temperatures sensors and a local weather station, instead of the weather forecast service, to primarily validate the model, before extrapolating to other geographic location [35].

The model is based on equation 2.8, which is a first-order, nonlinear, non homogeneous, ordinary differential equation. This energy balance is affected by weather conditions, material and geometric properties and environmental parameters, for instance, cloud coverage, season, solar position, rail size, shape, orientation and surface conditions. In addition, similarly to previous discussed model, the bottom of the rail is considered adiabatic, meaning that the heat transfer between the sleepers and ballast is ignored [35].

$$\dot{E}_{in} - \left(\dot{E}_{conv} + \dot{E}_{rad}\right) = \dot{E}_{st} = \frac{dE_{st}}{dt} \tag{2.8}$$

$\dot{E}_{in}$ = Rate of energy absorbed by the rail from the sun and atmospheric irradiation;
$\dot{E}_{conv}$ = Rate of energy emitted from the rail by convection;
$\dot{E}_{rad}$ = Rate of energy emitted from the rail by radiation;
$\dot{E}_{st}$ = Rate of energy change.

Applying energy and heat exchange relations to equation 2.8, it can be reformulated to eq. 2.9. Furthermore, an empirical relation between wind speed and convection coefficient is used, as shown in equation 2.10 and has been found to be sufficiently accurate for use with this model, although other relations can be used correlating other available variables [38].

$$SR \cdot \alpha_s A_s - \left[h_{conv} A_c (T_r - T_{air}) + \epsilon \sigma A_r (T_r^4 - T_{sky}^4)\right] = \rho C V \frac{dT_r}{dt} \tag{2.9}$$

$$h_{conv} = \begin{cases} 5.6 + 4 \cdot w_s & ; w_s \leq 5 m s^{-1} \\ 7.2 \cdot (w_s)^{0.78} & ; w_s > 5 m s^{-1} \end{cases} \tag{2.10}$$

SR = Solar radiation ($W\,m^{-2}$);
α_s = Solar absorptivity of rail (-);
A_s = Area of rail surface exposed to the sun (m^2);
h_{conv} = Convection coefficient ($W\,m^{-2}\,K^{-1}$);
A_c = Area of rail subject to convection (m^2);
T_r = Rail temperature (K);
T_{air} = Ambient air temperature (K);
ϵ = Emissivity of rail (-);
σ = Stefan-Boltzmann constant ($W\,m^{-2}\,K^{-4}$);
A_r = Area of the rail subject to radiation heat transfer (m^2);
T_{sky} = Atmospheric sky temperature (K);
ρ = Density of rail material ($kg\,m^{-3}$);
C = Specific heat of rail material ($J\,kg^{-1}\,K^{-1}$);
V = Volume of rail segment (m^3);
w_s = Wind speed ($m\,s^{-1}$).

Many parameters are presented in the model and they can be related to weather conditions, material properties, rail geometry and physical constants. In order to solve for rail temperature is necessary to determine all of them by measuring or by using empirical relation.

Solar radiation, wind speed and ambient temperature are easily acquired by weather stations. However, atmospheric sky temperature there is no simple equation to determine its value, although is known to be in the range from 0 °C to −60 °C bellow ambient temperature. In this model, the value of −20 °C bellow the ambient temperature was used to perform the simulation [38].

The solar absorptivity (α_s) depends on the material and surface conditions of the rail. This value express the amount of incident solar energy that is absorbed by the rail segment, and stays in the range from 0 to 1, meaning full reflection or full absorption. For rail steel it may vary between 0.75 to 0.85 and, while 0.75 being used in this model. The emissivity (ϵ) represents the ability that the material and surface have to emit radiation to the surroundings (ambient). The value for steel is in the range of 0.65 to 0.85 depending also on the surface condition. For this model, 0.75 was utilized [38]. This model does not explicitly account for a reduced view factor on the emitting radiation equation as mentioned in Chapman's model. It can be that the reducing factor is already implicit on the emissivity value.

A_s, A_c, A_r depend on the rail profile geometry and represent the different areas for distinct heat transfer methods. These parameters are the lateral area of the rail segment for a unitary length of rail segment [38]. It is important to mention that the A_s can vary with time due to sun's relative motion. This case will be discussed on the next model.

On the right side of the equation 2.9 are presented variables that depend on material properties: material density (ρ) and specific heat (C). These are well known values for steel (EN 1993-1-2 [39]). Finally the last variable: the rate of change of rail temperature (T_r). It can be solved by separating the equation parts and integrating over time [38].

To validate the model, the author collected weather and rail data in January and July 2006. The results are shown in figures 2.15 and 2.16. The model outputs an adequate result for rail temperatures according to the figures. The author mentions that the algorithm behave very well for sunny days, and underestimate the rail temperature for other. The latter effect appear on January 11 (fig. 2.15). This is possibly caused by simply assumption of wind and convection coefficient (h_{conv}) and the linear extrapolation of sky temperature (T_{sky}), affecting the heat radiation from the rail to the sky [35].

Figure 2.15 – January collected data.

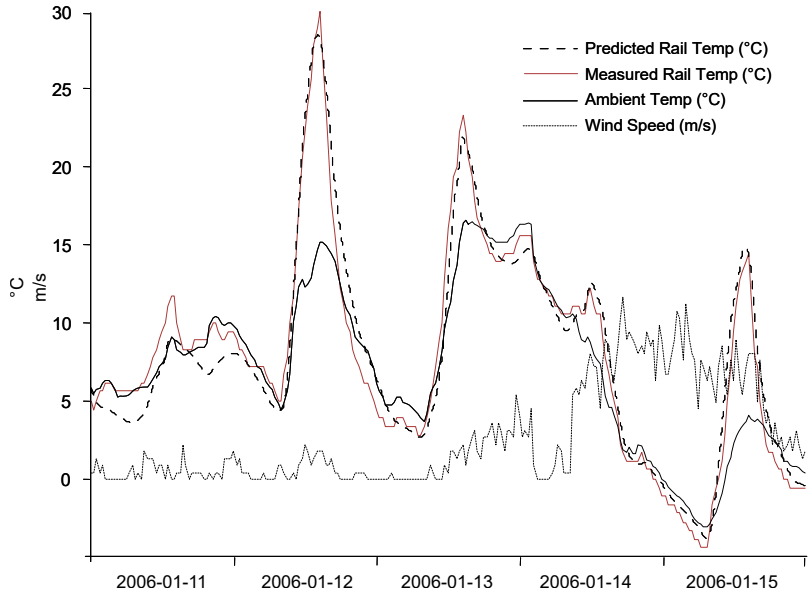

Source: Adapted from [35].

Figure 2.17 shows the correlation of daily predicted and measured peak temperatures for dates between February 1, 2007 to May 31, 2007. The model has a high correlation factor, meaning that it behaves well in predicting the maximum temperatures. The weather data were updated every 30 min using weather prediction system available in the US, for grids of the size 9 x 9 km. The forecast data were uploaded to a server and into a database, in which later a web application provides interface to view rail weather map. Important to mention that the accuracy of rail prediction inherits the error from the forecast service.

In conclusion, the model proved to work well both for local data and also using forecasted data, outputting a better result than linear correlation and empirical models. Furthermore, better assessment of parameters, such as, sky temperature, rail emissivity, and effect of wind are

Figure 2.16 – July collected data.

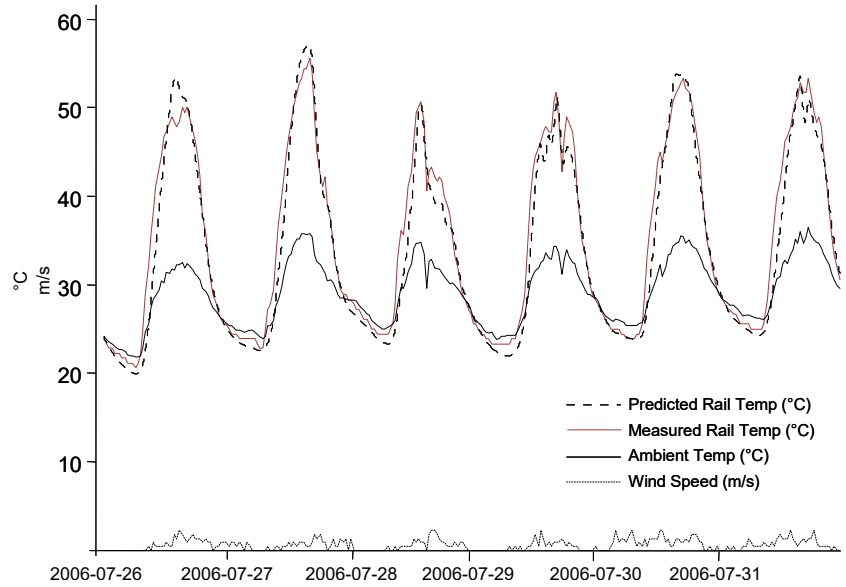

Source: Adapted from [35].

object of deep investigation and can lead to better result [35]. According to Wu *et al.* [4], both Chapman and Zhang developed models that are more accurate than empirical formulations. And since these models are based on physical and weather data, they can be used in any geographical location by adjusting the right parameters.

Figure 2.17 – Daily maximum temperatures correlation.

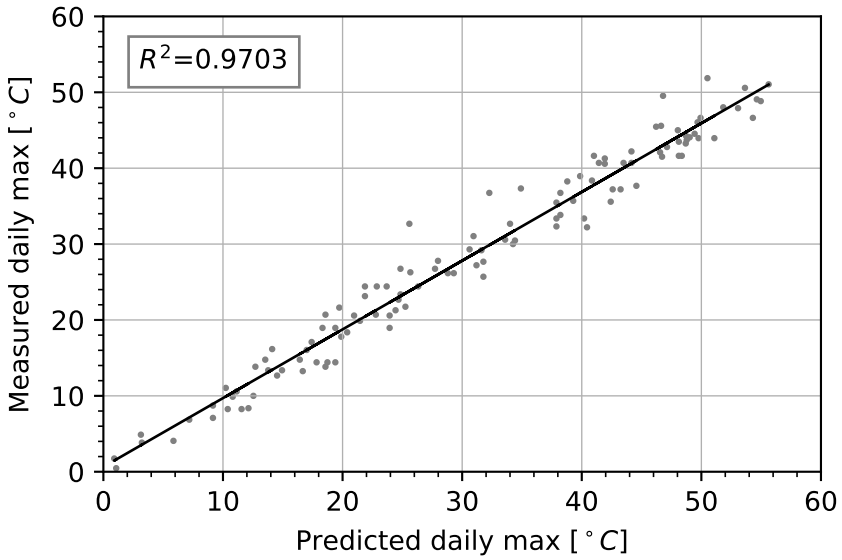

Source: Adapted from [35].

- CNU model

This model was developed by Hong *et al.* [36] on the basis of the work done by Chapman *et*

al. [29]. The improvement they added to the previous model is to consider the sun's position relative to the rail, affecting the area subjected to radiation absorption (A_s). Hence, they proposed a method to calculate this area, that consists in projecting the rail segment onto the ground and calculating the shadow it produces, and finally correlating it with A_s parameter. To determine the sun's position an algorithm called Michalsky's[40] method was used.

The improved method for rail temperatures was validated with field collected data between August 2016 and May 2017. They instrumented a rail segment of 500 mm located at Chungnam National University (CNU), Daejeon, Korea, with 16 K-type thermocouples and a weather station. All the instruments were set to collect data every 10 minutes. The model performed well, reaching 0.93 correlation and 3.80 °C of RMSE.

The method consists in a procedure to evaluate the area that effectively absorbs the incoming sun's radiation. In order to calculate, it assumes a relation between the shadow of the rail (S_{shadow}) onto the ground and the sun area (S_{sun}). And to calculate the shadow, it uses sun's position to create a direction vector, that is used to create a line and project it onto the ground. Further, with all the rail vertex on the ground, it is possible to extract the area of the shadow and convert it to the equivalent area of incident solar radiation. Once the area value is established, the heat equation is the one developed by Zhang *et al.*

Michalsky's method to find the sun's position depends on latitude, longitude and time and outputs the solar azimuth (ϕ_{sun}) and solar elevation (α_{sun}) as shown in figure 2.18a. The algorithm works well for dates between 1950 and 2050. The details of calculating the orientation of the sun will not be discussed. In fact any tool can be used, since the results are in accordance with the axes convention like shown in the figure. In addition, for this current work, another method to determine the sun's position was used, with help of Python libraries, that will be discussed in chapter 3.

Once the azimuth and the elevation of the sun are evaluated, is necessary to correlate the shadow it casts onto the ground and the area exposed to the sun. Figure 2.18b exemplify the procedure to accomplish the correlation. To determine the shadow, a simplified rail section is used (fig. 2.19a), define by points $A1$,$A2$,...,An, with their equivalent offset $B1$,$B2$,...,Bn. In this case, 14 points were used in each face. Each point is then projected onto the ground and the shadow area can be evaluated.

To derive the equations to project the rail points to a plane, a simple cube is used (fig. 2.19b), this can be later generalized to any geometry. First, defining the vector from the origin O with

Figure 2.18 – Sun position and areas relation.

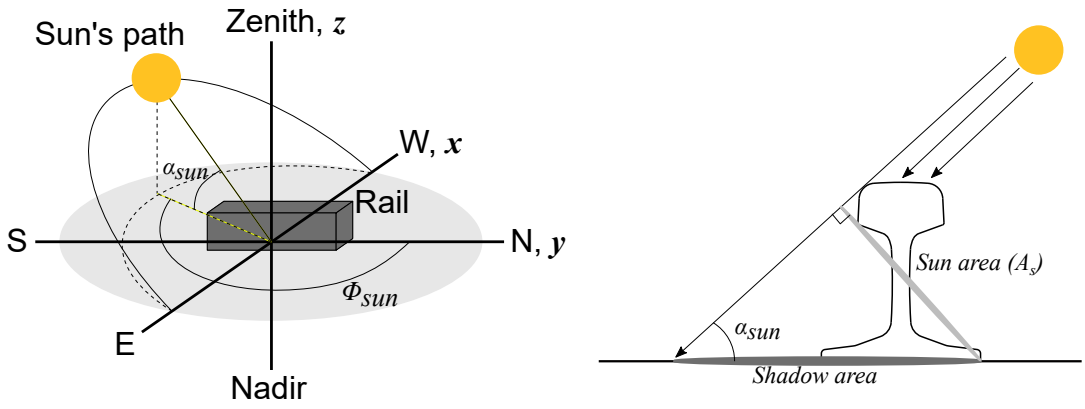

(a) Sun's position

(b) Shadow and sun areas

Source: Adapted from [36].

Figure 2.19 – Hong simplifications.

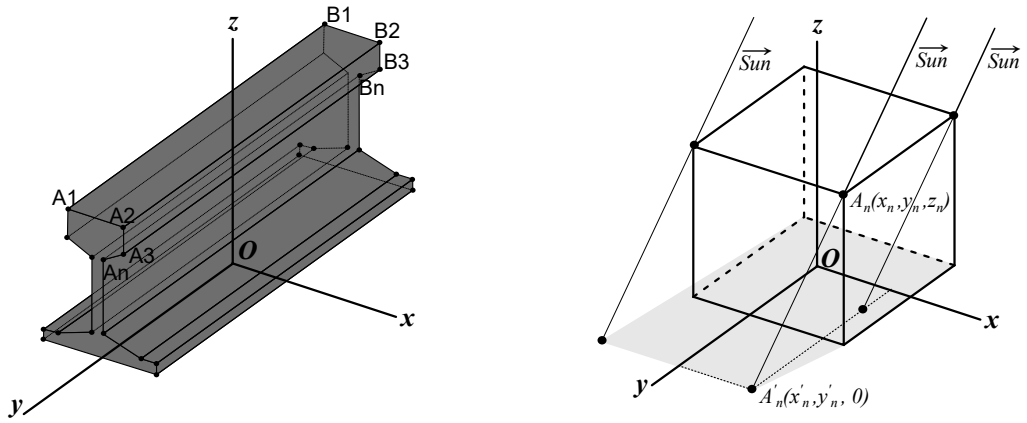

(a) Simplified rail profile

(b) Simplified case

Source: Adapted from [36].

direction to sun, it can be described with equation 2.11.

$$\overrightarrow{Sun} = (X,Y,Z) = (L_{sun}\cos\alpha_{sun}\sin\phi_{sun}, L_{sun}\cos\alpha_{sun}\cos\phi_{sun}, L_{sun}\sin\alpha_{sun}) \tag{2.11}$$

Given a point and a vector is possible to define a line. Using symmetric representation of this line, the equation 2.12 is achieved, where a, b and c are respectively X, Y and Z components of equation 2.11.

$$\frac{x - x_0}{a} = \frac{y - y_0}{b} = \frac{z - z_0}{c} \tag{2.12}$$

Let $A_n(x_n,y_n,z_n)$ be the set of points that represents the shape and $A'_n(x'_n,y'_n,0)$ the set of points projected on the ground. Making the following assumptions and managing equation 2.11 into 2.12.

$$\begin{aligned} L_{sun} &= 1 \\ (a,b,c) &= \overrightarrow{Sun} \\ A_n(x_n,y_n,z_n) &= (x_0,y_0,z_0) \\ A'_n(x'_n,y'_n,0) &= (x,y,z) \end{aligned}$$

The equation 2.13 can be derived and applied to all points, the results are (x,y) pairs of points projected onto the ground that represent the shadow of the geometric shape.

$$\begin{aligned} x'_n &= -\frac{\sin\phi_{sun}}{\tan\alpha_{sun}} z_n + x_n \\ y'_n &= -\frac{\cos\phi_{sun}}{\tan\alpha_{sun}} z_n + y_n \end{aligned} \tag{2.13}$$

In order to calculate the area, the authors used equation 2.14. Important to mention the fact that this equation requires the points to be ordered in a manner that they make a polygon with no crossing edges, otherwise the calculation will not return a valid value of area. In fact this can lead to errors when automating the procedure, since the algorithm should be aware of it.

$$S_{shadow} = \frac{1}{2}\sum_{i=1}^{n}(x_i + x_{i+1})(y_i - y_{i+1}) \tag{2.14}$$

Once the shadow area is obtained, to find the area that received direct sun's radiation, as shown in figure 2.18b, equation 2.15 expresses the relation.

$$A_s = S_{sun} = S_{shadow}\sin\alpha_{sun} \tag{2.15}$$

With all these steps, the solution can proceed to the energy balance equation (eq. 2.9). Important to mention, the value of S_{sun} is inputted on the parameter A_s on the latter equation. In addition the equation 2.10 was also used to correlate the convection coefficients (h_{conv}) and wind speed (w_s). Since the shadow area (S_{shadow}) changes for each time step, the solution needs to be iterative. The authors developed a LabVIEW program to automate the entire process. For a given file containing weather information and specifying the rail location, the program outputs a simulated rail temperature. To solve the energy balance equation, they used a MATLAB ordinary differential equation solver named ODE45.

By using the equation 2.9, some parameters are difficult to determine, such as emissivity (ϵ), sky temperature (T_{sky}) and solar absorptivity of the rail (α_s). The latter is the only parameter the author mention its value, since they have performed a laboratory test to assess the property. Two rail specimens (unused and used rail) were submitted to a reflectance test. The results are, respectively, 1.6 $\%$ and 18.9 $\%$. With these results, considering that there is no energy transmission through the material, the absorptivity is evaluated with $1 - reflectance$. The results for the used rail specimen were utilized to run simulations. Regarding the other two parameters, it is likely that they fall into the range values proposed by Zhang *et al.*

The results achieved are shown in table 2.8 and in figure 2.20. It was analyzed over 200 days of data, in total 35 300 data points. Hunt1 and Hunt2 were evaluated using equations 2.1 and 2.2. CNU1 was calculated using a fixed A_s value of 0.1 m^2. This value is the average solar incident area. CNU2 is calculated considering the proposed method, varying the solar incident area (A_s).

Table 2.8 – Hong *et al.* statistical results.

Model	**R^2**	**RMSE**	**Independent variable**
Hunt1	0.90	5.87 °C	Air temperature
Hunt2	0.90	15.11 °C	Air temperature
CNU1	0.93	4.21 °C	Air temperature, solar radiation and wind speed
CNU2	0.93	3.80 °C	Air temperature, solar radiation, wind speed, sun's azimuth and elevation

Source: Adapted from [36].

In summary, Hong *et al.* [36] have proposed a novel model to simulate rail temperatures under weather conditions. This was achieved by improving a previous model in a specific parameter: A_s. As recommendation, the author proposes that the method should be evaluated at other location in order to validate it. In fact, this model is utilized to perform simulations on the present work.

Figure 2.20 – Hong *et al.* simulations - September 2016.

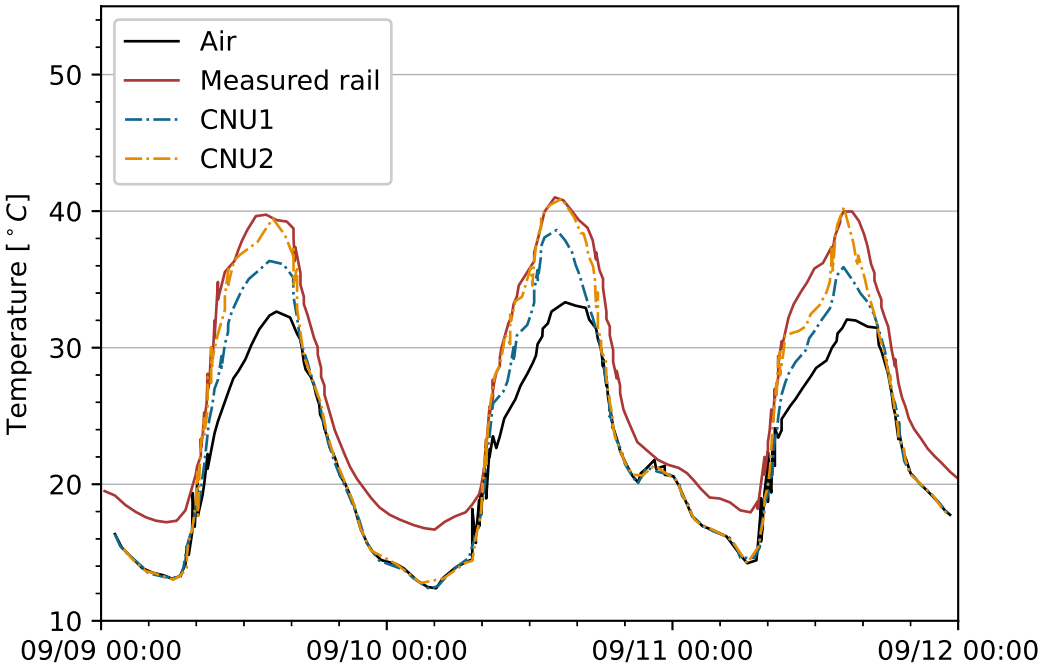

Source: Adapted from [36].

2.6 Rail Buckling

Buckling is the sudden change in deformed shape mode of a structure due to loading. It highly depends on the boundary conditions of the structure, level of imperfection and the action of its load. Railways are subject to thermal and mechanical loads in which, given the right circumstances, buckling may take places. Continuous welded rail (CWR) are more prone to this effect than jointed rails, since the longitudinal movement is restricted, and in presence of load, thermal deformation is not possible and it is converted to internal stresses. When the limit is reached, the actual shape is no longer stable and the rail releases energy by sudden and high lateral movement, until it reaches a new deformed shape (fig. 2.21).

This process can occur by the effect of thermal loads only, when the temperature increase gives enough energy to start the displacement, hence this is called thermal buckling or static buckling. However, the combination of temperature increase and mechanical load of moving trains can also lead to failure and at lower temperatures than static buckling, since the train load also contributes with compressive forces on the rail. This is then called dynamic buckling. Dynamic buckling is found to be more prevalent than static. Investigation shows that this is due to the uplift tendency of the track between the cars' trucks, lowering the lateral resistance creating the possible scenario for buckling to start [41].

Figure 2.21 – Lateral buckling examples.

(a) (b)

Source: Adapted from [41].

This problem raises great concern on the rail industry, since buckling can cause train derailments and accidents. Between 1993 and 2003 the annual average of train derailments in the US caused by track buckling was 34. These issues causes huge costs to the operators, and in 2002 the cost reached a peak value of 17 million USD [41]. Meanwhile, the UK reported 445 buckling occurrences between 2000 and 2009, 6 of them resulting in derailments [42].

According to Carvalho [42], since new connections for high speed trains between Portugal and Spain are in progress, understating and assuring the stability of tracks is essential to avoid accidents. Therefore, is necessary to give engineers the tools to maximize the safe operations of railways.

A variety of parameters have influence on buckling phenomenon, including track geometric characteristic (tangent and/or curved), material properties (rail's steel and ballast) and also environmental (temperature). Some of them are more important than others and small changes cause great effects. According to Kish *et al.* [41] and Van [3], the most important parameters of rail buckling are:

- Sleeper(tie)-ballast lateral resistance;
- Rail fastener longitudinal and torsional resistance;
- CWR neutral temperature;
- Track misalignment;
- Track curvature.

The typical response of the track structure can be described in terms of three temperature

values: neutral, buckling and safe temperatures. The neutral temperature is the one at which the track is free of thermal stress, presumably the temperature at which the track was laid. The buckling temperature is the temperature at which buckling will occur. The safe is a threshold that above this point buckling may occur, given the necessary amount of energy. Bellow that buckling can not happen. These concepts are shown in figure 2.22 [3], [43].

Figure 2.22 – Typical track response curve.

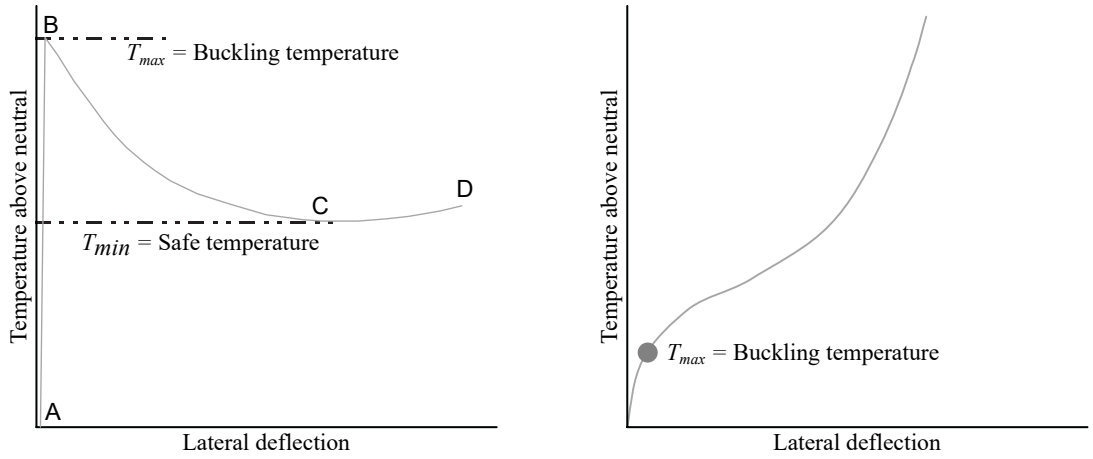

(a) Explosive buckling. (b) Progressive buckling.

Source: Adapted from [41], [43].

Figure 2.22a also shows that the buckling response can be divided in three branches: AB, BC and CD. Parts AB and CD represents the stables configurations before and after buckling, meanwhile BC contains the unstable configuration where the track's shape changes quickly until it reaches the post buckling deformed shape mode [43].

Kish *et al.* [41] states that the quality of the track has great effect on the buckling response. High quality tracks have buckling responses with well defined T_{max} and T_{min}, as shown in figure 2.22a and is called explosive buckling, with sudden snap trough. Meanwhile, low quality tracks show no difference between T_{max} and T_{min} and can be represented as a single value. Such tracks have no snap through and buckling occurs progressively, as shown in figure 2.22b.

Many models have been developed to study this process, some of them using analytical solutions and finite element analysis (FEA). The solutions can also be divided into two different approaches: beam models, in which a single equivalent beam is used to derive solutions, and rail-tie models, which treats the interaction of ties and rails separately [42], [43].

A Notable analytical model was developed by Kish *et al.* [41] using a beam approach. Furthermore, from these studies, a software was developed to help rail operators to assess the buckling probability and manage the risks, the software is called CRW-safe. These studies were

sponsored by the Federal Railroad Administration (FRA).

Van [3] utilized also a analytical approach similar to the latter model to conduct a sensitivity analysis and also to develop a computer program to manage the buckling risks. This work was supported by the European Railway Research Institute.

Lim *et al.* [43] developed their own finite element model in order to overcome the limitations of previous models and obtain the full track response (pre and post buckling). The authors modeled a 3D FEM to analyze both vertical and lateral buckling, considering geometric non-linearities. They have concluded that three dimensional models better express the buckling problem while two dimensional ones overestimate the track stability.

2.6.1 *Buckling Parameters*

The governing parameters of track buckling can be modeled as shown in figure 2.23. The rails are connected through torsional springs to the sleepers. The sleepers have their lateral and longitudinal displacements restricted by linear springs, which represent the ballast action on them. In case of dynamic buckling, a spring modeling the vertical action of the ballast must be included.

Figure 2.23 – Track model.

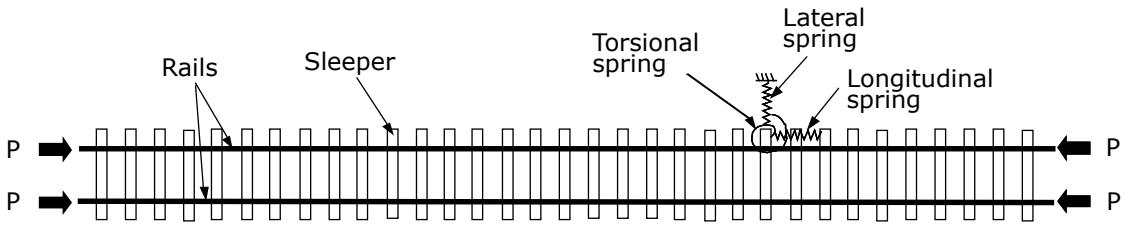

Source: Adapted from [41].

The force P is due to temperature changes and can be calculated using equation 2.16. In which A is the rail profile area, E Young's modulus, α thermal elongation coefficient, T current rail temperature and T_0 neutral rail temperature, also known as stress free temperature.

$$P = AE\alpha(T - T_0) \tag{2.16}$$

- Fastenings

Fasteners resist the rotation and longitudinal slip of the rail relative to the sleeper. It highly depends on the fastener type and sleeper material. Experiments have shown a linear behaviour

Table 2.9 – Fastenings torsional resistance.

Sleeper	Type	kN m rad^{-1}	Std
Wood	**Pandrol**	568	221
	8 spikes	245	67
	4 spikes	135	43
	2 spikes	43	16
Concrete	**Pandrol**	32	18
	McKay	39	9

Source: Adapated from [44].

regarding the torsional constant. In such tests, the rail is clamped by fasteners on a fixed sleeper and loaded by torsional moment. Figure 2.24 shows the results of such tests and the model simplification. Table 2.9 presents the torsional resistance of different fastenings methods and sleeper material, along with the standard variation of the measurements. This study is presented in Samavedam *et al.* [44].

Figure 2.24 – Fastener linear model.

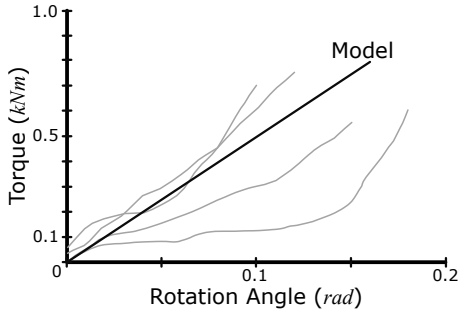

Source: Adapted from [3].

- Sleeper-ballast resistance

The ballast resistance act against the displacement of sleepers both in the longitudinal and lateral directions. The behaviour can be measured by pulling or pushing a single sleeper also known as single tie push test (STPT) in the longitudinal or lateral direction [3]. Typical results of these tests are shown in figure 2.25.

Figure 2.25a shows that the consolidation process due to passing trains increase the resistance. Furthermore the longitudinal ballast resistance is modeled as a bi-linear model [3]. This is then modeled as a non-linear springs as shown in figure 2.23.

The consolidation process also increases the resistance in the lateral direction, reaching a peak value and right exhibits a distinct drop, whereas the freshly tamped track continues at the peak limit [3], [41]. This behaviour is shown in figure 2.25b. The peak resistance value is

Figure 2.25 – Sleeper-ballast behaviour.

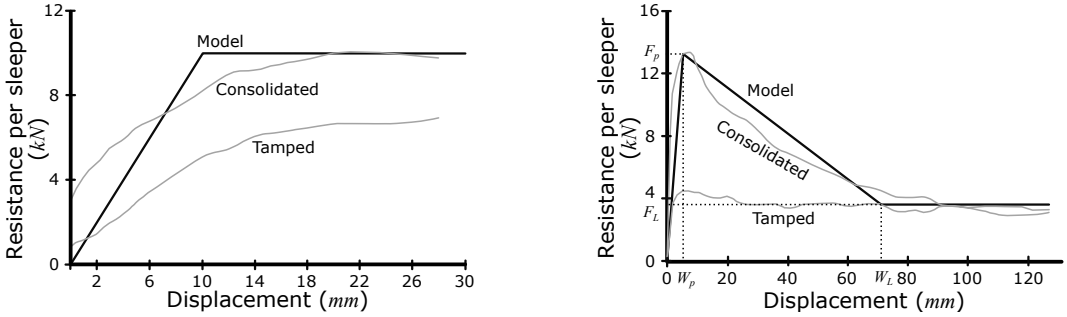

(a) Typical longitudinal resistance.

(b) Typical lateral resistance.

Source: Adapted from [3].

denominated F_p along with its deformation W_p, meanwhile the limiting values are denominated F_L and W_L [41].

Furthermore, the lateral resistance is a combination of the resistance of the sleeper side, bottom and end, each contributing for approximately 33 % of total resistance [3]. A recent study has shown that for loose tamped conditions the contributions are 50 %, 25 % and 25 %, respectively [45]. These forces appear due to the contact interaction between the sleeper and the ballast material.

According to Van [3], lateral ballast resistance correlate linearly with T_{max} and T_{min}. By increasing the resistance, the temperatures thresholds also increase. However the longitudinal resistance has little influence on the temperatures.

When studying dynamic buckling, is necessary to apply factors to account for increased and reduced friction between ballast and sleeper. This is due to the fact that when vertical loads are applied, sleepers move vertically in the ballast. The simple way to model this are vertical linear-elastic springs, known as a Winkler foundation [3]. This effect is shown on figure 2.26.

Figure 2.26 – Winkler foundation.

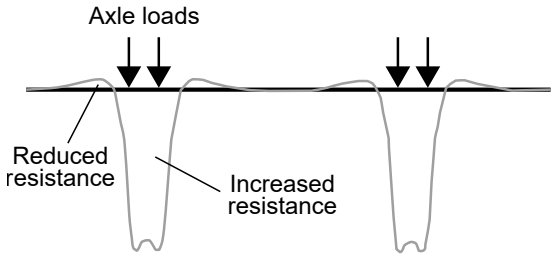

Source: Adapted from [3]

- Track misalignment

According to Van [3], the amplitude of track's misalignment has significant influence on the buckling temperature (T_{max}), while the safe temperature (T_{min}) is less affected.

Many factors cause the track's imperfection to increase, such as, initial imperfections during construction, localized poor ballast conditions, movement of trains, elevated thermal loads, excessive vertical loads from the rolling stock. Theses parameters should be monitored and due to safety concerns, maximum values for track misalignment were established [42].

- δ_0 - In the range of 1 mm to 4 mm after construction and maintenance operations;
- δ_m - Maximum allowed values before maintenance work, in the range of 4 mm to 8 mm;
- δ_c - Critical misalignment, in which maintenance must be done. The operation's safety is jeopardized.

In order to model the track's misalignment to be used in buckling simulations, a wave function is required. It is common to use a sinusoidal shape, which takes two parameters: amplitude and wave length. The modeled imperfection is shown in figure 2.27. Van [3] conducted analysis utilizing values for amplitude in the range of 8 mm to 50 mm. Lim *et al.* [43] performed simulations utilizing a constant value of 40.64 mm.

Figure 2.27 – Track misalignment.

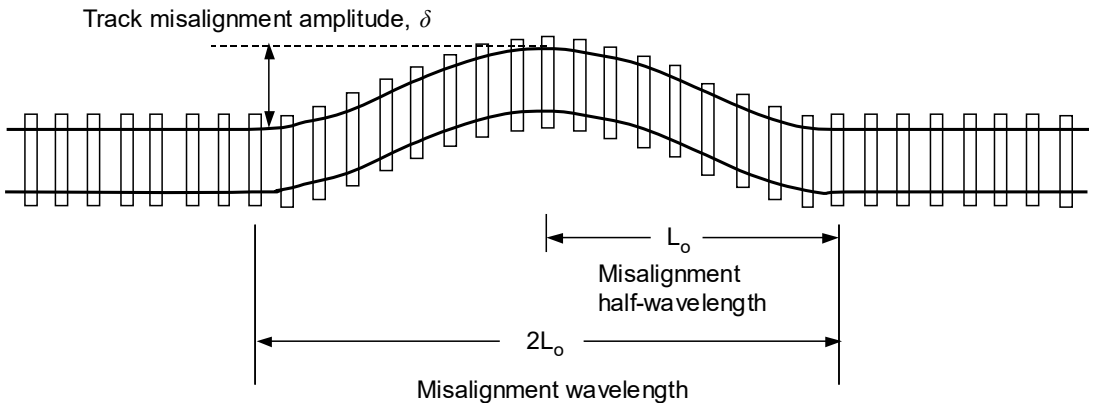

Source: Adapted from [41].

2.6.2 *Stress Free Temperatures*

The stress free temperature (SFT) is the value in which there are no thermal stresses on the rail. This value is set when the rail is welded during construction and plays an important role on CWR's buckling. According to [42], in Europe common values used for dimensioning of railways, are in the range of 23 °C to 27 °C, however, for extreme weather conditions, values in the range of 5 °C to 35 °C have been used.

Bonnett [1] states that ideally the stress free temperature of CWR's must fall exactly halfway between the hottest and coldest likely rail temperature. Rail temperatures are discussed in section 2.5.

2.6.3 *Finite Element Model*

As mentioned, the buckling problem on CWR can be solved utilizing the finite element analysis, by modeling simplified to complex 3-D models. It is very helpful when studying complex boundary conditions and non-linearities. Since the rail tracks have a complex interaction between different material, the FEA is suitable to determine the buckling response of the track.

Ansys is a software that helps with modeling and solving finite element models and provides various tools to deal with non linear problems. Carvalho [42] utilized the software to perform buckling analysis. In the other hand, to achieve better control of parameters a specialized software for rail buckling can also be developed, for instance Lim *et al.* [43] developed their own finite element model.

Figure 2.28 shows the cross section and the elements utilized by Lim *et al.* [43] to model the railway track. The rail element is assumed to have greater length than any other cross-section dimensions, the cross sections retain their original shape, it follows the Euler-Bernouli hypothesis and the shear strains along the middle surface of the thin-walled cross-section are not considered.

The sleeper element is modeled as a solid beam on an elastic foundation (Winkler foundation hypothesis), has an elastic behaviour and also follows the Euler-Bernouli hypothesis. The fastener is a 3-D spring element with 6 degrees of freedom, respectively to 3 translation and 3 rotation, which is placed between the sleeper and rail nodes. The ballast lateral and longitudinal are modeled with non-linear springs with a bi-linear plastic behaviour, as shown in figure 2.29. The authors modeled a rail with 199.92 m with 40.64 mm imperfection over the central 11.22 m of the track. They compared the results with previous model and field tests. The procedure proposed by the authors can determine the full buckling response (pre and post buckling) with well defined temperatures (T_{max} and T_{min}). The conclusion of this work is that three dimensional models better express the buckling problem while the 2-D overestimate the track stability, as mentioned before.

Carvalho [42] has utilized the software Ansys to solve rail buckling problems. The author utilized the same parameters as Lim *et al.* in order to compare the results, however by the time, the available solvers on the software could not solve the full buckling response.

Figure 2.28 – Lim *et al.* cross section model.

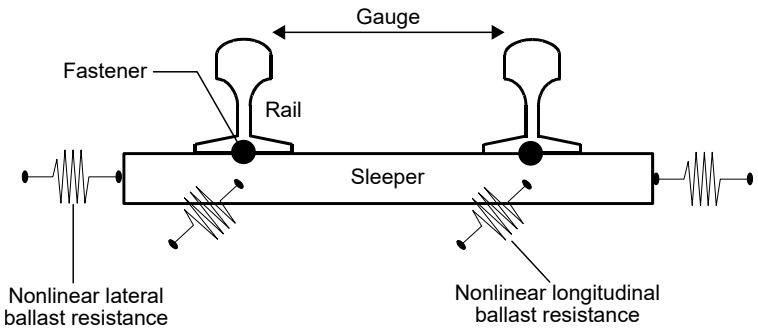

Source: Adapted from [43].

Figure 2.29 – Ballast lateral and longitudinal behaviour utilized by Lim *et al.*

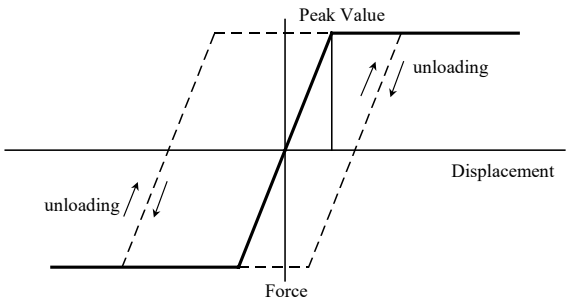

Source: Adapted from [43].

The software provides two methods to solve iterative solutions: Newton-Raphson and arc-length. For non-linear problems, a nonlinear stabilization can be set to help the convergence of the model, however, it is not possible to have negative increment of loads. On the other hand, the arc-length method overcomes this issue and can be used to solve snap-through problems, similar to figure 2.22a. However, the author simulated models utilizing thermal loads on fixed beams with arc-length solver and the software could not converge to a solution. It is likely that the arc-length method is not optimized to handle thermal loads [42].

Thus, when simulating rail thermal buckling with the software Ansys, depending on the track quality (explosive or progressive buckling), the safe temperature (T_{min}) can not be directly evaluated. Hence, Carvalho [42] proposed an indirect method do determine the full buckling response with a hybrid approach utilizing analytical and finite element models.

3 METHODOLOGY

Based on the previous discussions, is clear that buckling on railways is a great concern and it depends on many parameters. Rail temperatures are very important when it comes to design CWR's tracks, since the stress free temperature has to be carefully selected to assure the range of safe operation. Furthermore when studying rail buckling, the temperatures are thresholds to the phenomenon, as discussed in section 2.6.

The present methodology is divided in three main parts: field data collection, rail temperature simulations and rail thermal buckling simulations. Firstly, a weather station and a data logger were installed in a railway located in the city of Mirandela - Portugal to later be used to perform simulations. Secondly, a modified version of the CNU model is used to simulate rail temperatures and validated with experimental data and finite element model. Furthermore, the model is used to extend the simulation to other locations in Portugal utilizing weather information provided by the Portuguese Institute for Sea and Atmosphere (IPMA) for over the past 4 years. Lastly, the effects of these temperatures are discussed by simulating thermal buckling also using finite element models.

3.1 Experimental Data Acquisition

The data acquisition took place in the city of Mirandela, where a weather station and a logger were installed in order to collect the following parameters: solar radiation, wind speed, ambient temperature and rail temperature. The logging started on 27/07/2020 and finished on 15/02/2021, approximately 200 days of recorded data. In order to avoid loss of information, the download of data took place monthly.

Ideally, in order to perform analysis with the physical models described in section 2.5.2, the weather information should be collected as close as possible from the rail. However, due to technical reasons, the weather station had to be mounted 500 m away from the rail's instrumentation site. The positioning of the weather station, rail instrumentation, as well as the city's location are shown in figure 3.1.

Figure 3.1 – Map of instrumentation places.

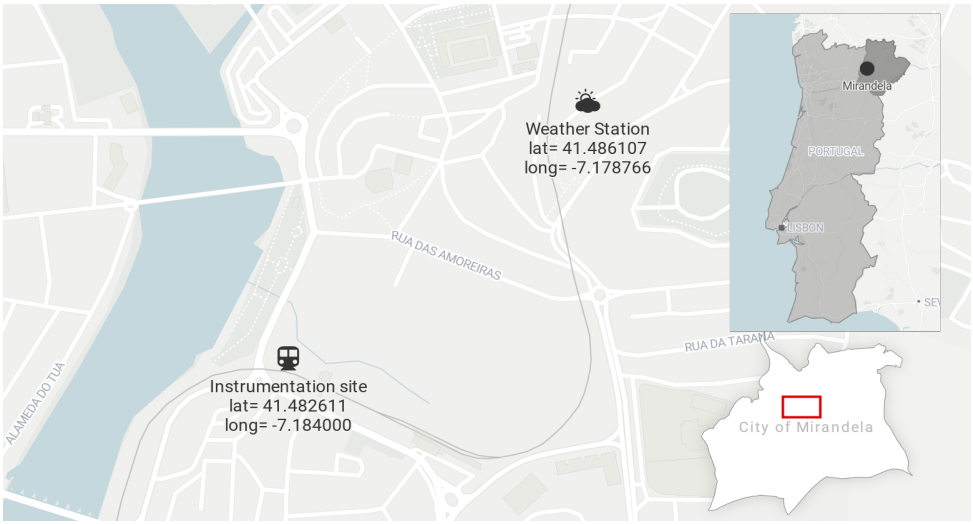

Source: Adapted from openstreetap [17].

3.1.1 *Track Instrumentation*

The monitored rail track is placed in the city center and is part of the Tua line, which connects the city of Mirandela and village of Brunheda. The line is deactivated since 2008 but is currently under renovation, fact that helped with the sensor's installation. The track is made of UIC54 profiles and utilizes metric gauge. In addition, it is constructed by jointed tracks, as described in section 2.4.6. The sleepers are made of wood and have 60 cm spacing.

To measure the temperature of the rail, a set of two K-Type thermocouples were properly welded on the rail's surface, in order to achieve a good joint between sensors and rail. Beyond that, a thermal putty paste was added to protect the joint from external deterioration. The probes were installed at the bottom and middle of rail's web, following the recommendation shown in figure 2.11. Due to technical aspects, only the north facing side of the rail could be monitored. A data logger DataTaker® model DT50 was installed in an electric control panel of the line, which enabled access to grid power, furthermore the logging interval was set to 5 minutes. The device and the sensors are shown in figures 3.2 and 3.3.

3.1.2 *Weather Station*

A weather station was installed on the roof of a building near the track's instrumentation site, as shown in figure 3.1. This building was chosen because of its proximity to the site and easy access to the roof. The weather station collects three parameters: wind speed (w_s), air temperature (T_{air}) and global solar irradiance (SR). The sensors utilized on the weather station

Figure 3.2 – Instrumentation site.

Figure 3.3 – Installed thermocouples.

are described in table 3.1 and in figure 3.4.

Similarly to track's instrumentation, a data logger DataTaker® D500 was used to collect and store the weather data. The interval of measurement was set to 5 minutes. The wind speed stored measurement is the average over 5 minutes and the other two parameters are measured once every logging interval cycle.

Table 3.1 – Weather station sensors.

Parameter	Sensor	Model	Output
Wind Speed	Anemometer	THIES BLET REF : 4.3515.30.000	$m\,s^{-1}$
Air Temperature	Thermocouple K-Type	T351-TR Vector Instruments	°C
Solar Irradiance	Silicon Pyranometer	SP Lite Kipp & Zonen	$W\,m^{-2}$

Figure 3.4 – Weather station sensors.

(a) Anemometer

(b) Air Temperature

(c) Pyramometer

Source: Adapted from internet.

3.1.3 *Logging Rail Temperatures - Additional Approach*

Programmable microcontrollers are getting easier to use and more accessible along with development boards like Arduino, Raspberry Pi and similar. In addition, the world is currently experiencing the easy access to Internet and, furthermore, simple everyday objects can now be connected whether to be controlled or to report status. This is known as Internet of Things (IoT).

Redundantly and simultaneously with the system described above, in order to read, store and display rail temperatures in real time over the internet, a data logger was developed using a development board based on ESP-32 microcontroller, named TTGO T-call. The prototype was designed to read K-type thermocouples and it was validated with experimental data collected with the data logger mentioned in 3.1.1. This section discusses the details of the prototype.

Figure 3.5 shows the basic diagram of the system. The microcontroller reads a thermocouple attached to the rail, then it connects to the mobile network through cellular network to Losant's API. A secure connection is established and a payload message is sent containing the values read by the sensor. Once the payload is successfully received on the platform, it can be used to render the information on dashboards (fig. 3.7) and also be manipulated and passed to external databases. Here the received data has been stored in a mongoDB instance.

In order to read temperature with thermocouples, is necessary to read voltage differences between the thermocouple wires. The working range of temperature in case is between $-20\,°C$ to $100\,°C$, therefore the voltage vary from $-0.78\,mV$ to $4\,mV$. To read accurately this range

Figure 3.5 – System Workflow.

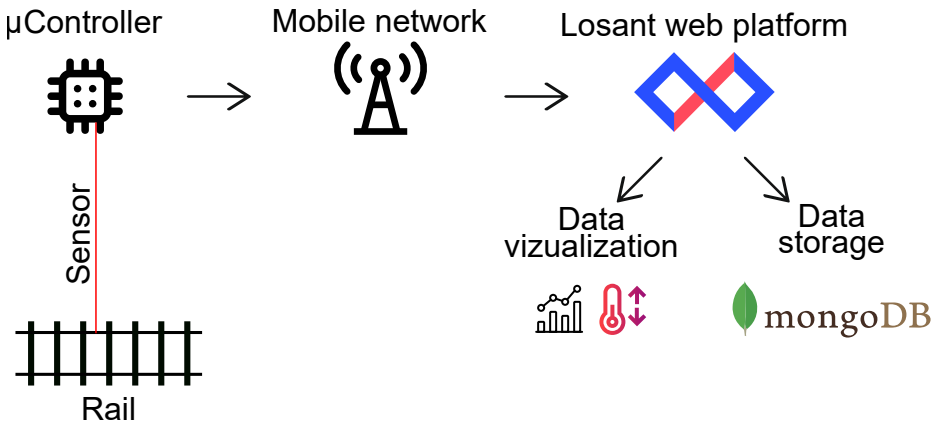

the ADS115 component was used, which is an analog to digital converter, with 16 bits of resolution. Furthermore, a different thermometer (DS18B20) was used to monitor the internal temperature of the device, which was used to compensate the thermocouple readings to achieve precise values of rail temperature. The system architecture is shown in figure 3.6a.

Figure 3.6b shows the programmed routine in the microcontroller. The program starts by reading V_m values and averaging over 10 samples. Then a value of internal temperature (cold junction temperature) T_{cj} is acquired and then these values are processed by a function (eq. A.3) that computes the actual value of the thermocouple temperature, making a cold junction compensation. Calibration and validation procedures are described in Appendix A. After these steps, the values are packed in a payload and sent to Losant's platform. Finally the microcontroller enter deep sleep mode for 5 minutes and start the routine once again.

Figure 3.6 – System overview.

(a) Architecture

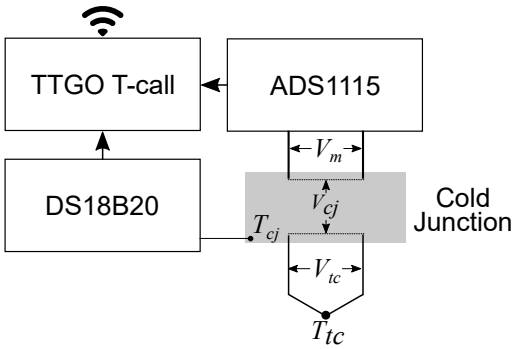

(b) Routine

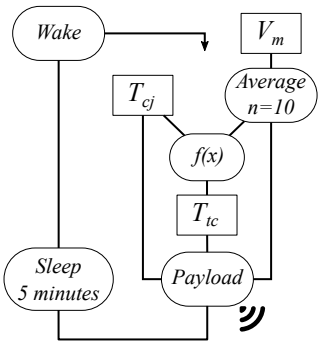

Even though this approach was not used as a main data source of this study, it shows a feasible way to monitor in real time the temperature of structures, in this case, a railway. However is necessary to take into account that this was possible because mobile network

Figure 3.7 – Losant dashboard.

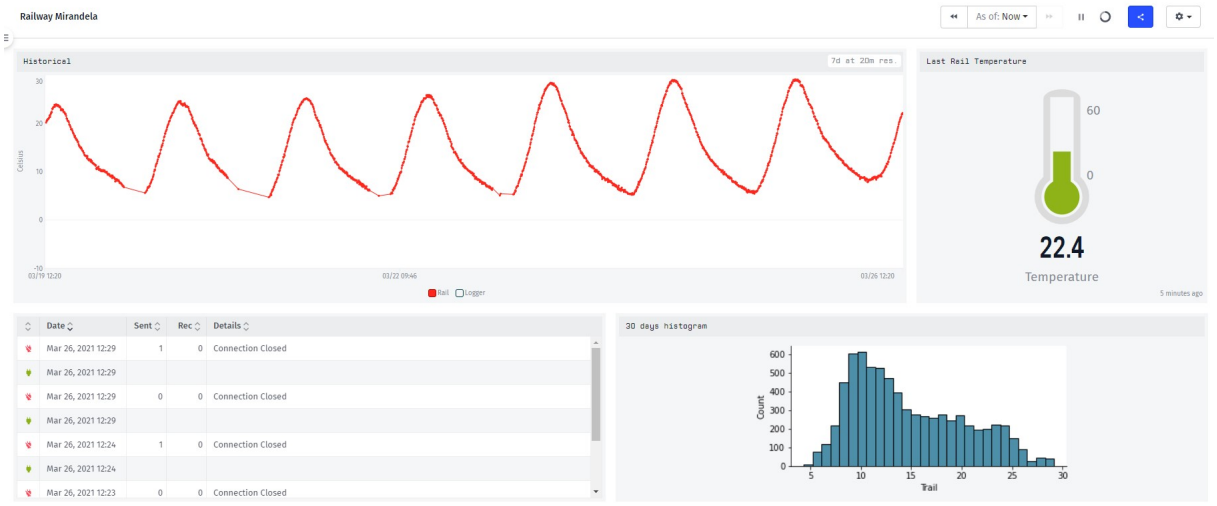

coverage is consistent and the power source constant, making no need of batteries, hence, power consumption was not optimized, although it has capabilities to do so. Furthermore, it is highly scalable and the association of any devices could build a system of real time rail temperature report and help the operation and management of the infrastructure.

3.2 Material Properties

This section describes all the material properties utilized in order to run thermal and mechanical simulations. The materials account for rail's steel properties and sleeper's wood properties.

3.2.1 *Rail's Steel Properties*

The R260 steel was utilized to perform analysis on this work. The stress-strain behaviour at room temperature is described by Maximov *et al.* [46] after experimental testing. The experimental data were fit into the Ramberg-Osgood model (equation 3.1) and the coefficients (a and n) were determined and presented a good approximation for the steel's behaviour.

$$\epsilon = \frac{\sigma}{E} + a\frac{\sigma_0}{E}\left(\frac{\sigma}{\sigma_0}\right)^n \tag{3.1}$$

By utilizing this model, one can describe a material behaviour by specifying only two parameters: Young's modulus (E) and yield stress (σ_0). So, in order to obtain the behaviour at higher temperatures, the reductions coefficients described by EN 1993-1-2 in table 3.1 were applied

Table 3.2 – Young modulus for R260 steel.

E (GPa)			
Experimental	**20 °C**	**100 °C**	**250 °C**
206	201	201	172

Figure 3.8 – Mechanical behaviour of R260 steel.

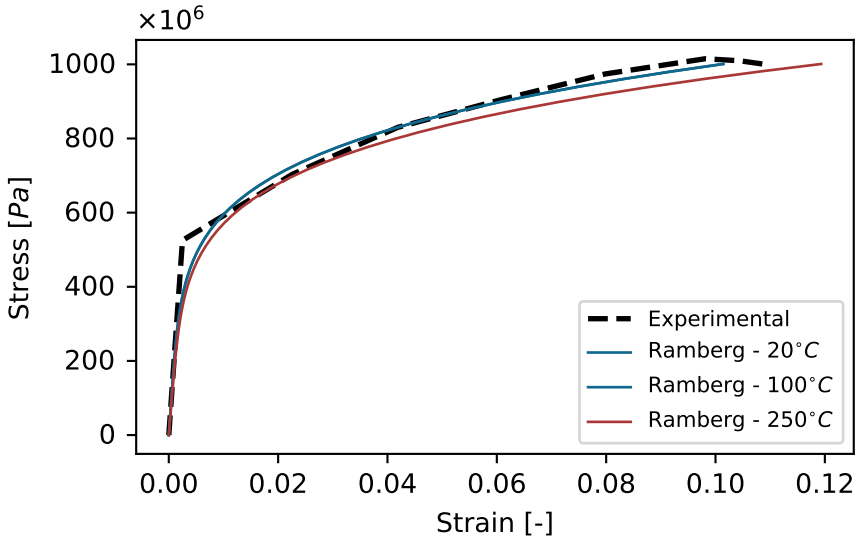

to the model. The results are shown in figure 3.8.

Noteworthy from figure 3.8 is that the curves for 20 °C and 100 °C are equal, since the properties do not change in this range. Beyond that, the Young's modulus (table 3.2) and the yield stress change as shown in figure. These curves were modeled in Ansys utilizing multilinear isotropic hardening option. The Poisson's ration were held constant with value of 0 3. Steel's density is set to 7850 kg m^{-3}.

Furthermore, thermal properties, such as, thermal expansion (α) and elongation, specific heat (C) and thermal conductivity (λ) were based on the equations proposed by EN 1993-1-2. Firstly, the thermal expansion (eq. 3.3) is archived by taking the derivative of the thermal elongation (eq. 3.2) with respect to the temperature (T). Specific heat is shown in equation 3.4 and lastly the thermal conductivity in equation 3.5. These parameters are shown in figures 3.9a and 3.9b, respectively. Lastly, the emissivity of the steel is also considered constant with a value of 0.7.

$$\frac{\Delta L}{L} = 1.2 \times 10^{-5} T + 0.4 \times 10^{-8} \cdot T^2 + 2.416 \times 10^{-4} \tag{3.2}$$

$$\alpha = 1.2 \times 10^{-5} + 0.8 \times 10^{-8} \cdot T \tag{3.3}$$

$$C = 425 + 7.73 \times 10^{-1}T - 1.69 \times 10^{-3}T^2 + 2.22 \times 10^{-6}T^3 \tag{3.4}$$

$$\lambda = 54 - 3.33 \times 10^{-2}T \tag{3.5}$$

Figure 3.9 – Steel's thermal dependent parameters.

(a) Thermal expansion

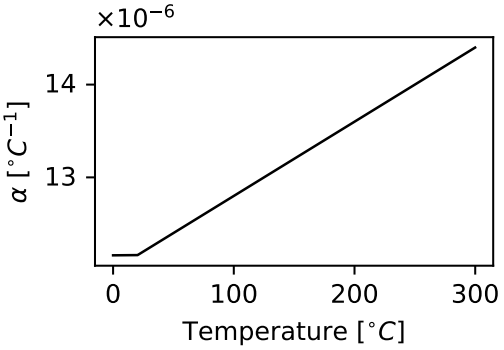

(b) Specific heat and thermal conductivity

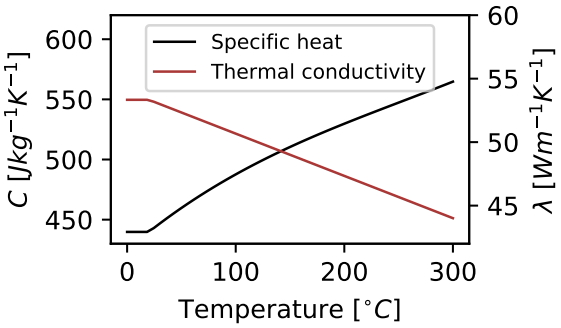

3.2.2 *Sleeper's Wood Properties*

There is a variety of woods utilized on the sleeper's construction and this fact may lead to different behaviour of the track. In addition, the deterioration of the wood sleepers can also affect track's behaviour. The wood specie used on this work's simulation is called *Pinho Bravo*, according to the track's maintenance personnel of Tua's line. Many studies have been conducted to characterize the mechanical behaviour of this material and it is described in [47] and [48]. The main parameter taken from these source was the longitudinal Young's modulus and it falls into the range of 3.4 GPa to 16 GPa. Thus, these two values were utilized as upper and lower bounds in order to cover the range.

Furthermore, it is well known that wood is an orthotropic material and its mechanical behaviour highly depends on the orientation of fibers. In order to better model this property in the simulation, reference ratio values for orthotropic parameters related to longitudinal Young's modulus were taken from Ross *et al.* [49]. Since no reference value for *Pinho Bravo* were available, these were taken from Red Pine and are shown in table 3.3, where E denotes the elasticity modulus, G the shear modulus and ν the Poisson's ratio. Axis orientation are shown in figure 3.10.

By utilizing these reference values presented and the experimental results for Young's modulus, it is possible to estimate the orthotropic behaviour for the desired wood species. Wood's

Table 3.3 – Orthotropic relations.

Specie	$\mathbf{E_T/E_L}$	$\mathbf{E_R/E_L}$	$\mathbf{G_{LR}/E_L}$	$\mathbf{G_{LT}/E_L}$	$\mathbf{G_{RT}/E_L}$	$\nu_{\mathbf{LR}}$	$\nu_{\mathbf{LT}}$	$\nu_{\mathbf{RT}}$
Red Pine	0.044	0.088	0.096	0.081	0.011	0.347	0.315	0.408

Source: adapted from [49].

Figure 3.10 – Axis orientation for orthotropic wood parameters.

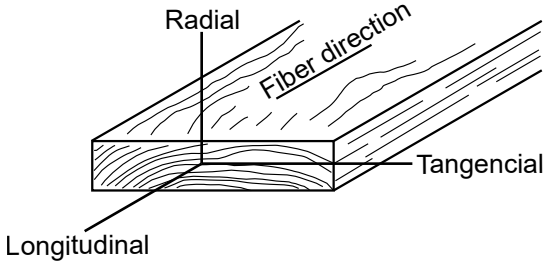

Source: adapted from [49].

thermal properties are not discussed, since the thermal simulation do not account for heat transfer through the sleeper, as explained in section 2.5.

3.3 Thermal Simulations - Rail Temperatures

In order to simulate rail temperatures based on the weather information that have been collected, this work makes use of the CNU model, described in 2.5.2, with modifications to overcome issues and facilitate the simulation procedure. This model was chosen since it considers the geographical position of the rail track. Also, as mentioned in section 2.5.2, the authors suggest that this approach should be evaluated in other locations as means of validation.

Furthermore, to ease and automate the process, a simple software/package was developed utilizing python programming language, which is discussed in section 3.3.2. The software's solving procedure was validated by comparing with a finite element model (section 3.3.3), as well as with experimental rail temperatures. Additionally, the simulation extends to other locations in Portugal, utilizing weather data provided by IPMA.

3.3.1 *Model Modifications*

As a brief recap, the CNU model uses the heat balance equation (eq. 2.9) proposed by Zhang *et al.* [35] and modifies the calculation of the sun area parameter (A_s) by relating it to the area of the shadow produced by the sun's rays and rail track on a given latitude, longitude, date and time.

Two main procedures are modified in this present work: sun's position evaluation and shadow area calculation (see figs 2.18b and 2.19b). Differently from the original model, which a set of equations based on Michalsky method were utilized to determine the sun's position in the sky in terms of elevation and azimuth, the python package utilizes the Pysolar library to calculate these parameters, which algorithm is described in Reda *et al.* [50]. This approach enable a easy-to-use interface to determine the sun's position, making the integration with the main program effortless.

The second main difference appear on the rail profile simplification and consequently on the shadow area calculation (S_{shadow} in eq. 2.15). Rather than using 14 vertex in each face to represent the rail segment, the software utilizes more than 30 points in each face, depending on the profile type (e.g. UIC54, UIC60). And this modification may lead to miscalculation when evaluating the area formed by the rail's projected points utilizing the equation 2.14. To use this equation, the points should be ordered sequentially in such manner that no crossing edges exists. Beyond that, some points may fall "inside" the shadow (see fig. 2.19b) and should be excluded from the calculation.

To overcome this issue, once more, the package adopts a specialized algorithm to evaluate this parameter: *scipy.spatial.ConvexHull*, This algorithm is used to find the most external points and use them to evaluate the area they create. Furthermore, it already features a built-in function to output this area.

3.3.2 *Python Package*

Python is an open source and powerful programming language for many fields, including scientific programming. To solve the CNU model, automate and ease the process of simulation, a package for python programming language was developed. The package called **railtemp** is available for download[1] aiming further improvements and collaboration. Besides, a brief example of utilization is presented in appendix B.

This software is written on top of the following python libraries:

- SciPy [51] - Ecosystem for scientific computing;
  - Pandas [52] - Data manipulation;
  - NumPy [53] - Array calculations;
  - IPython [54] - Interactive computing;
- Pysolar [55] - Solar irradiation simulation and ephemeris calculation.

The package has four main classes which contain all the functions and parameters needed to solve the equations proposed by Hong *et al.* [36]. The steps to perform a simulation with the package is similar to the use of Ansys software: define material properties, create geometry, apply loads, specify initial conditions and solve the model. For instance, all the material properties are associated to the *RailMaterial* class, *WeatherData* contains weather information, *Rail* inherits the attributes of *RailMaterial* and also has other geometric related parameters. Finally, the *CNU* class contains all the methods to solve the model and depends on the aforementioned classes. Figure 3.11 shows all methods and parameters each class has and their relations.

The advantage of having this architecture is that enables one to perform multiple simulations varying specific parameters just by creating multiple objects of the same class. Also, since the program is built with these blocks, one can easily create other class for model modifications but will still be able to access the geometric, weather information and material properties of the upper classes.

The *run()* method starts the solving process of the model. The sequence of steps are shown in figure 3.12. First all temperatures are converted to Kelvin, since it is necessary to correct

[1] Source code and example available in https://github.com/aryvini/railtemp

Figure 3.11 – Railtemp: classes, attributes, methods and dependencies.

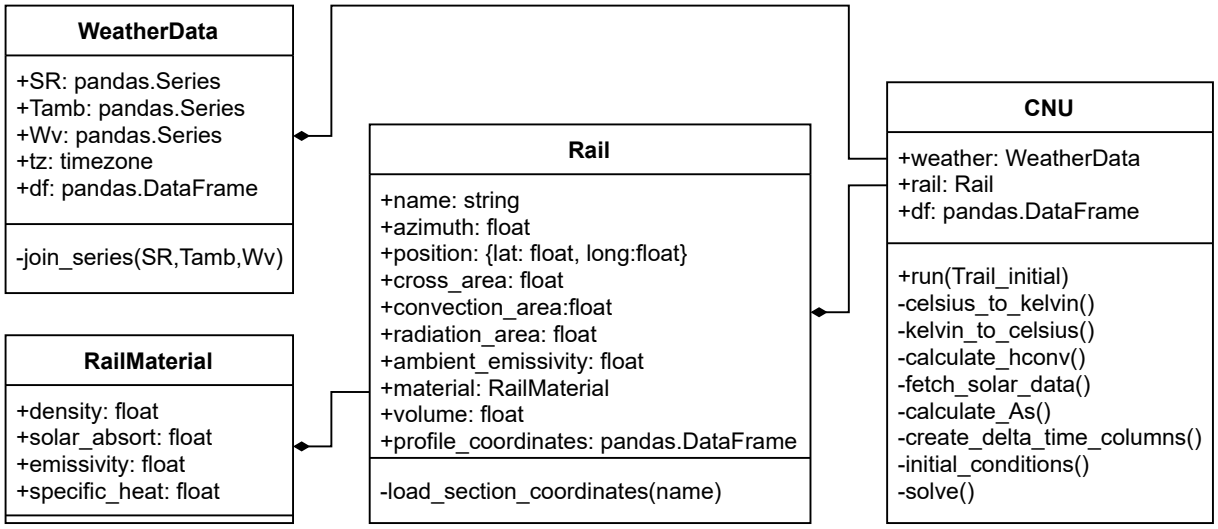

quantify energy exchange when dealing with radiation. Next, with use of equation 2.10, the convection coefficient is evaluated. Following, the module PySolar is used to fetch the solar data (elevation and azimuth) for every time step of the simulation and then these data are used to perform the evaluation of the sun area (A_s) parameter.

The steps (determine ΔT and initial conditions) prepares the data to be used on the equation's solving process. The procedure to solve the differential equation (eq. 2.9) of the CNU model is presented in figure 3.13, it is first divided in 4 parts (A,B,C,E,K) and derivatives defined on a finite interval. Managing the equation and setting equal 0, results in a equation in which one can find the root. The package makes use of the *scipy.optimize.newton* algorithm to find the T_{ri} in which the condition is true with a tolerance of 1×10^{-5}. Once the rail temperature converges for all time steps, the package convert the temperatures to Celsius and finishes the solution.

3.3.3 *Finite Element Validation*

To validate the solving process and the usability of the python package, a validation was conducted by comparing with a thermal finite element model solution. The details and procedures of this validation are discussed in this section.

The finite element model was built using the Ansys software and is built using two elements: *PLANE55* and *COMBIN39*. The plane element is used to solve 2D heat conduction problems. It is defined by four nodes, each with temperature as degree of freedom. This element features

Figure 3.12 – Package solution steps.

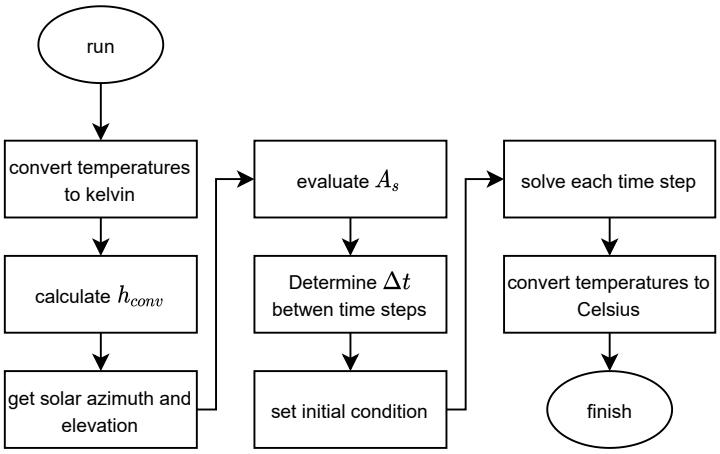

Figure 3.13 – Differential equation discrete solution.

$$\underbrace{SR \cdot \alpha_s A_s}_{A} - \underbrace{\left[h_{conv} A_c (T_r - T_{air})}_{C} + \underbrace{\epsilon_{res} \sigma A_r (T_r^4 - T_{air}^4)\right]}_{E} = \underbrace{\rho C V \frac{dT_r}{dt}}_{K}$$

$$\underbrace{\frac{1}{K_i}[A_i - C_i - E_i]}_{F_i(T_{ri})} = \frac{T_{ri} - T_{ri-1}}{\Delta t}$$

$$[F_i(T_{ri})\Delta t + T_{ri-1}] - T_{ri} = 0$$

i: Current time step
$i-1$: Previous time step

linear interpolation and full gauss integration. The element accepts nodal loads in terms of radiation and convection or heat flux (not both). This is a limitation, since the CNU model uses the three heat flow modes concurrently. This is overcome by using the combination element. *COMBIN39* is an unidirectional element with nonlinear relation between heat flow and the temperature difference. It also features linear shape function and exact integration. Its use is detailed further. The key options utilized for each element are shown in table 3.4.

Table 3.4 – Main key options of elements.

	PLANE55			COMBIN39	
Key option	**Value**		**Key option**	**Value**	
K1	0	Average film coefficient	**K3**	8	Tempearture
K2	0	Plane			

In order to overcome the issue with three heat transfer modes, an arch were meshed above the rail profile and it receives the radiation loads and transfers to rail's nodes through the *COMBIN39* elements. The FEM mesh is shown in figure 3.14 and illustrates this approach

Figure 3.14 – FEM mesh for simplified thermal model validation.

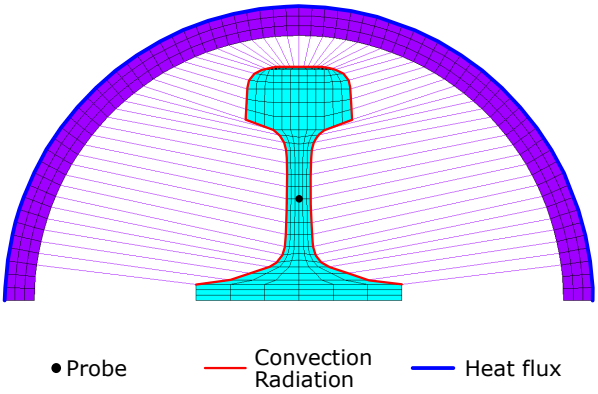

together with the surface in which each load is applied.

The mesh of the arch is made with plane elements and of a material in which features high thermal conductivity, unitary density and low heat capacity. This allows a instantly energy transfer from the arch to the rail profile. The material is referred as *radiation transfer material* and its properties are in table 3.5. Besides that, the rail profile is also made using plane elements however the material properties of the steel (see section 3.2) are assigned to them.

Table 3.5 – Radiation transfer material properties.

Density	**Specific heat**	**Emissivity**	**Thermal conductivity**
1	1	1	1000

The profile utilized in this validation is the UIC54, since it is the one being monitored, as mentioned in section 3.1. In total the mesh contains 502 elements and 554 nodes and this size has been determined after a convergence test.

The input loads depend on weather information, and for the purpose of this validation, the data between 2020/07/26 until 2020/07/28 were chosen to this analysis. The reason was because the solar radiation presented no interruptions, meaning a clear sky day and the air temperature reached over 35 °C. These conditions are presented in figure 3.15 and 3.16. Hence, high rail temperatures are expected during these days, what is later confirmed in section 4. The sun's elevation and the equivalent sun area (A_s) parameter are presented in figure 3.17. It is possible to see the variation of the parameters as far as the sun changes its altitude.

An important fact to mention about the input loads is that the heat flux is inserted taking into account the solar absorptivity of the rail (α_s) and beside that, since the arch has a greater perimeter than the rail profile, the solar radiation is converted to match the same amount of

Figure 3.15 – Solar radiation and convection coefficient for validation.

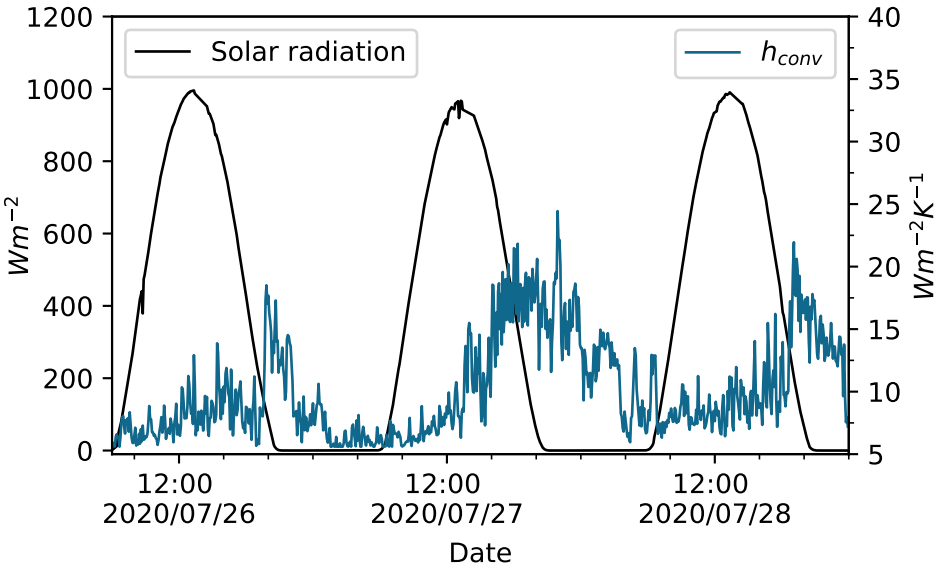

Figure 3.16 – Air temperature for validation.

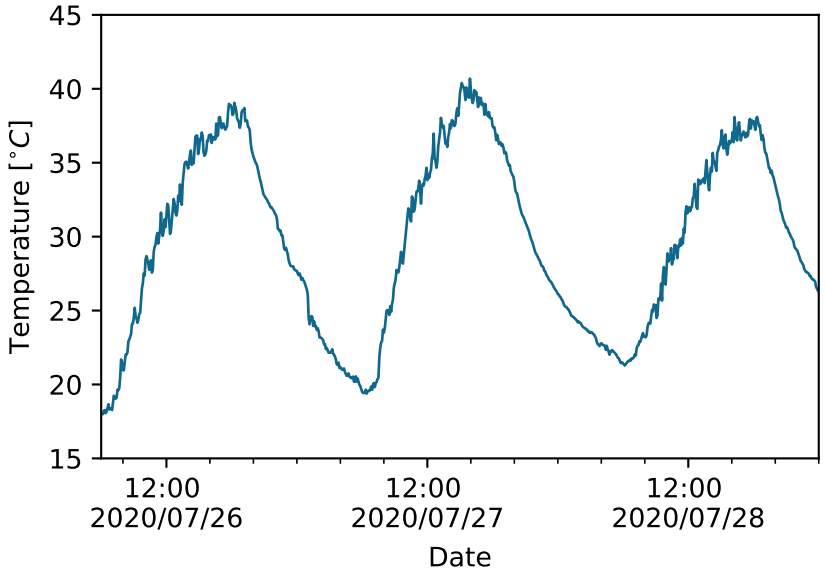

energy that would be received directly by the rail profile. Table 3.6 shows a summary of the constant parameters utilized to perform the simulation with the CNU model. The emissivity (ϵ) presented in equation 2.9 is calculated as the product of the rail (ϵ_r) and ambient (ϵ_{amb}) emissivities.

Table 3.6 – Constant parameters for thermal simulations.

ρ (kg m^{-3})	α_s	ϵ_r	ϵ_{amb}	T_{sky} (°C)	A_c (m^2)	A_r (m^2)	V (m^3)
7850	0.85	0.7	0.6	T_{air}	472.8×10^{-3}	472.8×10^{-3}	7.16×10^{-3}

Regarding the solution control parameters, a full transient analysis is configured and the time

Figure 3.17 – Sun's parameters for validation.

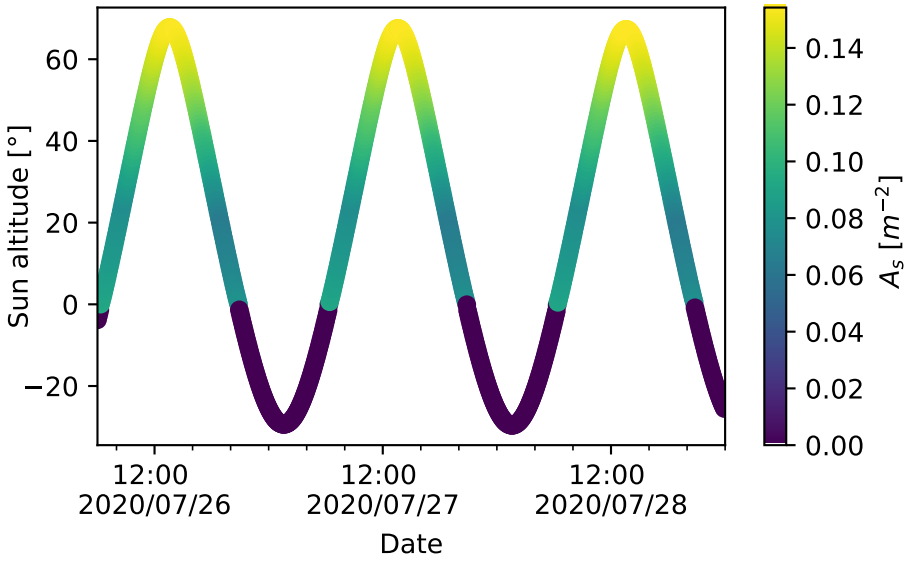

step is set to 60 seconds and in case of easy convergence the maximum allowed step is 200 seconds. On the other hand the minimum possible time step is 10 seconds. The thermal analysis is incremental and iterative, using heat flow criterion for convergence, with a tolerance of 1×10^{-3} and reference value of 1×10^{-6}.

3.3.4 *Simulating other Locations in Portugal*

As discussed in section 2.5.2, physical models show advantages when compared to statistical ones because they can be used in any location, once the weather conditions are known. Hence, in order to extend the simulation of the rail temperatures to other locations in Portugal, the CNU model was utilized with the help of the python package mentioned in section 3.3.2.

In total, six locations were chosen to run analysis. This choice was made taking into consideration the availability of an IPMA's weather station and also the existing railways nearby. Train stations or maintenance yards locations were utilized to extract coordinates and rail orientation. Table 3.7 shows these places with their coordinates and azimuth. The same information are shown in figure 3.18

In order to estimate the maximum rail temperature, it was assumed that it happens when the air temperature is also maximum. Thus, among 4 years of recorded data, 10 days were selected around the day in which the maximum air temperature takes place. Important to mention that, similarly to the monitored track in Mirandela, the weather station is not at the same place as the simulation. Furthermore, the UIC60 profile was utilized in these other places, since it is the

Table 3.7 – Coordinates of simulated rail tracks in Portugal.

City	Latitude	Longitude	Track azimuth
Alvega	39.472212	-8.046025	90
Coimbra	40.225813	-8.440641	175
Évora	38.550388	-7.916778	35
Guarda	40.537631	-7.233397	160
Lisboa	38.819434	-9.088660	15
Porto	41.172193	-8.571092	40

Figure 3.18 – Analyzed cities in Portugal.

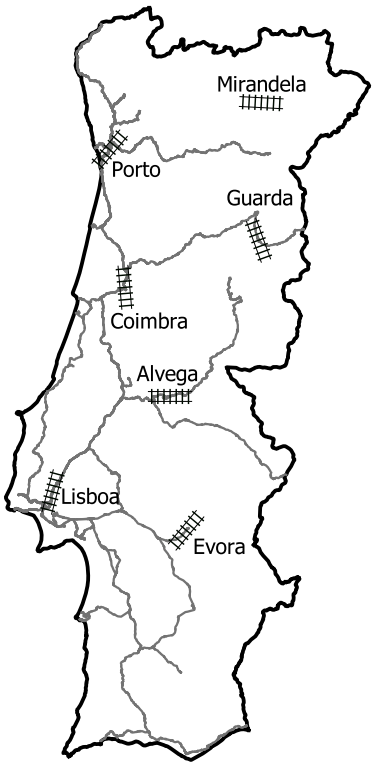

most used nowadays. The material properties remain equal to the mentioned before.

3.4 Thermomechanical Simulations - Rail Buckling

In order to evaluate the static buckling temperatures (not taking into account vertical loads) on tangent railway tracks, this work makes use of non linear finite element models. This section describes all the parameters utilized to build and solve them using the software Ansys. The models utilized in this work are similar to the ones mentioned in section 2.6.3 with modification. Furthermore a parametric evaluation is made regarding the following variables: track gauge, rail profile, initial imperfection amplitude, sleeper's elasticity modulus, torsional resistance of

fastenings and ballast resistance.

3.4.1 *Elements Definition*

Ansys provides a variety of finite elements formulations to build models, and in this work uses two: *BEAM188* and *COMBIN39*. Their definition, features and key options are described bellow.

The beam element is suitable for analyzing slender to moderately thick beam structures and it is based on Timoshenko beam theory. It has six or seven degrees of freedom at each node, which includes translations and rotation in three axis (x,y,z) and a warping magnitude as the last DOF. The latter being optional and has not been utilized. The element is defined by two (or three) nodes, which defines the beginning, ending and orientation (optional) of the cross section. The shape functions can be linear, quadratic or cubic, linear being utilized in this work. This choice can affect the quality of the results if a adequate number of elements is not utilized. The key options of this element are described in table 3.8. The element was used to model both rail and sleepers. Details are later explained in the geometry section.

Table 3.8 – *BEAM188* key options.

Key option	**Value**	
K1	0	Six DOF per node
K2	1	Rigid: transverse strain is neglected
K3	0	Linear shape function

Another element that has been utilized is the *COMBIN39*. It has been already defined on the section about thermal models. However it also features other capabilities to be used on mechanical simulations. It features longitudinal or torsional capabilities in 1-D, 2-D or 3-D applications. It has been used to model the non linear behaviour of the ballast (both lateral and longitudinal) and the torsional resistance of the fastening type between sleeper and rail. The element requires a real constant which defines the force-deflection (or moment-rotation) behaviour of it.

For each application (ballasts and fastenings) of the *COMBIN39* an unique element type instance in the software was necessary in order to assure the desired behaviour. Thus Table 3.9 shows the key options utilized and its application. Their real constants are later explained in the geometry section.

Table 3.9 – *COMBIN39* key options.

Application	Key option	Value
Fastening	**K3**	6 ROTZ (Rotation about nodal Z axes)
Lateral ballast	**K4**	3 2-D longidutinal (UX and UY)
Longidutinal ballast	**K3**	2 UY (Displacement along nodal Z axes)

3.4.2 *Geometry Definition*

As discussed before, many rail profiles and gauges are utilized to build railway tracks. Therefore, in order to evaluate the behaviour of rail buckling for different tracks, many geometries were used, varying both gauge and profiles.

UIC54 and UIC60 profiles were used and their technical drawing and geometric parameters can be found in annex E. Regarding the gauges: metric, UIC and iberian gauges were employed (see section 2.4.2), respectively: 1000 mm, 1432 mm and 1664 mm. Only one sleeper cross section was used and it is a rectangular shape measuring 24 cm of width and 12 cm of height. The length changes depending on the gauge utilized.

Figure 3.19 shows the construction of the model with its elements, main boundary conditions, dimensions and axes orientation. The plane view is presented in figure 3.19a and the cross section in figure 3.19b. As displayed, the *COMBIN39* element type has three application and differs from their key option sets.

BEAM188 is used for both sleepers and rails and their material properties have been defined in section 3.2. The sleeper is considered orthotropic, as mentioned before, however, a full orthotropic behaviour is not possible to achieve with this element type, since in its formulation matrix not all three dimensional orthotropic parameters are considered.

Since the fastenings connect sleeper and rail, it must be placed between these element's nodes. The details are shown in figure 3.20. As a remark, the entire model is designed on the XY plane, and in the figure the nodes have a vertical offset to illustrate that the fastening element is placed between the sleeper and rail element's nodes. These specific nodes have the same nodal coordinates, however they are two different nodes (superposed) with their own DOF. Since the displacement of the sleeper and the rail at this nodes are equal, it was necessary to couple the following degrees of freedom: x, y, z displacements and x, y rotations. The remaining DOF is the rotation about the z axes, in which the fastening element is set to actuate. Without the coupling, the solution do not converges.

Regarding the boundary conditions, as shown in figure 3.19a, the rail's ends have the following

Figure 3.19 – Geometry of the model.

(a) Plane view

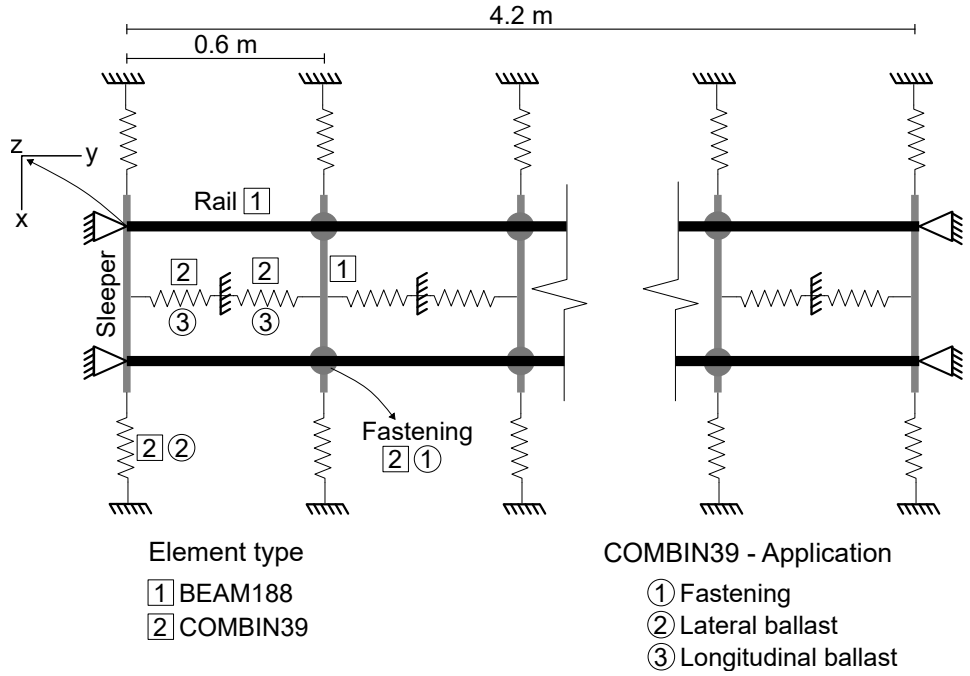

(b) Cross section

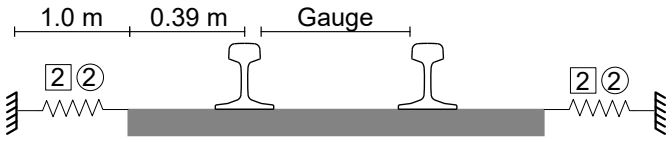

DOF restrictions: x, y, z displacements and x, y rotations. In addition, all nodes are set to have null displacement along the z axis.

Figure 3.20 – Detail of fastening elements.

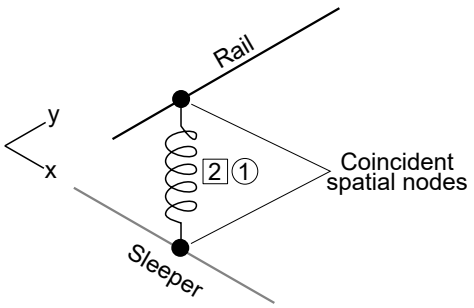

3.4.3 *Real Constants*

The real constants define the spring behaviour of the *COMBIN39* elements. As discussed in section 2.6, the ballast has non linear behaviour meanwhile the fastening can be modeled with linear relation. This section describes the real constants of these elements to be used in the simulations.

Differently from the finite element models utilized by Lim *et al.* [43] and Carvalho [42], in which simplify the ballast behaviour with a bi-linear curve (see figure 2.29), in this work, the ballast have a full non linear behaviour following experimental measurements, as described in figure 2.25. The figure presents two ballasts situations: tamped and consolidated, the latter being with the highest peak resistance, for both lateral and longitudinal orientations. Therefore, as a simplification, it is here called as "strong", meanwhile the tamped curve is named as "weak". Tables 3.10 and 3.11 show the values of the real constants for lateral and longitudinal spring elements for both weak and strong behaviour. The values are ordered as they were inserted in Ansys.

Table 3.10 – Real constant of longitudinal ballast

Strong		**Weak**	
D (m)	**F (N)**	**D (m)**	**F (N)**
−0.05	−10 000.1	−0.05	−5000.1
−0.01	−10 000.0	−0.01	−5000.0
0	0	0	0
10	0.01	10	0.01
11	0.011	11	0.011

Table 3.11 – Real constant of lateral ballast

Strong		**Weak**	
D (m)	**F (N)**	**D (m)**	**F (N)**
−1.0	−4000.2	-	-
−0.12	−4000.1	−1.0	−4000.2
−0.0832	−4000.0	−0.12	−4000.1
−0.0067	−13 200.0	−0.0032	−4000.0
0	0	0	0
10	0.01	10	0.01
11	0.011	11	0.011

The ballast actuates only against compressive forces, however, the *COMBIN39* element type does not provide an option to work only on the compressive curve. Thus, the element is set to have both compression and tension curves, and the tensile forces are set to very small values,

thus offering almost null resistance when pulled. However as a remark of calculation purpose they are not null, but negligible.

Regarding the real constants of the fastening elements and considering that they have linear behaviour, they do not require a multi line table input. For this analysis, two values of the torsional resistance were utilized: 136 kN m rad^{-1} and 44 kN m rad^{-1}. The source of these values can be found in table 2.9, respectively for 4 and 2 spikes (nails).

3.4.4 *Initial Imperfections*

The track is modeled with a sinusoidal imperfection with the half wavelength of 4.2 m, which is the length of the geometry. The amplitude (δ) of the function changes according to equation 3.6, where L is the length of the model, and L_0 is an arbitrary value, usually varying in the range of 200 to 1000. Here, the values of 200, 500 and 1000 were used. Therefore, the values of the imperfection amplitude are, respectively: 21 mm, 8.4 mm and 4.1 mm. The bigger the L_o, the smaller imperfections. The shape of the imperfection and its amplitude are shown in figure 3.21

To implement the imperfection on the model, first an elastic buckling analysis was conducted. From it the modes of instability were extracted and the desired one is used to update a new geometry by applying a scaling factor, which matches the maximum deformation on the eigen-buckling analysis and the desired amplitude (δ) in the new geometry.

$$\delta = \frac{L}{L_0} \tag{3.6}$$

Figure 3.21 – Initial imperfection of the model.

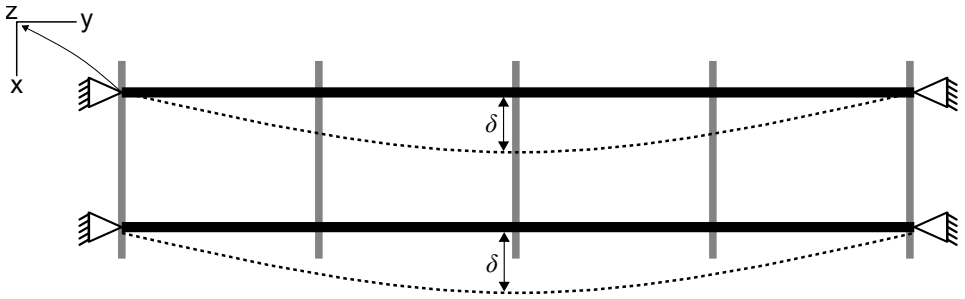

3.4.5 *Mesh Sizing*

Figure 3.22 shows the size control of each *BEAM188* elements and figure 3.23 shows the 3D view of the model. There is no need to define the size control of *COMBIN39*, because they are defined only by two nodes and their length do not play a role on the model. The number of divisions of the sleeper and rails has been defined after a convergence test, by increasing the number of divisions and comparing the results. However, the higher the number of elements, the bigger the computational cost. Therefore the values presented in the figure have shown adequate results with reasonable duration of the simulation, taking about 1′50″ on average. In total the models have 434 elements and 575 nodes of both element types.

Figure 3.22 – Model mesh sizing.

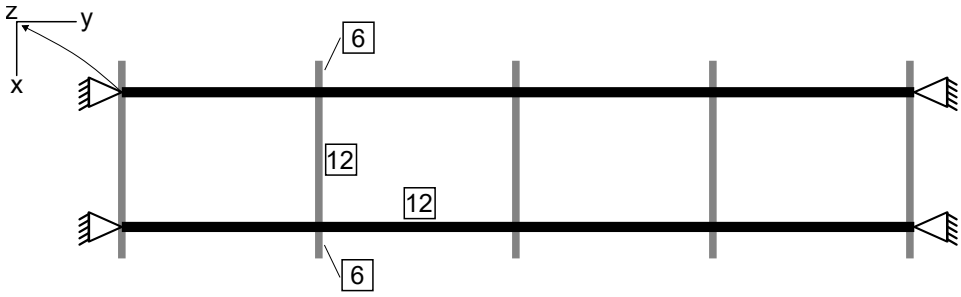

Figure 3.23 – Model mesh - 3D view.

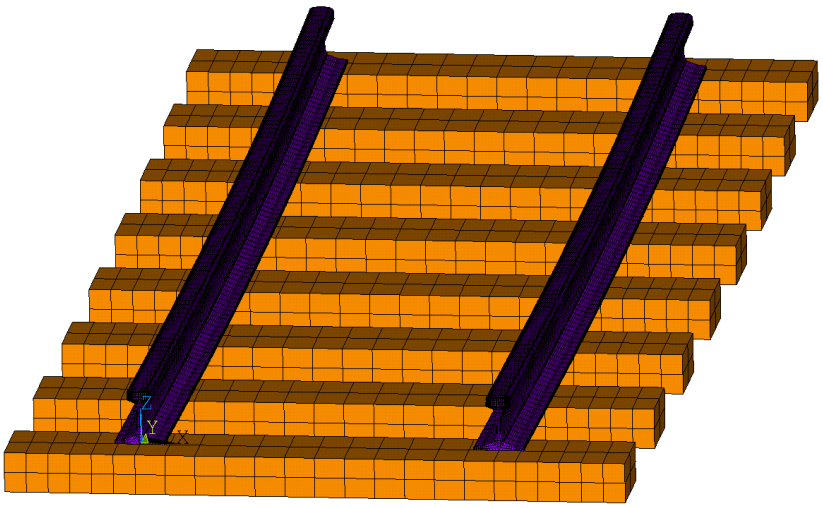

3.4.6 *Loads and Solution Options*

The thermal loads were applied to all nodes, regardless the element type. However, since only the rail's steel has temperature dependent properties, these elements will experience

thermal expansion, leading to internal compressive stresses. The reference temperature for strain calculation was set to 20 °C, which is the stress free temperature, where any changes from this value will cause compressive or tensile stresses. The thermal load was inserted as a table, varying from 20 °C to 200 °C in 200 seconds, hence, the rail in all its extension has the same temperature at a given time. In some cases, at 200 °C the buckling curve could not be defined and then it was increased up to 250 °C.

The simulations have the following solution controls:

- Static solution;
- Large displacement;
- Time step size: 1 °C;
- Minimum time step: 0.001 °C;
- Maximum time step: 5 °C;
- Constant energy dissipation: 0.0001.

The solution method is incremental and iterative, based on the Newton–Raphson algorithm. The convergence criteria of the simulations are based on the force and moment equilibrium, with a tolerance of 1×10^{-3} units.

3.4.7 *Summary of Simulation Parameters*

To summarize the analyzed parameters of the analysis, table 3.12 shows the values of each of them: profiles, gauges, imperfection (L_0), longitudinal elasticity modulus of the sleeper's wood (E_l), ballast behaviour and the torsional resistance of the fastener.

Table 3.12 – Summary of parametric study.

Geometry			**Properties**		
Profile	**Gauge (mm)**	$\mathbf{L_0}$	$\mathbf{E_l}$ **sleeper (GPa)**	**Ballast**	**Fastener (kN m rad^{-1})**
UIC54	1000	200	3.4	Weak	43
UIC60	1435	500	16	Strong	135
	1664	1000			

Varying all these parameters, a total of 144 simulations were done. In order to facilitate and automate the process, scripts with APDL language were built, simulating batches of 8 analysis per run.

4 RESULTS

4.1 Analysis of Experimental Data

Before presenting the result of the simulation, a brief exploratory analysis of all collected data (weather and rail temperatures) in Mirandela is presented. Since IPMA has provided four years of data from the cities mentioned in table 3.7, the summary of them is presented in appendix C.

4.1.1 *Collected Rail Temperatures*

As mentioned before, the logging started on 27/07/2020 and finished on 15/02/2021. Figure 4.1 presents the measured rail temperatures during the time range of data collection as a calendar, where each box is one day, the vertical axes represents the days of the week and the horizontal axes the months. Figure 4.1a shows the maximum recorded temperature of the day, while figure 4.1b shows the minimum. Furthermore the difference between maximum and minimum (amplitude) is presented in the figure 4.1c. The boxes with red indicators mean lack of data.

The highest recorded rail temperature was 58.06 °C, on 2020/07/27. In contrast, the minimum was −2.40 °C on 2021/01/13. This represents a total thermal amplitude of 60.46 °C. On daily basis perspective, from figure 4.1, it is possible to notice that the maximum daily change in temperature happens during the months of August, September and October, reaching an average value of 29.31 °C. The lighter boxes during these months are possibly due to cloud cover, avoiding the rail to receive solar radiation, thus not increasing the temperature.

From figure 4.1a it is clear to notice the graded variation in temperature as far as the seasons changes. As expected, during the summer months the rail temperatures reach values up to 58 °C and slowly shift to the winter reaching values of 0 °C, as mentioned before.

Figure 4.2 shows that the daily maximum rail temperature occurs mostly between 14:00 and 15:00. Important to mention that the time expressed in the image corresponds to the local time. This distribution may change for different locations, mainly varying the latitude, since it effects the sun's path during the day. The maximum temperatures before 13:00 and after 15:00 may due to cloud covered days and in case of any temporally cloud clearance, the temperature rises for a while.

Figure 4.1 – Heat-map calendar of measured rail temperatures.

(a) Daily maximum

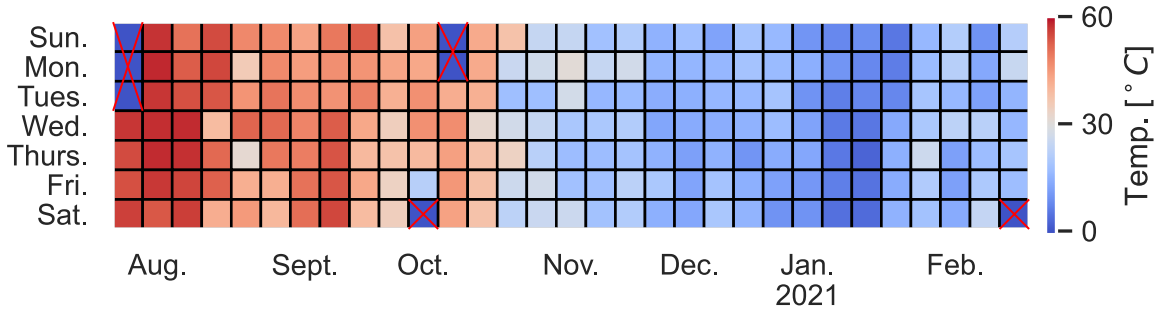

(b) Daily minimum

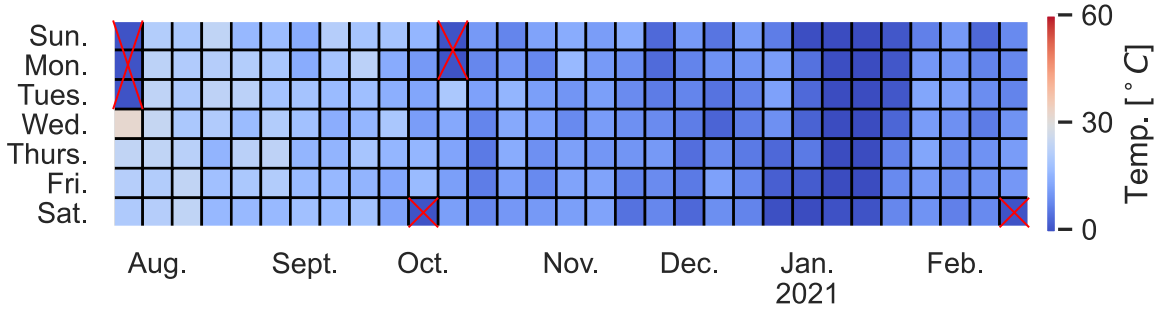

(c) Daily amplitude

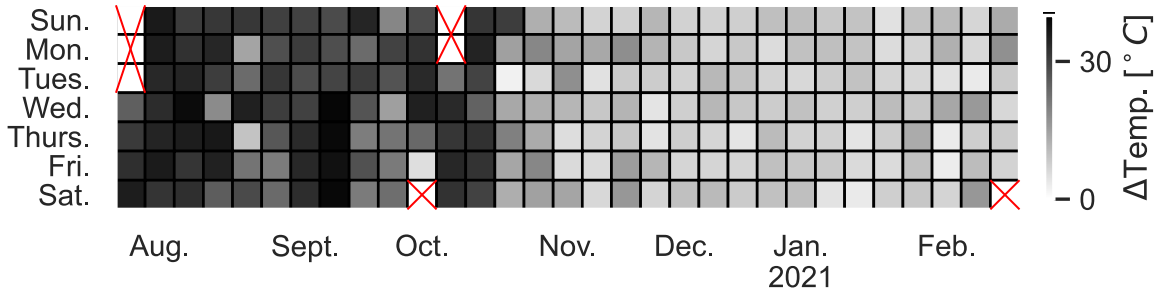

Analysing all collected rail temperatures with a histogram it is possible to identify the most frequent value. Figure 4.3 shows the frequency distribution of all measurements (fig. 4.3a), as well as the temperature during daylight (fig. 4.3b) and night-time (fig. 4.3c). The data was split according to the sun's altitude, where above horizon means daylight and bellow horizon means night-time.

It is notable that the most frequent temperatures falls into the range of 5 °C to 15 °C, according to figure 4.3a. Looking into daylight and night-time, it is possible to conclude that temperatures higher than 30 °C only take place during the day, as expected. Meanwhile, low temperatures near 0 °C take place both during day and night, although it is more frequent during night-time.

Although the goal of this work is to use physical modeling to correlate weather and rail

Figure 4.2 – Histogram of the time for daily maximum measured rail temperatures.

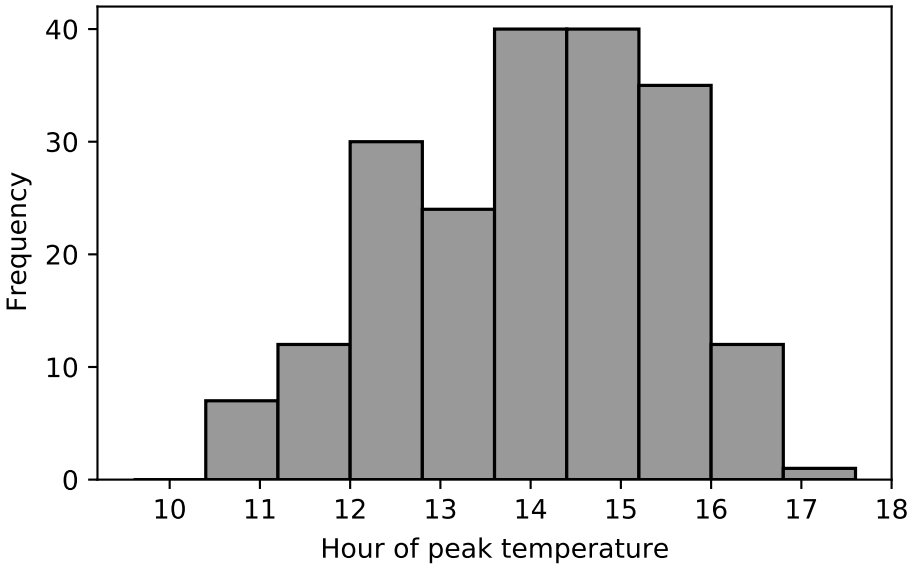

Figure 4.3 – Histogram of collected rail temperatures.

(a) All rail temperatures

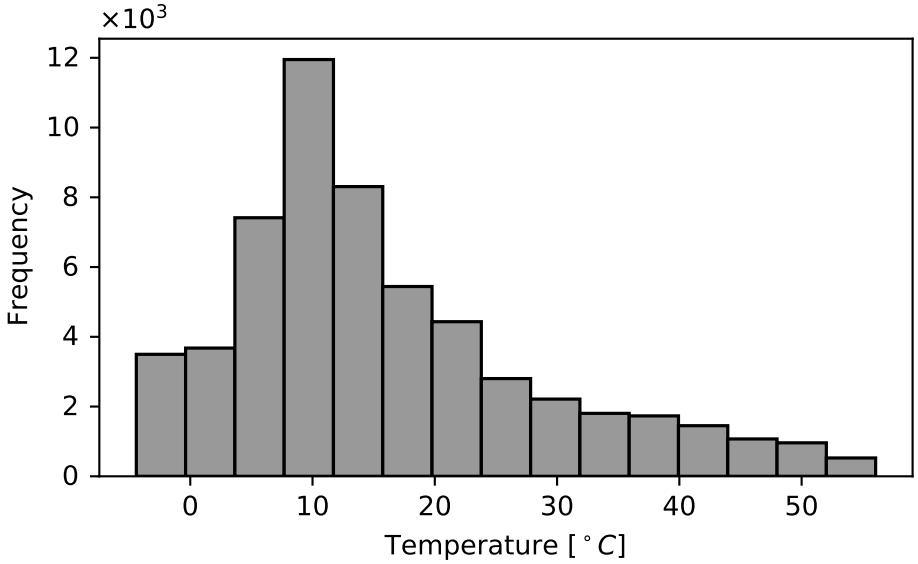

(b) Daylight temperatures

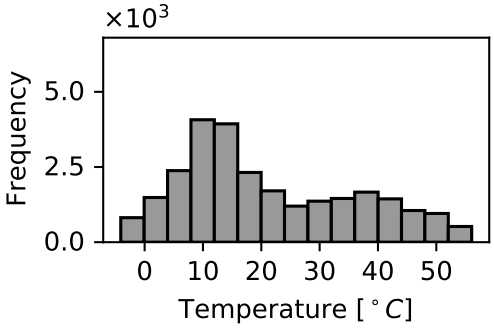

(c) Night-time temperatures

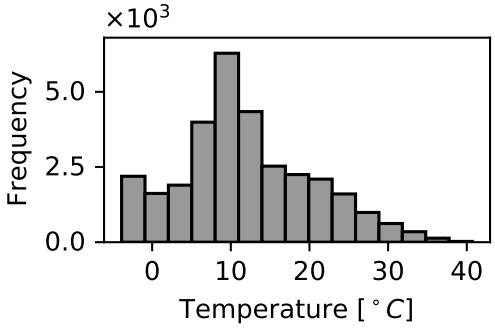

Figure 4.4 – Correlation of measured rail and air temperatures.

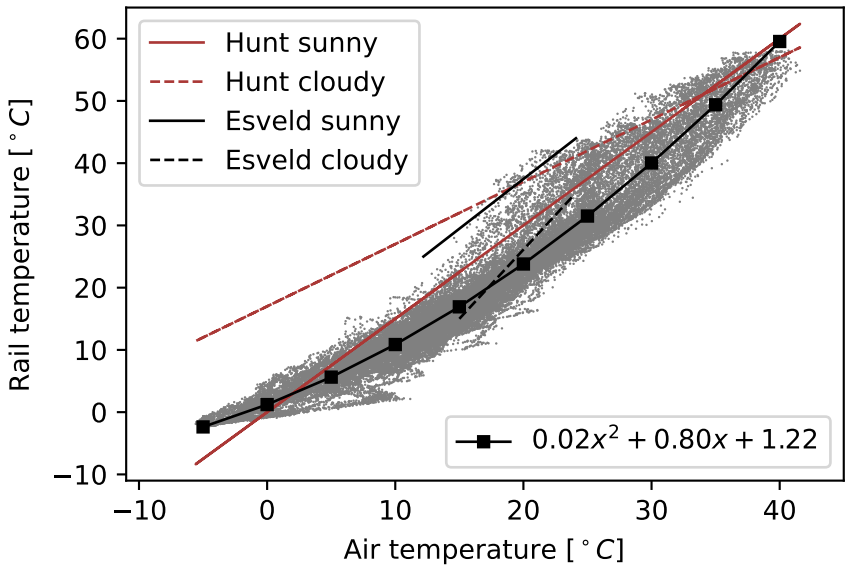

temperatures, it is worth verifying the correlation between air and rail temperatures, since is the most used on empirical models, as discussed in section 2.5.1. Figure 4.4 shows the correlation of all measured rail and air temperatures, similarly to figure 2.13. One can conclude that there is a multi linear relation between air and rail temperature, however the data shows a great spread perpendicular to the relations. Furthermore there is an offset of almost 20 °C between maximum air and rail temperature.

As a simplification, an 2-order polynomial equation was fit into the data where the x variable is the air temperature, the output is the rail temperature, and its coefficients are expressed in figure 4.4. This naive simplification reached an R^2 score of 0.946 and $RMSE$ of 2.95 °C.

4.1.2 *Collected Weather Data*

Equivalently the last section, an overview of the collected weather data are presented. The data correspond to air temperature, solar radiation and wind velocity. The results are presented in figure 4.5 as a histogram. Air temperature is shown in figure 4.5a, solar radiation in figure 4.5b and wind velocity in figure 4.5c. For visualization purposes, the solar radiation presented was filtered by the threshold of 15° of the sun's elevation, in order to cut off the small readings when the sun is starting to rise above the horizon and the zero readings during night-time.

The maximum recorded air temperature was 41.58 °C on 2020/08/06 and the minimum was −5.57 °C on 2021/01/06. Meanwhile the most frequent measures fall into the range of 8 °C to 14 °C. The solar radiation reach peaks over 1000 W m^{-2} which is expected for clear sky

Figure 4.5 – Histogram of collected weather data.

(a) Air temperature

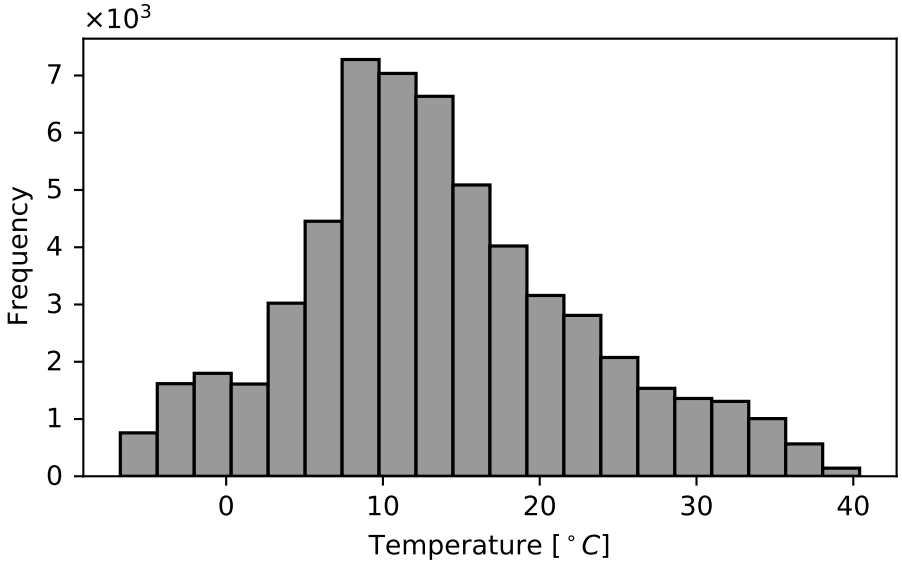

(b) Solar radiation

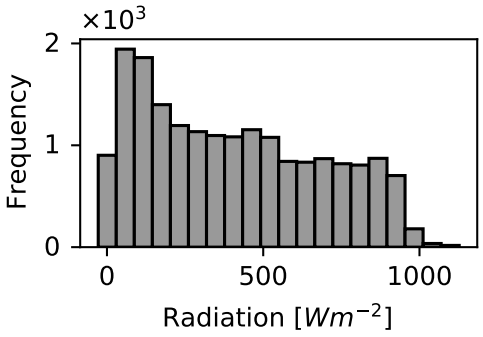

(c) Wind velocity

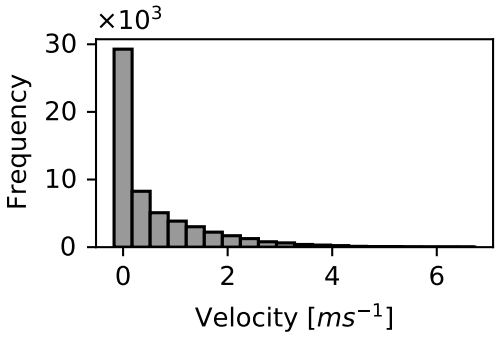

days. The wind velocity shows frequent values around $0\,\mathrm{m\,s^{-1}}$ indicating that calm winds are predominant in this location.

4.2 Thermal simulations - Rail Temperatures

In this section, the results regarding the thermal simulations are discussed. The validation of the use of the *railtemp* package is presented, as well as the extrapolation of the simulations throughout Portugal. Beyond that, an overall performance of the model when simulating over all experimental collected data is also presented.

4.2.1 *Finite Element Validation of Python Package*

Performing the simulation utilizing finite element model and the thermal lumped model with help of the *railtemp* package developed in python showed no significant difference. This means that instead building a complete finite element model, the package can be easily utilized to perform such simulations and predict rail temperatures based on given weather conditions, and at the same time, verify the possibilities of occurrence of critical temperatures. The results of the validation are shown in figure 4.6.

Figure 4.6 – Comparison between finite element and lumped model.

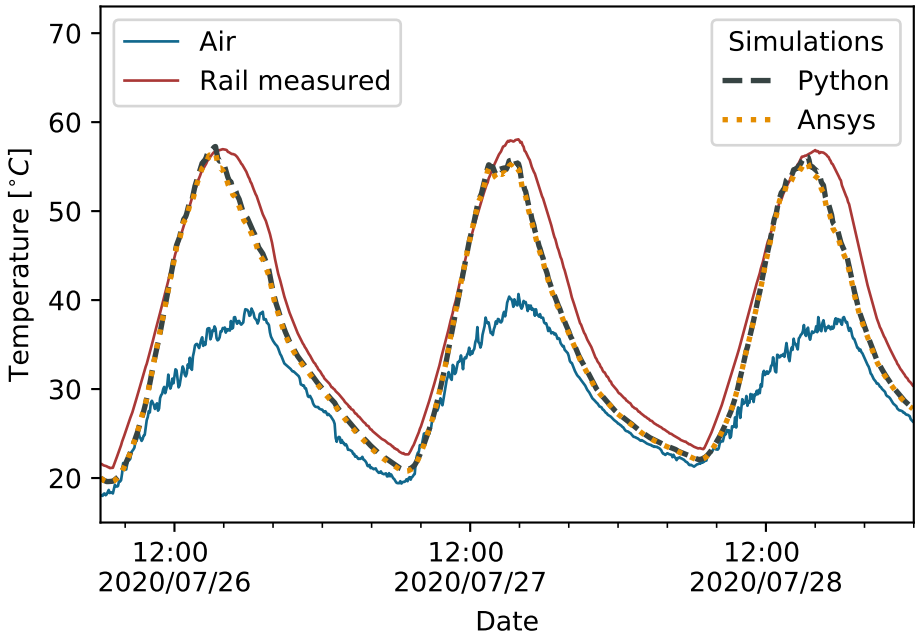

A FEA result of a specific time instant is shown in figure 4.7. It notable that the variation of temperatures within the profile is negligible (0.2 °C maximum difference). This is in accordance with the thermal lumped model, in which assumes a uniform temperature distribution along the rail section profile for each time step. However this assumption means a limitation of the model, since the temperature distribution is not uniform during the day and along the profile, as reported in [30].

Regarding the performance of the model to predict rail temperatures, it shows a good behavior, reaching a coefficient of determination (R^2 score) of 0.914 and a root means squared error ($RMSE$) of 3.44 °C within 792 samples utilized on the simulations. However it is notable that during the cooling stage, the simulation lose energy and decrease the temperatures earlier than measured. This may be related to the parameters used for the boundary conditions, mainly the heat loss by convection. Despite this fact, the model has a good performance.

Figure 4.7 – FEA results for 2020/07/26 15:15.

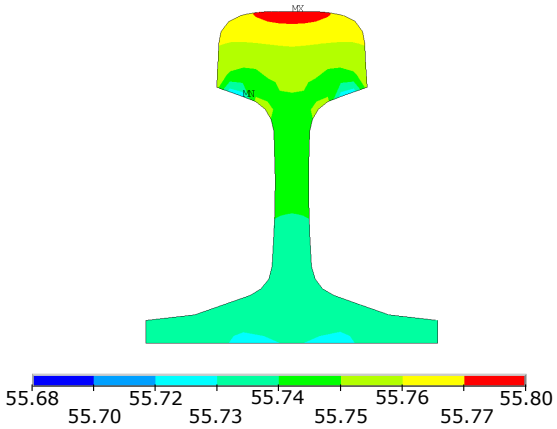

The peak temperatures exhibit differences in a range of 3 °C and also demonstrates a delay, staying behind the actual measured maximum rail temperature. After all the model presents a good approximation to estimate the maximum rail temperatures based on weather conditions. Furthermore, by utilizing weather forecast information, it is possible to use it to predict the instant and maximum rail temperature under specific circumstances.

4.2.2 *Overall Performance of the Model*

For purpose of validation of the simplified model, only few days of data were utilized and discussed in the last section, however this do not represent a good statistical sample to extrapolate the model, since the weather conditions vary along the year. Therefore, in this section the performance of the model is discussed when utilizing over 150 days of weather data to simulate the rail temperature and comparing it with experimental measures.

Due to some missing data, it was not possible to simulate all data continuously. Therefore the simulations were divided into six time ranges and they are presented in table 4.1. Also this fact helps comparing the model under different weather conditions and various seasons. The material properties and constant parameters utilized for these simulations are equal to the section 3.3.3.

Figure 4.8 shows the result of each simulation with a correlation scatter between measured and simulated rail temperatures. The R^2 score of each simulation is displayed, together with a dashed line representing a perfect correlation. It is notable the shifting in temperature from simulation 1 to 6, what is expected, according to figure 4.1, which shows the temperature shifting during the year. Besides that, the performance of the simulation also drops significantly,

Table 4.1 – Time range of rail temperature simulations in Mirandela.

Simulation	From	To	Duration	Sample size
1	2020/07/23	2020/07/29	6 days	1920
2	2020/08/03	2020/09/12	40 days	11 723
3	2020/09/13	2020/09/30	17 days	5098
4	2020/10/07	2020/10/24	17 days	5100
5	2020/11/12	2021/01/12	61 days	17 772
6	2021/01/13	2021/02/15	33 days	9709

what indicates that for specific weather conditions the model does not behave well.

Figure 4.8 – Correlation between measured and simulated rail temperatures in Mirandela.

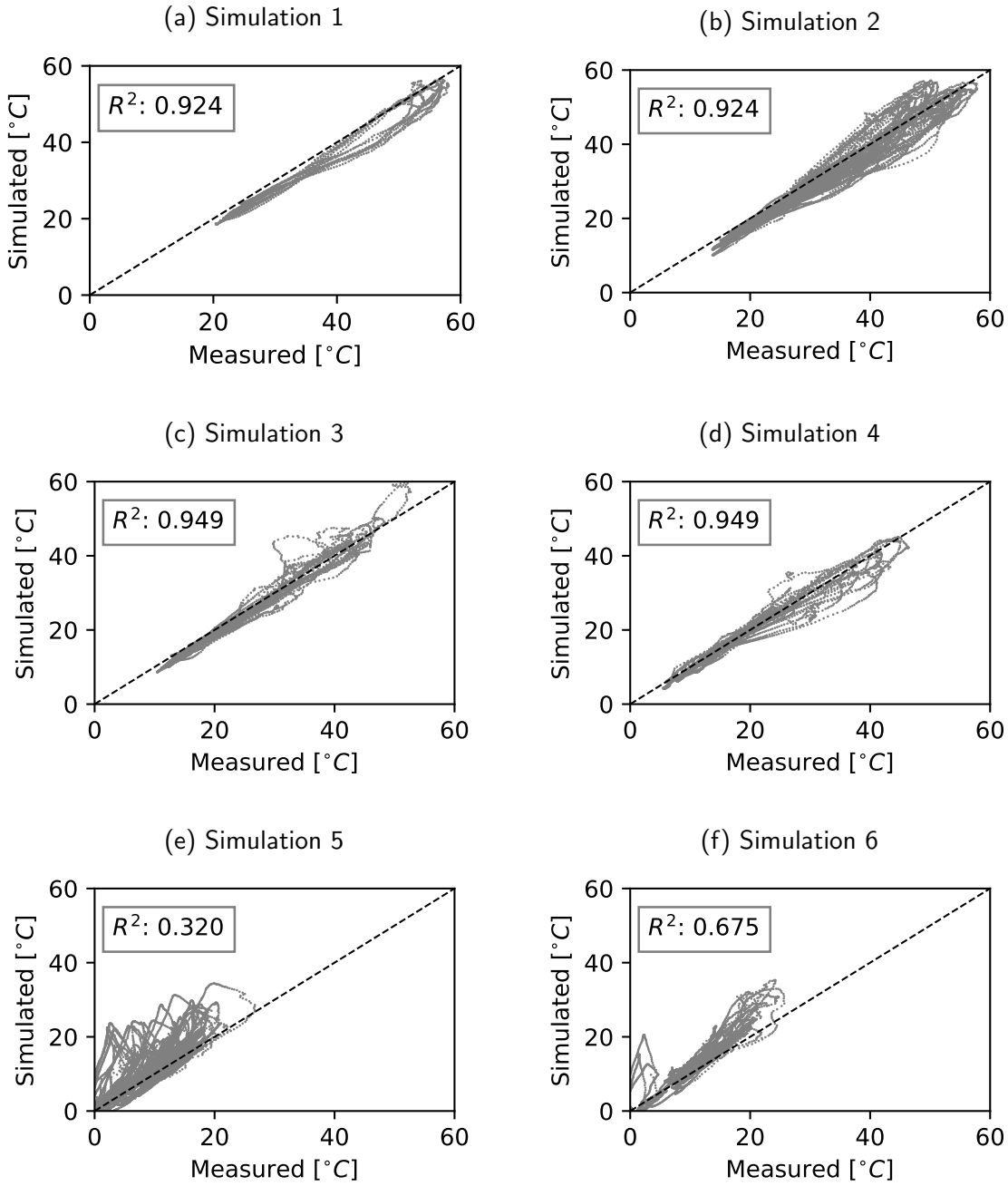

In order to understand what causes the drop in performance of the model, a summary of the weather parameters of each simulation is presented in table 4.2. The data were aggregated to daily values, in order to verify the behaviour of the simulated days. The standard deviation of the daily solar energy correlates with the number of cloud covered days during this period. From simulation 1, it is notable that the deviation is low, what may indicate that for clear sky days the model behaves well. As an opposite example, simulations 5 and 6 present a high deviation compared to their average value and their correlation factor of the simulations are lower than the other.

However, the wind speed may also have a great influence on the model's performance, since the simulation 5 has the lowest daily average value and also the lowest R^2 score. Perhaps the equation (eq. 2.10) to correlate the wind speed and convection coefficient needs further investigation.

Table 4.2 – Weather summary of simulation in Mirandela.

Simulation	**Solar energy ($MJ\,m^{-2}$)**		**Wind speed ($m\,s^{-1}$)**		**Air temp. (°C)**	
	avg	**std**	**avg**	**std**	**avg**	**std**
1	29.90	0.45	1.20	0.25	29.45	1.71
2	24.58	4.70	0.94	0.62	24.39	3.05
3	18.90	3.95	0.69	0.44	19.89	3.26
4	13.88	5.33	0.65	0.44	15.16	2.37
5	6.35	3.04	0.48	0.43	8.02	4.29
6	6.09	3.65	0.80	0.66	9.23	5.42

From figure 4.8 it is clear that the model does not have a good correlation under all weather conditions and a further analysis must take place to understand in which circumstance it can not be used. Still by concatenating all simulations and performing the correlation analysis, the model reached a R^2 score of 0.932 and mean squared error ($RMSE$) of 3.38 °C, within a total sample of 51 322 data points.

Worth it also to analyze the ability of the model to predict the daily maximum temperature. Figure 4.9 shows daily values of predicted and measured rail temperatures and its R^2 score, which reach a value of 0.876. The figure shows that the model predicts reasonable values of rail temperature over 30 °C. However, below this threshold, there is a great spread between the data.

In general, the CNU model presented good capability of predicting rail temperatures, however further investigation is necessary to understand under which weather combination the model needed to be improved, according to figure 4.8. In addition, the overall performance of the model reached similar values as reported by Hong *et al.* [36] (R^2 of 0.93 and $RMSE$ of 3.8 °C - table 2.8). The mean squared error shows slight difference between this work and Hong's work,

Figure 4.9 – Correlation of predicted and simulated daily maximum rail temperatures.

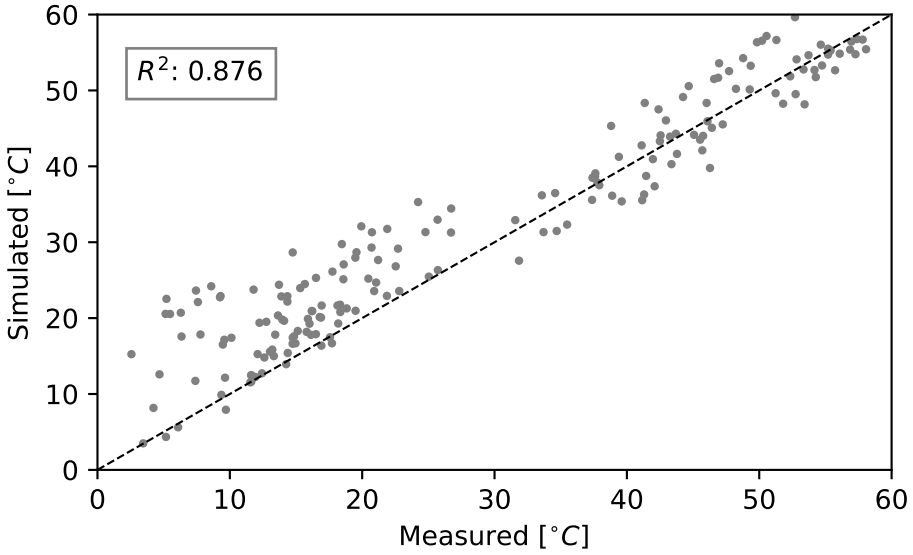

meanwhile the R^2 are almost equal. Regarding the maximum daily predicted temperatures, the model also shows a good prediction capability.

4.2.3 *Rail Temperatures in Portugal*

As mentioned, in order to estimate the maximum rail temperatures across Portugal, weather data from IPMA were utilized. As a remark, among four year of hourly weather information, only a few days were utilized. The days with the highest air temperature in each location were selected. The results of the simulation are presented in figure 4.10 and besides that, the lines represent the main railway tracks of Portugal. The results were interpolated for the extend of the continental territory of Portugal utilizing inverse distance weighting method.

Weighting is assigned to sample points through the use of a weighting coefficient that controls how the weighting influence will drop off as the distance from new point increases. The greater the weighting coefficient, the less the effect points will have if they are far from the unknown point during the interpolation process. As the coefficient increases, the value of the unknown point approaches the value of the nearest observational point [56].

Similarly to the weather summary of simulations in Mirandela, table 4.3 shows the weather summary of the simulations in the cities.

The temperatures presented in figure 4.10 can be considered a good estimate taking into account the accuracy of the model reported on section 4.2.2. Only by measuring rail temperature in these locations and simulating it with mutual weather information the validation of these

temperatures are possible. This may be subject for further investigation. This would also help to further validate the usability of the model in other locations.

Table 4.3 – Weather summary of simulation in other cities.

City	Solar energy ($MJ\,m^{-2}$)		Wind speed ($m\,s^{-1}$)		Air temp. (°C)	
	avg	std	avg	std	avg	std
Alvega	24.69	1.44	1.74	0.25	30.55	2.36
Coimbra	25.09	2.77	1.92	0.22	27.72	4.26
Evora	15.31	10.52	2.20	0.66	24.56	2.84
Guarda	29.39	1.49	2.73	0.45	28.78	1.71
Lisboa	25.20	1.23	2.81	0.74	30.61	4.14
Porto	25.00	1.41	3.99	1.01	24.14	3.25

Figure 4.10 – Interpolated maximum rail temperatures for continental Portugal.

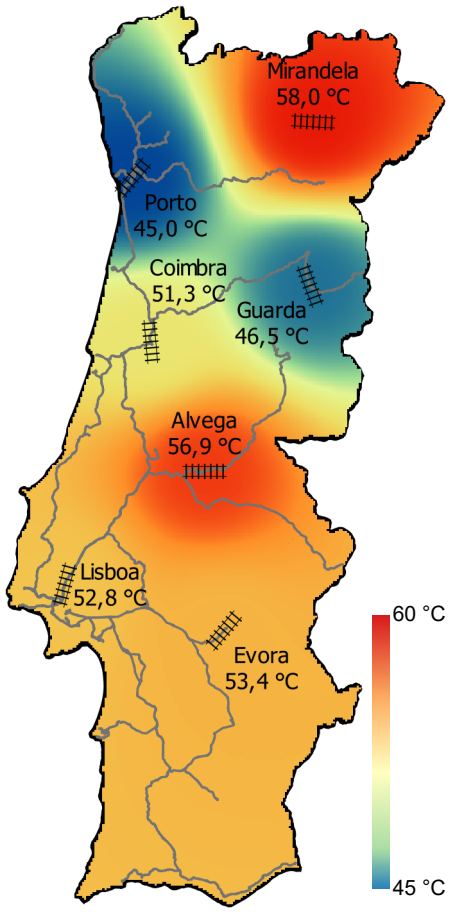

4.3 Mechanical Simulations - Rail Buckling

It is important to mention that this 3D model analysis only considers the lateral deflection deflection (buckling in a 2D plane), although studies have shown that this phenomena happens in three dimensions, as discussed in section 2.6. Another limitation of the present work is that there are no vertical loads, hence there were no need to model a winkler foundation (see fig. 2.26), which means that this is a static thermal non linear geometrical and material analysis.

Another important fact is that, as mentioned in section 2.6.3, Ansys could not solve the full buckling curve, and during the unstable path an horizontal line appears, meaning that this is the the snap-through movement. When the solver reaches a stable equilibrium position, it starts to increase again. This fact has been reported by Carvalho [42].

As a remark, the safe temperature is defined at the value where buckling may occur given enough extra energy to the track and the buckling temperature is defined where small energy input will lead the track to buckle. Also there are two types of responses: explosive and progressive buckling, where the first these two temperatures are well defined and the progressive response shows no difference between the two temperature parameters. This is defined in figure 2.22.

With these two facts, the analysis presented in this section can not determine the safe temperature, since the unstable path of the buckling response can not be determined utilizing this methodology. However, on the other hand, the buckling temperature is well defined by analyzing the lateral deflection by increasing track temperature.

The results presented in this section correspond to the lateral deformation of the central span of the rail, on the sleeper-rail junction. As a remark, since at these junctions there are two nodes at same coordinates, only the "upper" node (or rail node, see fig. 3.20) was utilized to extract displacement and rotation data to be later compared within all the 144 simulations. Figure 4.11 shows an example of Ansys contour plot for lateral displacement and the point utilized to extract the results. All results can be found in appendix D.

The analysis have shown that among all analyzed parameters the ones that play an important role on the buckling temperature are three: imperfection (L_o), ballast resistance and fastener torsional resistance. Elasticity modulus of the sleeper, gauge and profile have shown no great difference when determining the critical temperature. Furthermore, it was noted that the steel reaches the plastic behaviour before reaching the buckling temperature, meaning that from a certain temperature, permanent displacement will happen.

Figures 4.12 and 4.13 shows the buckling response, where y axis displays the temperature (°C) and x axis the lateral displacement (m) for different sleepers, gauges and rail profiles, the other

Figure 4.11 – Example - Contour plot x-axis.

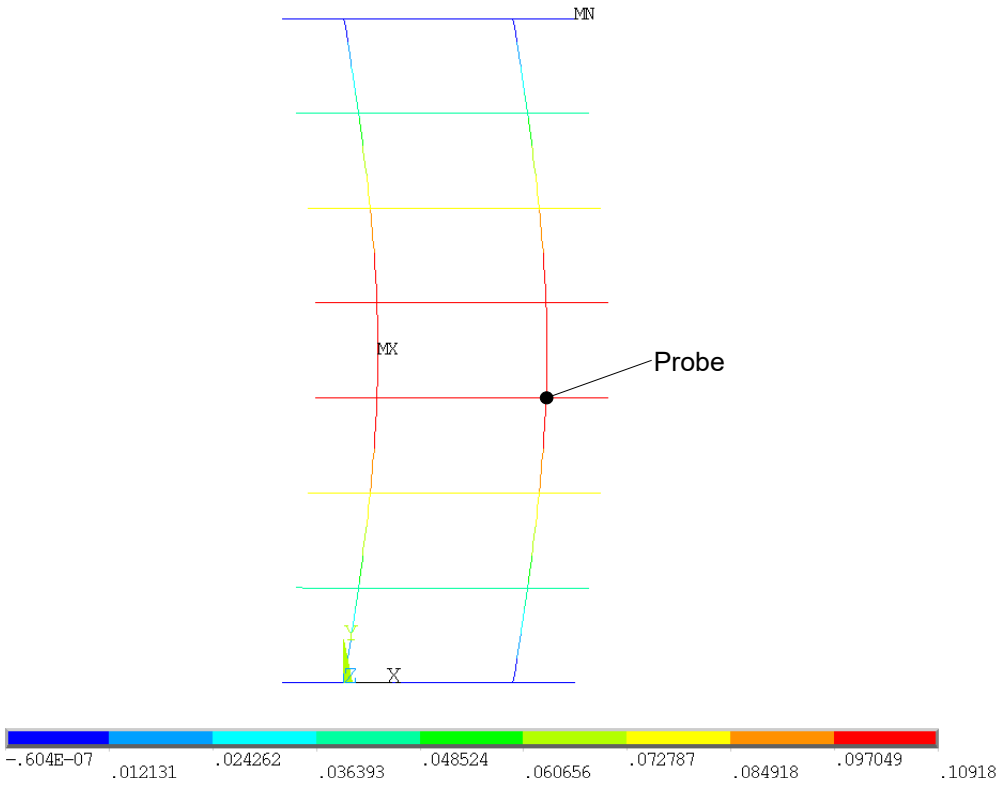

three parameters are displayed on top of the plot. From these figure it is possible to notice that the gauge and the sleeper longitudinal elasticity do not affect the buckling temperature. However, when it comes to different profiles, little difference can be seen for strong ballast, meanwhile for weak ballast this is not the case anymore.

Furthermore from these figures is it possible to identify the critical temperatures. In case of strong ballast, the value is in the range of 110 °C to 125 °C. Meanwhile for weak ballast, it is a single value of 60 °C. Which is very close to the maximum measured temperature in Mirandela, as mentioned in section 4.1.

Figure 4.14 shows important parameters that affect the buckling temperature. As expected, the initial miss-alignment of the track is the most important parameter and it follows an inverse relation: The higher the imperfection, the lower the buckling temperature. Following, the ballast quality also plays a very important role. When it has weak or poor quality, the simulations show that buckling temperatures are bellow 100 °C. The same behaviour is seen with different profiles and gauges.

Still from figure 4.14 in some cases for weak ballast a progressive buckling takes places, where no sudden movement happens and the displacement increase gradually. This situation occur for poor track conditions, as discussed in section 2.6.

Figure 4.12 – Buckling curve for different sleeper, gauge and profiles.

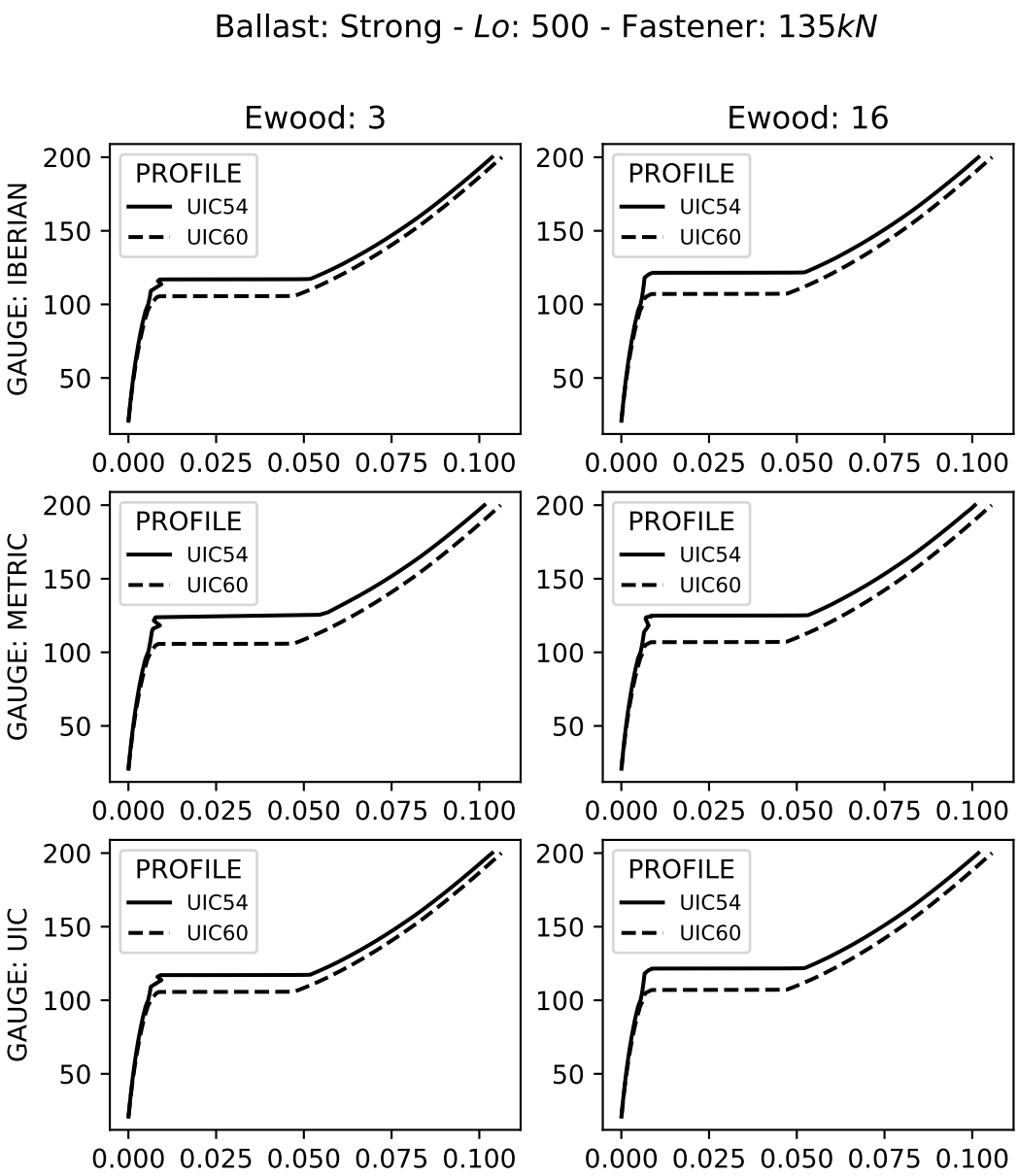

In summary, these analyses are in accordance with important parameters stated by Van [3]. Unfortunately, the safe temperature could not be determined, however, it can be calculated by using analytical solution or hybrid methods, as described by Carvalho *et al.* [57] and Carvalho [42]. Still, since previous models have shown that the safe temperature is bellow the buckling threshold, one can expect that if a track lacks maintenance, this phenomena can occur, given the temperatures measured in Mirandela, reaching almost 60 °C.

Figure 4.13 – Buckling curve for different sleeper, gauge and profiles.

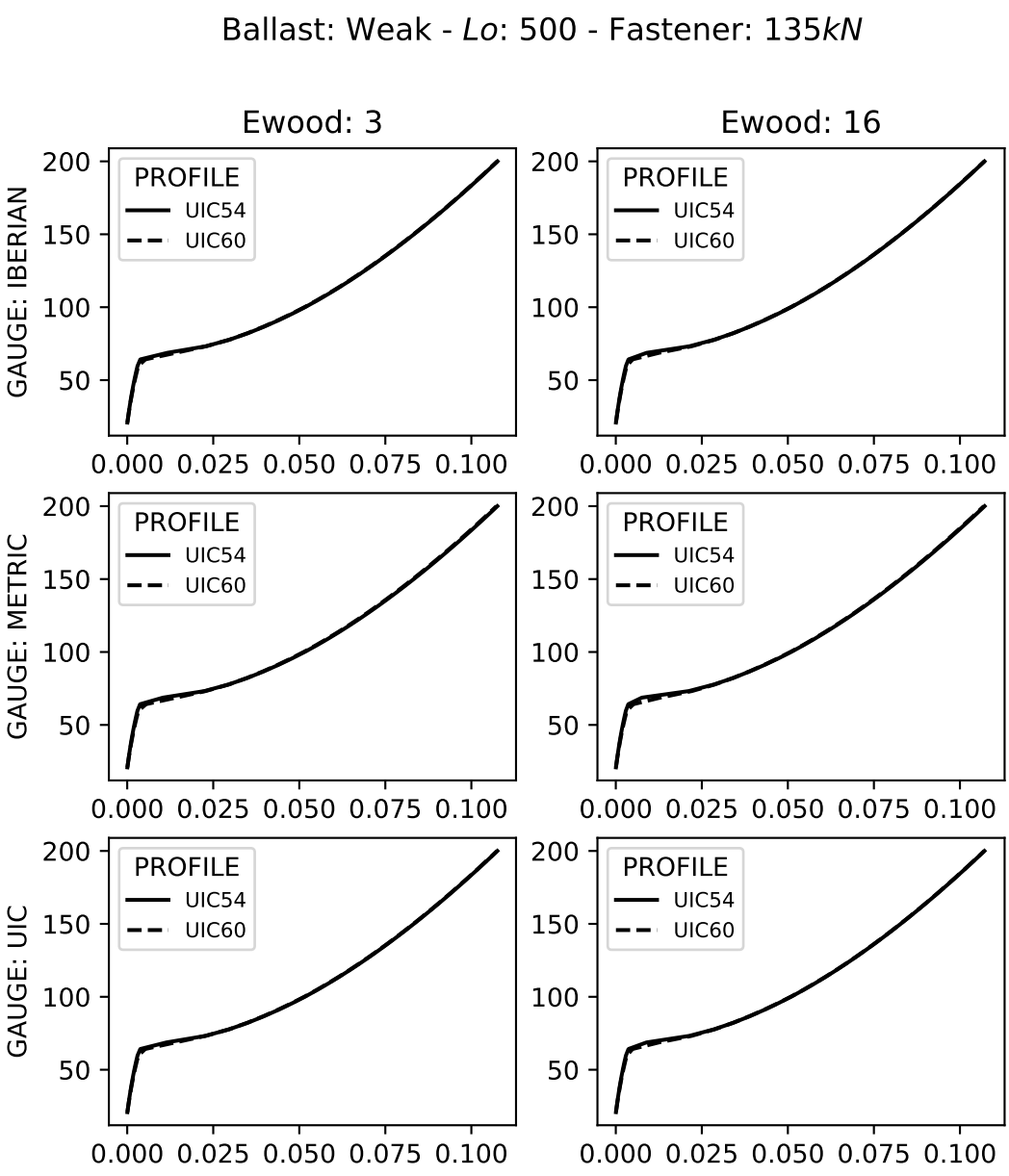

Figure 4.14 – Buckling curve for different ballasts, fasteners and imperfections.

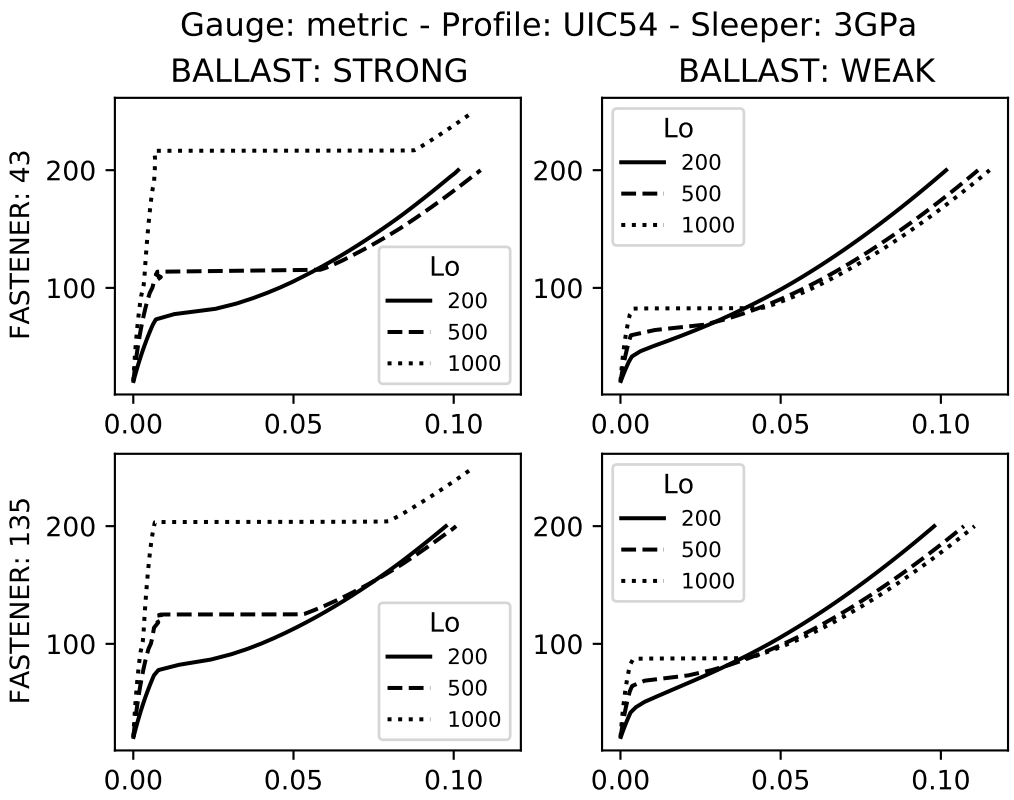

5 CONCLUSION AND FUTURE WORKS

This section summarizes all the achievements of the work and discuss the further improvements and which topics could be better explored in order to reach better results, both in thermal and mechanical analysis.

5.1 Conclusion

The present work has discussed about two main topics about thermal buckling of railways. First thermal model was discussed, including empirical relations and physical models, in order to predict rail temperatures to be used in thermal buckling studies, based on the current and also predicted weather conditions. Then an previous model was improved by researchers at Chungnam National University (CNU) [36], by including the effect of the sun's position. Second, mechanical analysis were conducted to study the buckling behaviour under various track conditions.

In order to validate the usage of this model to simulate and predict rail temperatures, a segment of a rail track in the city of Mirandela-Portugal was instrumented with thermocouples, as well as a weather station nearby. Besides that a software called *railtemp* was developed utilizing Python programming language in a format of a package to automate and facilitate the process of fetching solar data (elevation and azimuth) and also solving the differential equation of the CNU model. Furthermore, a thermal finite element model was utilized to validate the solving process of the package and both solutions are in good agreement, meaning that the package can be used to perform such analysis.

When compared to measured rail temperatures, the model features high correlation factors (R^2), reaching up to 0.949 for some simulations. However, for some weather conditions, the correlation drops to 0.320 (subject for future works). The overall performance, when comparing all simulations and measured data, reached a R^2 score of 0.932 and a $RMSE$ of 3.38 °C. By analyzing only the capability of the model to predict daily maximum rail temperatures, the R^2 score is 0.876.

Regarding the buckling analysis, they have demonstrated that the ballast quality, track's initial miss alignment and fastening resistance are the most important parameters when determining the buckling temperature of railways. In case of poor ballast quality, simulations have shown that the buckling occurs around 65 °C, which can already triggers concern, since the maximum registered temperature in Mirandela was near 60 °C.

These results shows that track maintenance should be always up to date in order to avoid buckling problems. As a remark the present study has analyzed only static buckling, which according to studies, may overestimate the critical temperature, meaning that it can happen bellow the values presented here. This may be subject for further study.

5.2 Future Works

As mentioned above, understanding on what weather combination the CNU model can be used with a good confidence level can be subject of further studies. Furthermore, combing the model with weather forecast model creating future prediction and then comparing with actual measurements could complete validate the usage of this model to predict rail temperatures. Also, creating an Graphical User Interface (GUI) for the *railtemp* package would facilitate even more the usage of such a tool.

Furthermore, by experimentally assessing physical parameters of the model, such as the convection coefficient (h_Pconv) and the rail emissivity (ϵ) can possibly improve the results of the model.

Beside that, since a continuous monitoring of the rail temperature is intended with the *IoT* device that was briefly discussed, a large amount of data are being collected and will continue to further enable advanced statistical analysis of the data. Preliminary investigations have shown that machine learning techniques such as artificial neural networks can be used to predict rail temperatures.

Regarding mechanical analysis, improvements can be made by considering dynamic buckling and instead of a 2-D plane analysis, perform three dimensional simulations. Also, utilizing approaches to characterize the full buckling curve, since Ansys still cannot solve the unstable path of the solution. This can be achieved by using another FEM software or by hybrid solution as discussed.

Also, by conducting buckling experiments in laboratory, subjecting rail profiles under thermal loads utilizing electric resistance wires could validate the mechanical simulations of this work.

By assessing the parameters that were used, with experiments on the local track would help to determine critical conditions of the track and also improve the results, both for mechanical and thermal simulations.

BIBLIOGRAPHY

[1] C. F. Bonnett, *Practical railway engineering*, 2. ed. Imperial College Press, 2005, ISBN: 1-86094-515-5.

[2] C. E. L. Paiva, *Super e Infraestruturas de Ferrovias*. Campus, 2014, 328 pp., ISBN: 85-352-8039-1.

[3] M. A. Van, "Buckling analysis of continuous welded rail track", *Heron*, vol. 41, no. 3, pp. 175–186, 1996.

[4] Y. Wu, P. Munro, M. G. Rasul, and M. K. M. Khan, "A Review on Recent Developments in Rail Temperature Prediction for use in Buckling Studies", in *Conference on Railway Engineering*, Wellington, Sep. 12, 2010.

[5] J. E. S. C. Branco, "A Segregação da Infra-Estrutura como Elemento Reestruturador do Sistema Ferroviário Brasileiro", PhD thesis, UFRJ, 2008.

[6] M. Lewis, "Railway in the greek and roman world", 2001.

[7] M. Hallberg, *Railroads in north america*, Dec. 21, 2009. [Online]. Available: http://www.personal.psu.edu/faculty/m/c/mch/railroad/ (visited on 08/31/2020).

[8] L. Scaggiante, "Le strade ferrate: l'Italia preunitaria e gli elementi dell'identità nazionale", Mar. 7, 2014, Accepted: 2014-02-05 Publisher: Università Ca' Foscari Venezia. [Online]. Available: http://dspace.unive.it/handle/10579/4403 (visited on 09/01/2020).

[9] N. M. G. Teixeira, "Sistemas de Transporte Ferroviário: Evolução e perspetivas de desenvolvimento", Accepted: 2018-03-09T11:54:43Z, M.S. thesis, 2016. [Online]. Available: https://recipp.ipp.pt/handle/10400.22/11089 (visited on 09/01/2020).

[10] Imperial War Museums, *Transport and supply during the first world war*. [Online]. Available: https://www.iwm.org.uk/history/transport-and-supply-during-the-first-world-war (visited on 09/02/2020).

[11] Directorate-General for Mobility and Transport, *EU transport in figures : statistical pocketbook 2019*. Office for Official Publications of the European Communities, Oct. 11, 2019, ISBN: 978-92-76-03843-6 978-92-76-03842-9. [Online]. Available: http://op.europa.eu/en/publication-detail/-/publication/f0f3e1b7-ee2b-11e9-a32c-01aa75ed71a1 (visited on 10/01/2020).

[12] OpenRailwayMap contributors. (2017). OpenRailwayMap, [Online]. Available: https://www.openrailwaymap.org/ (visited on 04/15/2021).

[13] Steer Davies Gleave, *Study on the cost and contribution of the rail sector*, 2015. [Online]. Available: https://ec.europa.eu/transport/sites/transport/files/modes/rail/studies/doc/2015-09-study-on-the-cost-and-contribution-of-the-rail-sector.pdf (visited on 10/05/2020).

[14] D.-G. for Mobility {and} Transport, *EU transport in figures: statistical pocketbook 2015*. Luxembourg: Office for Official Publications of the European Communities, 2015, OCLC: 930773071, ISBN: 978-92-79-43915-8.

[15] European Commission, *Roadmap to a Single European Transport Area – Towards a competitive and resource efficient transport system*, Mar. 28, 2011. [Online]. Available: https://eur-lex.europa.eu/legal-content/EN/ALL/?uri=CELEX:52011DC0144 (visited on 10/02/2020).

[16] D. A. T. Carmona, "Contributo Biobibliográfico para o estudo do Caminho-de-ferro em Portugal (1856 – 2006)", Accepted: 2013-03-19T16:12:34Z, M.S. thesis, 2013. [Online]. Available: https://recil.grupolusofona.pt/handle/10437/3287 (visited on 10/08/2020).

[17] OpenStreetMap contributors. (2017). OpenStreetMap, OpenStreetMap, [Online]. Available: https://www.openstreetmap.org/ (visited on 04/16/2021).

[18] Comboios de Portugal. (). Cronologia | CP - Comboios de Portugal, CP.PT | Comboios de Portugal, [Online]. Available: https://www.cp.pt/institucional/pt/cultura-ferroviaria/historia-cp/cronologia (visited on 10/19/2020).

[19] Instituto Nacional de Estatísticas, "Estatísticas dos Transportes e Comunicações: 2018", INE, Lisboa, 2019. [Online]. Available: https://www.ine.pt/xurl/pub/358630755 (visited on 10/20/2020).

[20] M. Lopes, *A REDE FERROVIÁRIA DO SÉCULO XXI*, Nov. 28, 2011. [Online]. Available: http://cip.org.pt/wp-content/uploads/2017/01/Ref-18.pdf (visited on 10/19/2020).

[21] Revista Cargo. (Aug. 31, 2020). IP: 'Ferrovia 2020' com 78% do investimento em fase de obra ou já finalizado | Revista Cargo, Revista Cargo - Transportes e Logística, [Online]. Available: https://revistacargo.pt/ip-ferrovia-2020-com-78-do-investimento-em-fase-de-obra-ou-ja-finalizado/ (visited on 10/21/2020).

[22] ——, (Oct. 13, 2020). Plano Ferroviário: Executivo pretende ferrovia a ligar todas as capitais de distrito | Revista Cargo, Revista Cargo - Transportes e Logística, [Online]. Available: https://revistacargo.pt/plano-ferroviario-2021-executivo-pretende-ferrovia-a-ligar-todas-as-capitais-de-distrito/ (visited on 10/21/2020).

[23] E. M. C. Fortunato, "Renovação de plataformas ferroviárias : estudos relativos à capacidade de carga", Accepted: 2012-07-27T01:53:05Z, PhD thesis, 2005. [Online]. Available: https://repositorio-aberto.up.pt/handle/10216/11441 (visited on 11/09/2020).

[24] American Railway Engineering and Maintenance-of-way Association, *Manual for Railway Engineering*, 4 vols. USA, 2010, vol. 1 - Track.

[25] A. S. C. Moreira, "Métodos de dimensionamento de vias-férreas", Accepted: 2015-07-14T14:10:25Z, M.S. thesis, 2014. [Online]. Available: http://repositorium.sdum.uminho.pt/ (visited on 11/09/2020).

[26] V. Profillidis, *Railway Management and Engineering*, 4th edition. Farnham, Surrey, England: Routledge, Mar. 31, 2016, 552 pp., ISBN: 978-1-4094-6463-1.

[27] M. R. S. V. D. Leite, "Especificações Técnicas da Via-Férrea", Accepted: 2018-10-09T15:46:34Z, M.S. thesis, 2017. [Online]. Available: https://recipp.ipp.pt/handle/10400.22/12054 (visited on 09/01/2020).

[28] *Pandrol*, in *Wikipedia*, Page Version ID: 946559077, Mar. 20, 2020. [Online]. Available: https://en.wikipedia.org/w/index.php?title=Pandrol&oldid=946559077 (visited on 11/28/2020).

[29] L. Chapman, J. E. Thornes, Y. Huang, X. Cai, V. L. Sanderson, and S. P. White, "Modelling of rail surface temperatures: A preliminary study", *Theoretical and Applied Climatology*, vol. 92, no. 1, pp. 121–131, 2008, Publisher: Springer Wien, ISSN: 14344483. DOI: 10.1007/s00704-007-0313-5.

[30] S. U. Hong, H. Jung, C. Park, H. Lee, H. U. Kim, N. H. Lim, H. U. Bae, K. H. Kim, H. J. Kim, and S. J. Cho, "Prediction of a representative point for rail temperature measurement by considering longitudinal deformation", *Proceedings of the Institution of Mechanical Engineers, Part F: Journal of Rail and Rapid Transit*, vol. 233, no. 10, pp. 1003–1011, 2019, Publisher: SAGE Publications Ltd, ISSN: 20413017. DOI: 10.1177/0954409718822866.

[31] B. Marmash and M. Ryan, "Management of stressed continuously welded track. rail stress free temperature measurement techniques (t359 report)", RSSB, UK, PB009533, 2006.

[32] G. Hunt, "An analysis of track buckling risk", British Railways, Internal Report RRTM013, 1994.

[33] C. Esveld, *Modern railway track*, 2. ed, in collab. with T. U. Delft. Zaltbommel: MRT-Productions, 2001, 654 pp., OCLC: 249551699, ISBN: 978-90-800324-3-9.

[34] P. Munro, *Management of track infrastructure in hot weather: a practical application*, 2009.

[35] Y.-J. Zhang and S. Lee, "Modeling rail temperature with real-time weather data", in *Transportation Research Circular*, ser. E-C126, ISSN: 0097-8515 Issue: E-C126 Number: Weather08-001, Indianapolis, Indiana, Jun. 16, 2008. [Online]. Available: https://trid.trb.org/view/863329 (visited on 12/21/2020).

[36] S. U. Hong, H. U. Kim, N. H. Lim, K. H. Kim, H. Kim, and S. J. Cho, "A Rail-Temperature-Prediction Model Considering Meteorological Conditions and the Position of the Sun", *International Journal of Precision Engineering and Manufacturing*, vol. 20, no. 3, pp. 337–346, 2019, Publisher: SpringerOpen, ISSN: 20054602. DOI: 10.1007/s12541-019-00015-1.

[37] J. E. Thornes, "The prediction of ice formation on motorways in Britain", Publication Title: Doctoral thesis, University of London., Doctoral, University of London, 1984, 404 pp. [Online]. Available: https://discovery.ucl.ac.uk/id/eprint/1348922/ (visited on 12/19/2020).

[38] K. Kesler and Y.-J. Zhang, "System and method for predicting future rail temperature", U.S. Patent 20070265780A1, Nov. 15, 2007.

[39] EN 1993-1-2, *Eurocode 3: Design of steel structures - part 1-2: General rules - structural fire design*, 2005.

[40] J. Michalsky, "The Astronomical Almanac's algorithm for approximate solar position (1950–2050)", *Solar Energy*, vol. 40, pp. 227–235, Dec. 31, 1988. DOI: 10.1016/0038-092X(88)90045-X.

[41] A. Kish and G. Samavedam, "Track buckling prevention: Theory, safety concepts, and applications track systems safety", U.S Departament of Transportation, Cambridge, Mar. 2013, p. 168. [Online]. Available: www.fra.dot.gov..

[42] J. F. C. V. d. Carvalho, "Estabilidade estrutural da via ferroviária", 2010, Accepted: 2012-02-08T02:30:45Z. [Online]. Available: https://repositorio-aberto.up.pt/handle/10216/57680 (visited on 01/21/2021).

[43] N.-H. Lim, N.-H. Park, and Y.-J. Kang, "Stability of continuous welded rail track", *Computers & Structures*, vol. 81, no. 22, pp. 2219–2236, Sep. 1, 2003, ISSN: 0045-7949. DOI: 10.1016/S0045-7949(03)00287-6. [Online]. Available: https://www.sciencedirect.com/science/article/pii/S0045794903002876 (visited on 02/15/2021).

[44] G. Samavedam, A. Kish, A. Purple, and J. Schoengart, "Parametric analysis and safety concepts of CWR track buckling", U.S Departament of Transportation, Springfield, VA 22161, Dec. 1993, p. 120. [Online]. Available: https://railroads.dot.gov/elibrary/parametric-analysis-and-safety-concepts-cwr-track-buckling (visited on 01/18/2021).

[45] A. d. Iorio, M. Grasso, F. Penta, G. P. Pucillo, S. Rossi, and M. Testa, "On the ballast-sleeper interaction in the longitudinal and lateral directions", *Proceedings of the Institution of Mechanical Engineers, Part F: Journal of Rail and Rapid Transit*, vol. 232, no. 2, pp. 620–631, 2018, Number: 2, ISSN: 20413017. DOI: 10.1177/0954409716682629. (visited on 02/04/2021).

[46] J. Maximov, G. Duncheva, I. Amudjev, A. Anchev, and N. Ganev, "A new approach for pre-stressing of rail-end-bolt holes", *Proceedings of the Institution of Mechanical Engineers, Part C: Journal of Mechanical Engineering Science*, vol. 231, no. 12, pp. 2275–2283, Jun. 2017, ISSN: 0954-4062, 2041-2983. DOI: 10.1177/0954406216630003. [Online]. Available: http://journals.sagepub.com/doi/10.1177/0954406216630003 (visited on 10/01/2020).

[47] C. D. P. Pinto, "Caracterização das propriedades físicas e mecânicas da madeira de pinho bravo e de freixo do nordeste transmontano", Accepted: 2015-01-20T09:44:42Z, M.S. thesis, 2014. [Online]. Available: https://bibliotecadigital.ipb.pt/handle/10198/11598 (visited on 11/18/2020).

[48] C. L. Santos, A. M. P. d. Jesus, J. J. L. Morais, and J. L. P. C. Lousada, "Bearing properties of portuguese pine wood beneath a laterally loaded dowel", *Ciência & Tecnologia dos Materiais*, vol. 20, no. 1, pp. 45–51, Jan. 2008, ISSN: 0870-8312. [Online]. Available: http://www.scielo.mec.pt/scielo.php?script=sci_abstract&pid=S0870-83122008000100007&lng=en&nrm=iso&tlng=en (visited on 01/15/2021).

[49] R. J. Ross and F. P. L. USDA Forest Service., "Wood handbook : Wood as an engineering material", U.S. Department of Agriculture, Forest Service, Forest Products Laboratory, Madison, WI, FPL-GTR-190, 2010, FPL–GTR–190. DOI: 10.2737/FPL-GTR-190. [Online]. Available: https://www.fs.usda.gov/treesearch/pubs/37440 (visited on 03/08/2021).

[50] I. Reda and A. Andreas, "Solar Position Algorithm for Solar Radiation Applications (Revised)", National Renewable Energy Lab. (NREL), Golden, CO (United States), NREL/TP-560-34302, Jan. 1, 2008. DOI: 10.2172/15003974. [Online]. Available: https://www.osti.gov/biblio/15003974 (visited on 04/28/2021).

[51] SciPy 1.0 Contributors, P. Virtanen, R. Gommers, T. E. Oliphant, M. Haberland, T. Reddy, D. Cournapeau, E. Burovski, P. Peterson, W. Weckesser, J. Bright, S. J. van der Walt, M. Brett, J. Wilson, K. J. Millman, N. Mayorov, A. R. J. Nelson, E. Jones, R. Kern, E. Larson, C. J. Carey, İ. Polat, Y. Feng, E. W. Moore, J. VanderPlas, D. Laxalde, J. Perktold, R. Cimrman, I. Henriksen, E. A. Quintero, C. R. Harris, A. M. Archibald, A. H. Ribeiro, F. Pedregosa, and P. van Mulbregt, "SciPy 1.0: Fundamental algorithms for scientific computing in python", *Nature Methods*, vol. 17, no. 3, pp. 261–272, Mar. 2020, ISSN: 1548-7091, 1548-7105. DOI: 10.1038/s41592-019-0686-2. [Online]. Available: http://www.nature.com/articles/s41592-019-0686-2 (visited on 02/04/2021).

[52] W. McKinney, "Data Structures for Statistical Computing in Python", presented at the Python in Science Conference, Austin, Texas, 2010, pp. 56–61. DOI: 10.25080/Majora-92bf1922-00a. [Online]. Available: https://conference.scipy.org/proceedings/scipy2010/mckinney.html (visited on 02/04/2021).

[53] C. R. Harris, K. J. Millman, S. J. van der Walt, R. Gommers, P. Virtanen, D. Cournapeau, E. Wieser, J. Taylor, S. Berg, N. J. Smith, R. Kern, M. Picus, S. Hoyer, M. H. van Kerkwijk, M. Brett, A. Haldane, J. F. del Río, M. Wiebe, P. Peterson, P. Gérard-Marchant, K. Sheppard, T. Reddy, W. Weckesser, H. Abbasi, C. Gohlke, and T. E. Oliphant, "Array programming with NumPy", *Nature*, vol. 585, no. 7825, pp. 357–362, Sep. 17, 2020, ISSN: 0028-0836, 1476-4687. DOI: 10.1038/s41586-020-2649-2. [Online]. Available: http://www.nature.com/articles/s41586-020-2649-2 (visited on 02/04/2021).

[54] F. Perez and B. E. Granger, "IPython: A System for Interactive Scientific Computing", *Computing in Science Engineering*, vol. 9, no. 3, pp. 21–29, May 2007, Conference Name: Computing in Science Engineering, ISSN: 1558-366X. DOI: 10.1109/MCSE.2007.53.

[55] B. Stafford, *pysolar*, version 0.8, Sep. 28, 2018. DOI: 10.5281/zenodo.1461066. [Online]. Available: https://zenodo.org/record/1461066 (visited on 02/02/2021).

[56] QGIS Development Team, *QGIS Documentation*, 2021. [Online]. Available: https://docs.qgis.org/3.16/en/docs/user_manual/index.html (visited on 04/19/2021).

[57] J. Carvalho, J. Delgado, R. Calçada, and R. Delgado, "A NEW METHODOLOGY FOR EVALUATING THE SAFE TEMPERATURE IN CONTINUOUS WELDED RAIL TRACKS", *International Journal of Structural Stability and Dynamics*, vol. 13, no. 2, p. 1 350 016, Mar. 2013, ISSN: 0219-4554, 1793-6764. DOI: 10.1142/S0219455413500168. [Online]. Available: https://www.worldscientific.com/doi/abs/10.1142/S0219455413500168 (visited on 01/20/2021).

Appendix

APPENDIX A – CALIBRATION AND VALIDATION OF IoT DEVICE

Since the working range of temperatures is small, in contrast with the total range of K-type thermocouples, the relation between voltage and temperature was assumed to be linear, as shown in equation A.1. Furthermore, the tabular data available for thermocouples to convert voltage into temperature are provided considering a junction temperature of 0 °C. Hence, a compensation is necessary, since the junction of thermocouple wires and device is not constant.

$$\begin{aligned} T_{tc}(V_{tc}) &= aV_{tc} + b \\ T_{cj}(V_{cj}) &= dV_{cj} + c \end{aligned} \tag{A.1}$$

Since the junction temperature (fig 3.6a) is not 0 °C, the voltage reading corresponds to the voltage of thermocouple wires and junction metals, as demonstrated on equation A.2. The compensation is done by reading the junction temperature and finding the equivalent value of voltage, then is possible to find the real value of V_{tc}. In this case, the relation between junction voltage and temperature is also considered to be linear. Working equations A.1 and A.2 result in equation A.3. This is the function described in figure 3.6b.

$$V_m = V_{tc} - V_{cj} \tag{A.2}$$

$$T_{tc}(V_m) = a\left(V_m + \frac{T_{cj} - c}{d}\right) + b \tag{A.3}$$

From this equation is possible to proceed with a curve fitting using experimental data. Values of V_m and T_{cj} are collected with T-call and T_{tc} is the rail temperature collected with the data logger used on the research. The fitting was done using around 3000 data points. Then the values of the parameters a, b, c and d are programmed into the microcontroller.

After months of collected data both with data logger and TTGO, the correlation of the readings are shown in figure A.1. With around 20 000 data points evaluated, the results are in good accordance. For the purpose of this research, the error is totally acceptable, since small changes lower than the error are expected to have no effect on the rail.

Figure A.1 – IoT equipment - correlation plot

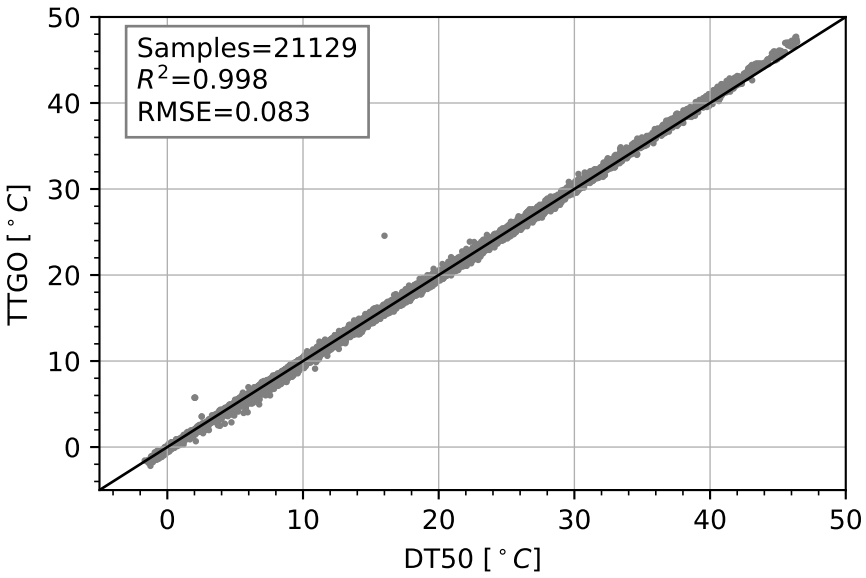

Figure A.2 – IoT device and conventional data logger

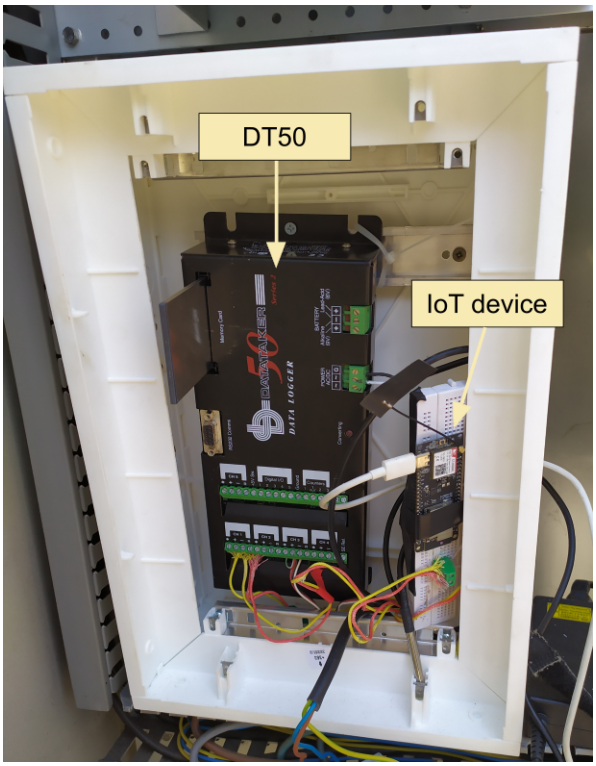

APPENDIX B – EXAMPLE OF RAILTEMP PACKAGE USAGE

```
#Import auxiliary libs
import numpy as np
import pandas as pd

#Import railtemp package
from railtemp import *

#Import weather data from any source
#In this example from a MySQL database
#The data contains the following columns:
#datetime, air, radiation, wind

df = pd.read_sql_query(query,con=mydb)

#Initializing components

#Material definition
steel = RailMaterial(density=7850,
                     solar_absort=0.85,
                     emissivity=0.7)

#Rails
UIC54 = Rail(name='UIC54',
             azimuth=93,lat=41.123,long=-7.123,elev=123,
             cross_area=123,convection_area=123,
             radiation_area=123,
             ambient_emissivity=0.6,
             material=steel)

UIC60 = Rail(name='UIC60',
             azimuth=93,lat=41.123,long=-7.123,elev=123,
             cross_area=123,convection_area=123,
             radiation_area=123,
             ambient_emissivity=0.6,
             material=steel)
```

```
#Weather
weather = WeatherData(solar_radiation=df['radiation'],
                      wind_velocity=df['wind'],
                      ambient_temperature=df['air'],
                      timezone=pytz.timezone('Europe/Lisbon'))

#Creating CNU simulation objects for
#UIC54 and UIC60 and same weather data
simu_uic54 = CNU(UIC54,weather)
simu_uic60 = CNU(UIC60,weather)

#Running the simulations
simu_uic54.run(Trail_initial=20)
simu_uic60.run(Trail_initial=20)

#Results
simu_uic54.result
simu.uic60.result
```

APPENDIX C – SUMMARY OF IPMA WEATHER DATA

Figure C.1 – IPMA temperature data.

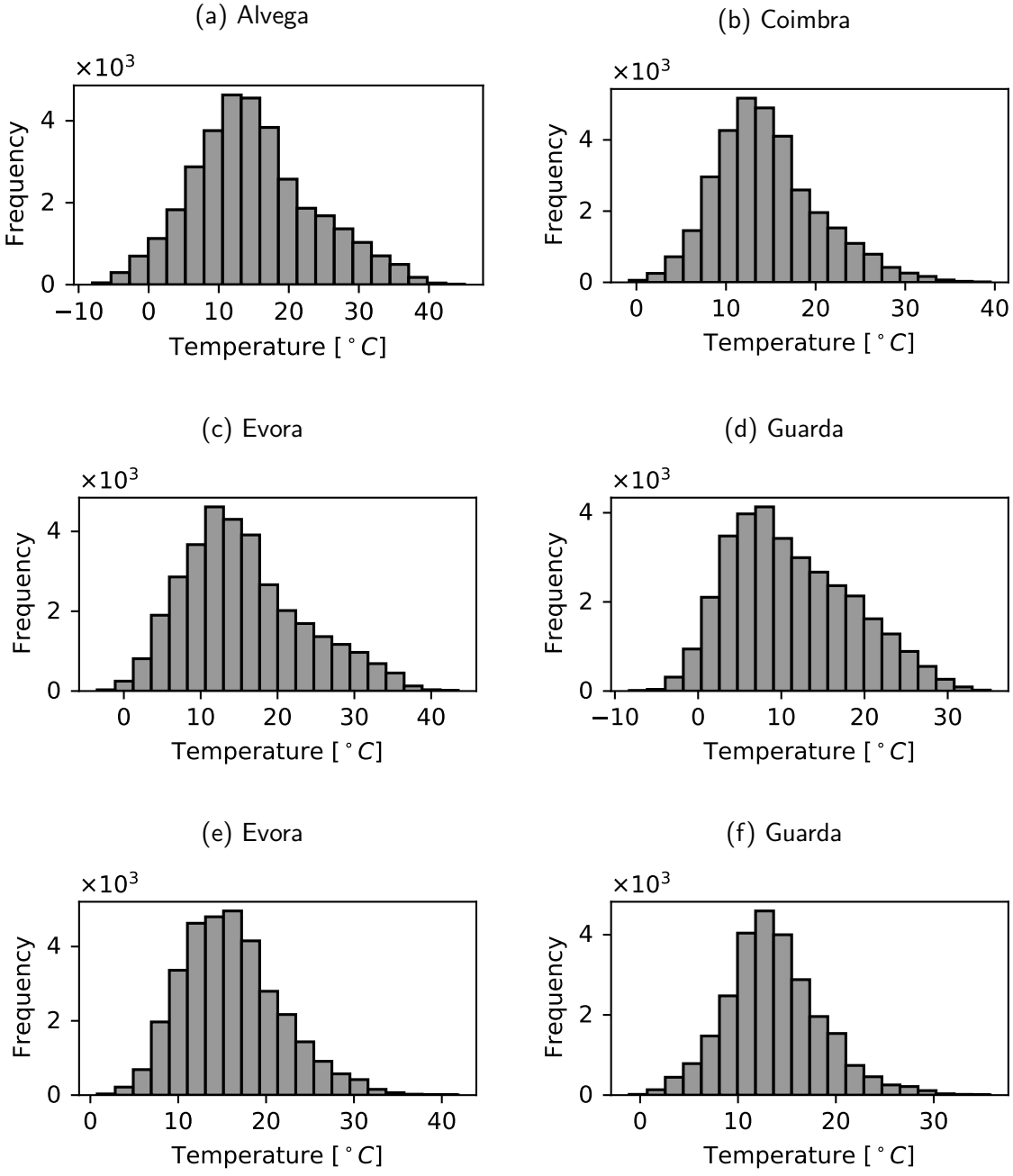

Figure C.2 – IPMA solar radiation data.

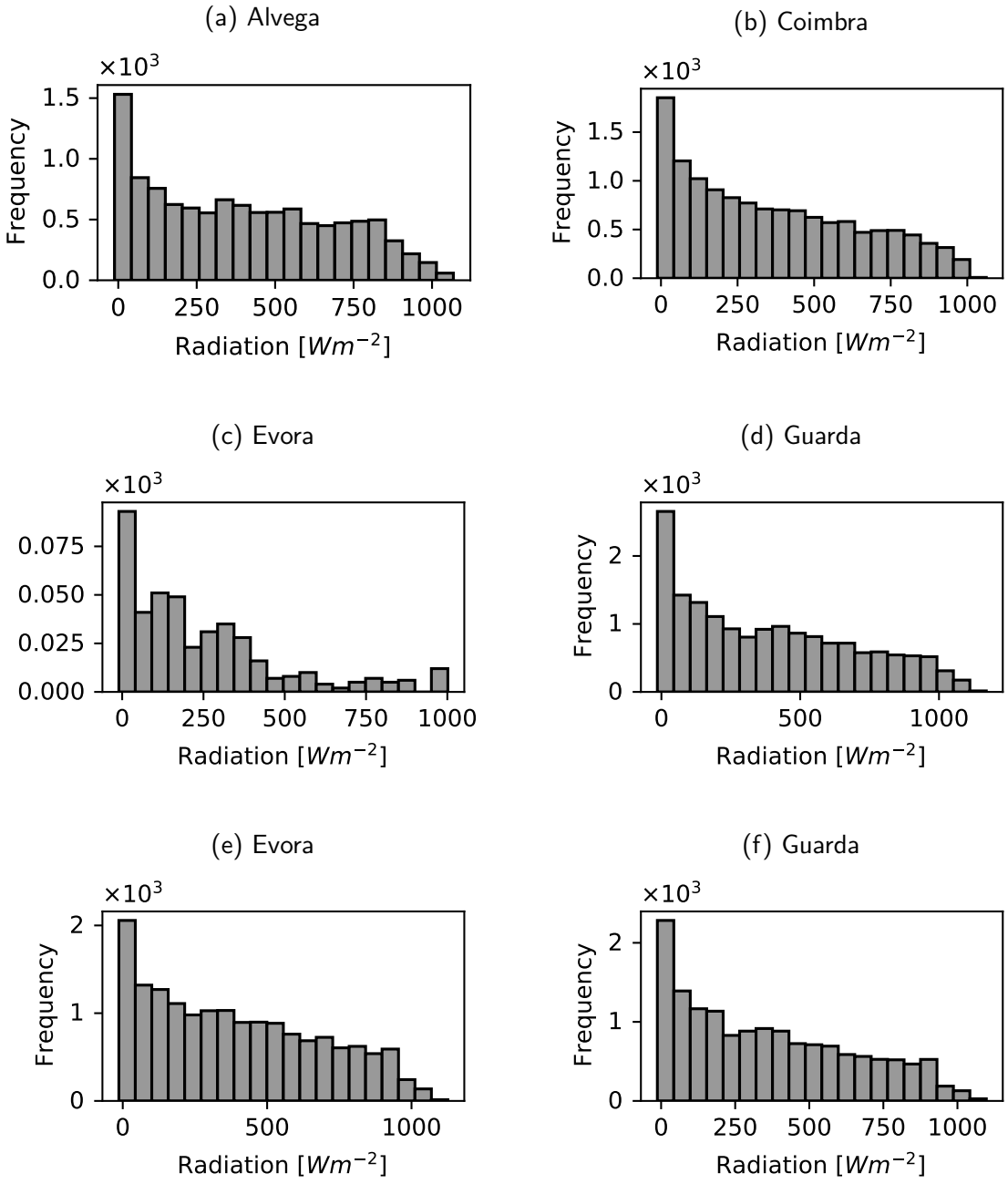

Figure C.3 – IPMA wind data.

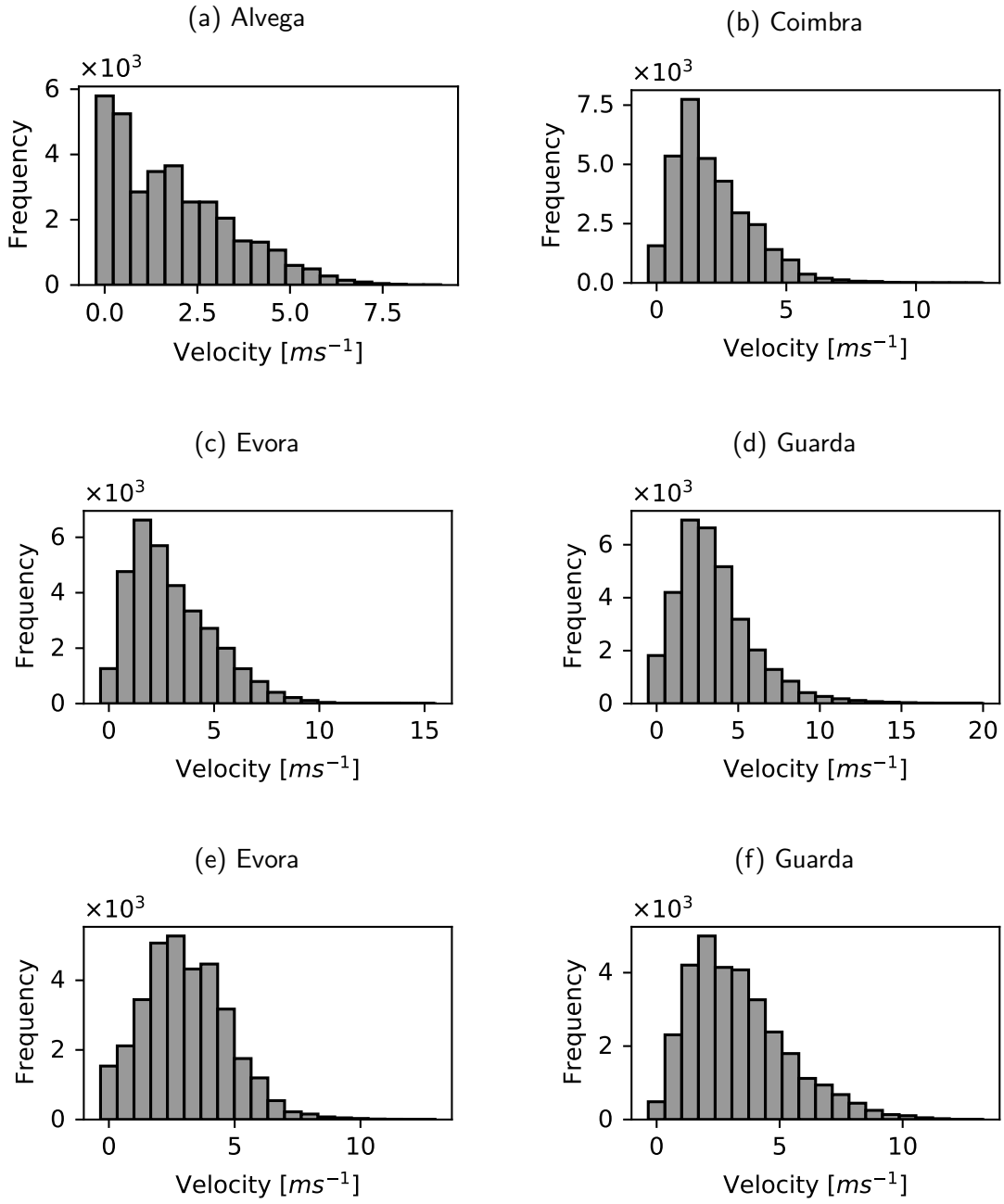

APPENDIX D – RESULTS OF MECHANICAL SIMULATIONS

This section present all the results of the mechanical simulations for each combination of rail and gauge. As a remark, the neutral temperature of the simulation is 20 °C. The y axis represent temperatures and x-axis the displacement in metres on the lateral axis of the track or the rotation in radians about the z axis of the track.

Figure D.1 – Displacement - UIC54 metric gauge

(a) 3.0 GPa sleeper

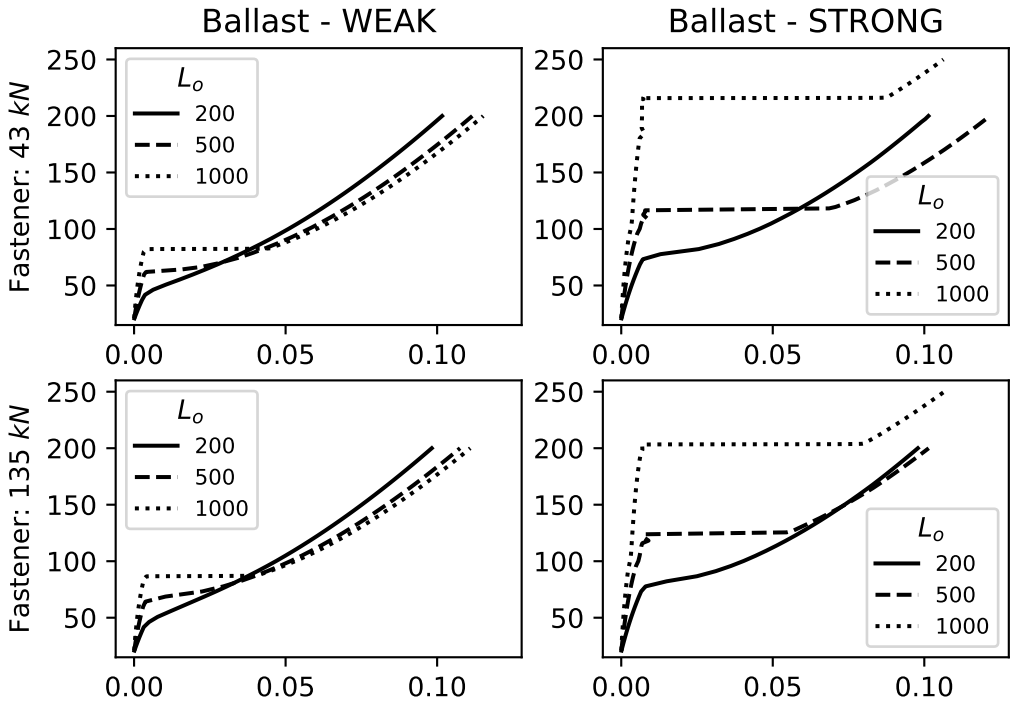

(b) 16.0 GPa sleeper

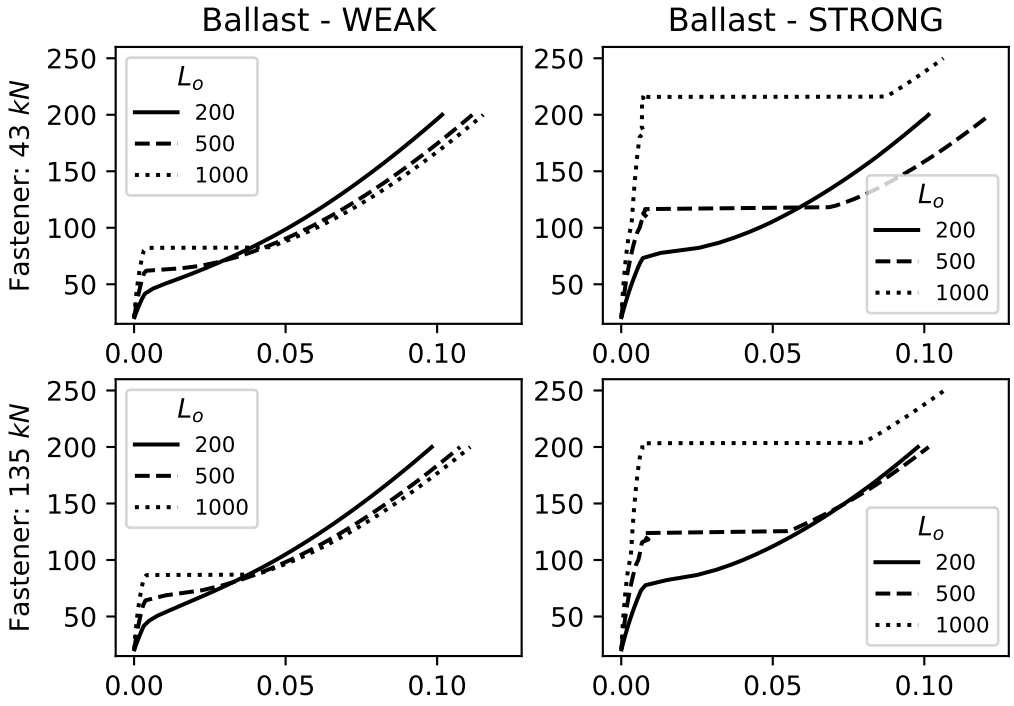

Figure D.2 – Displacement - UIC54 uic gauge

(a) 3.0 GPa sleeper

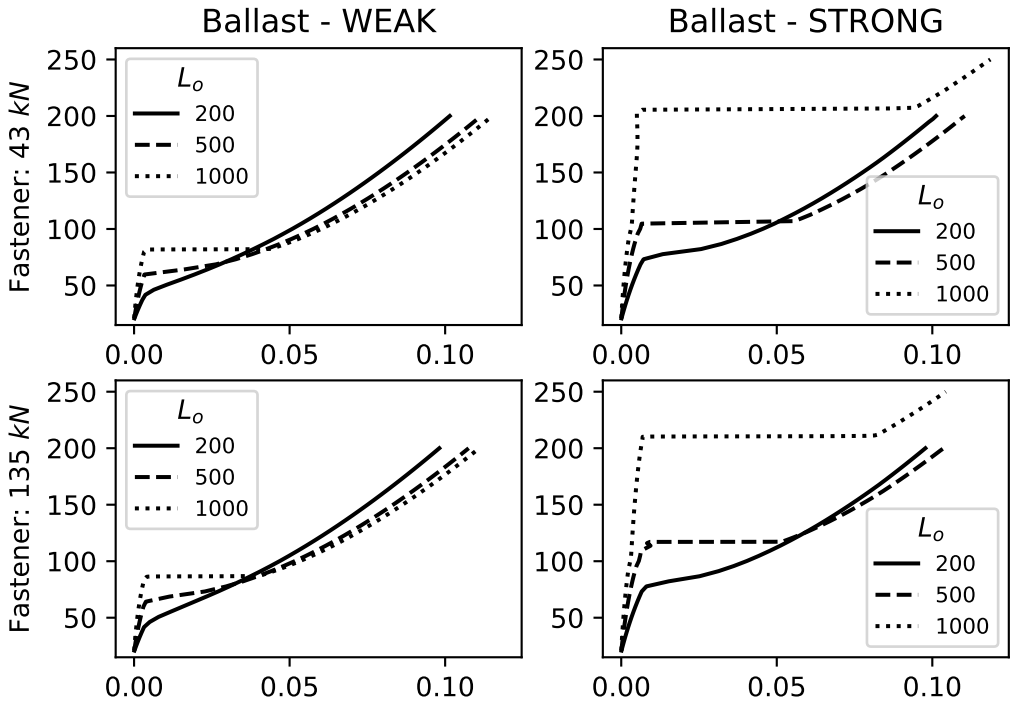

(b) 16.0 GPa sleeper

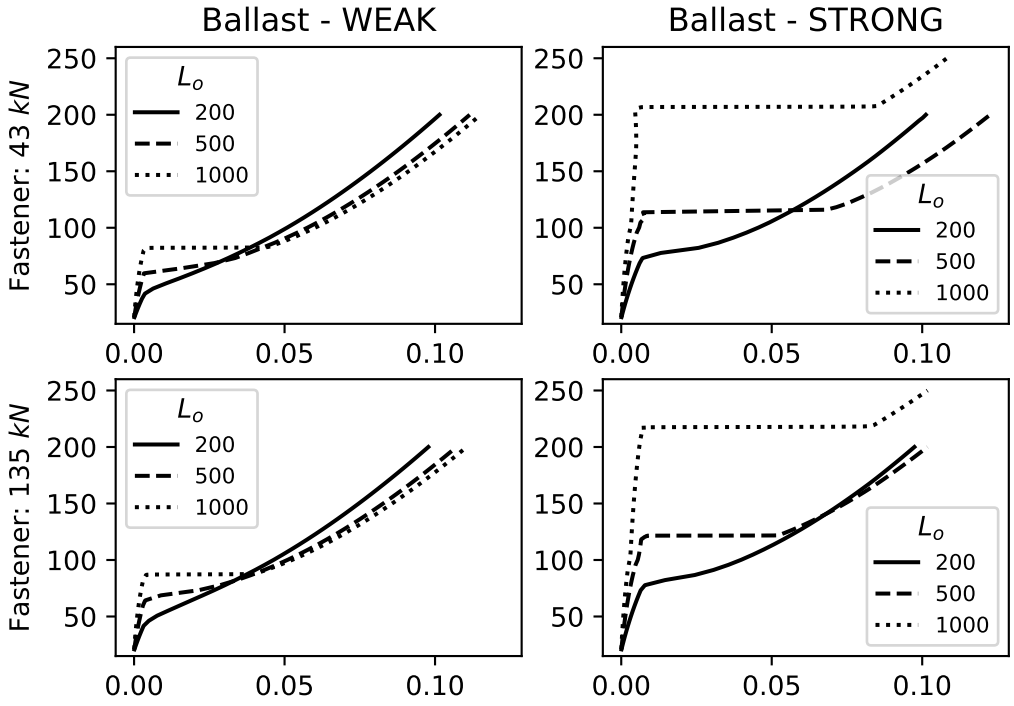

Figure D.3 – Displacement - UIC54 iberian gauge

(a) 3.0 GPa sleeper

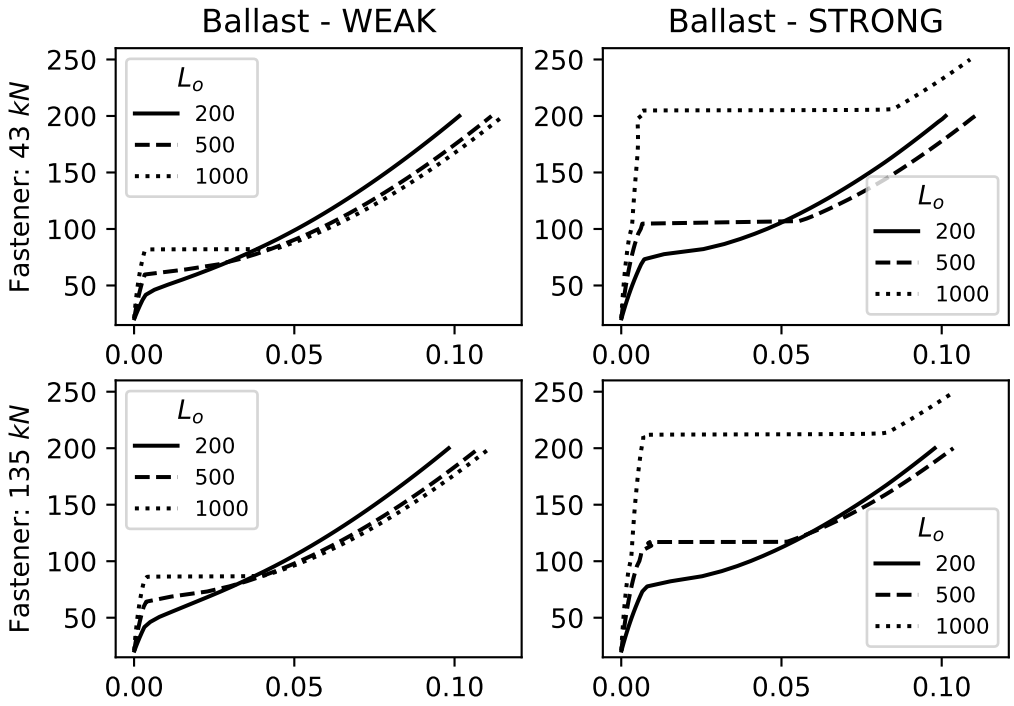

(b) 16.0 GPa sleeper

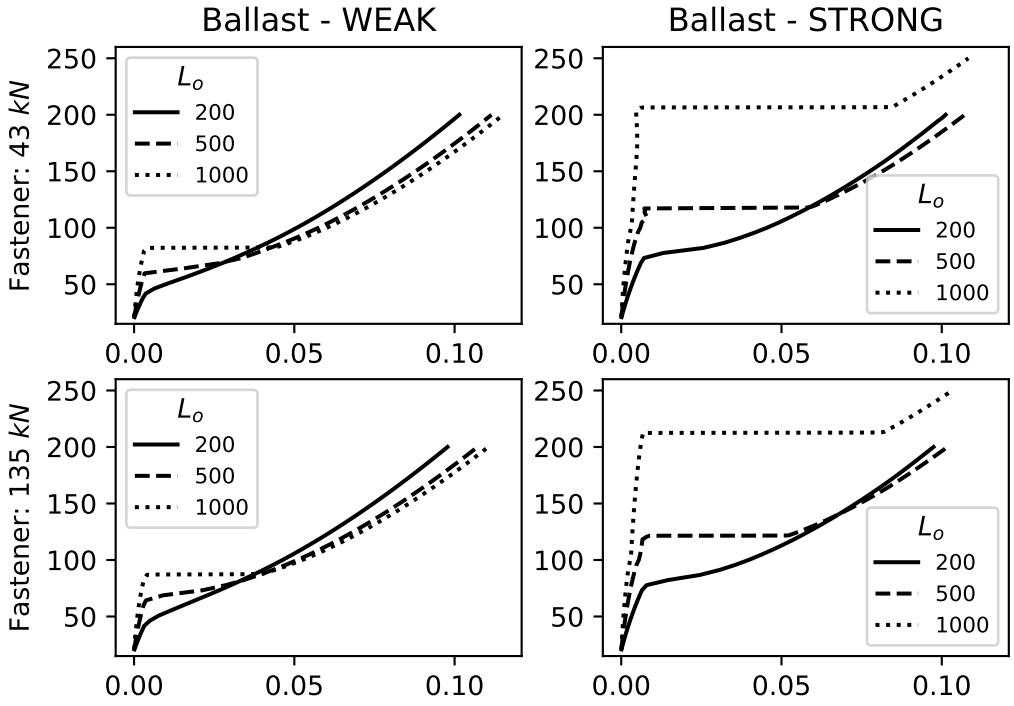

Figure D.4 – Displacement - UIC54 metric gauge

(a) 3.0 GPa sleeper

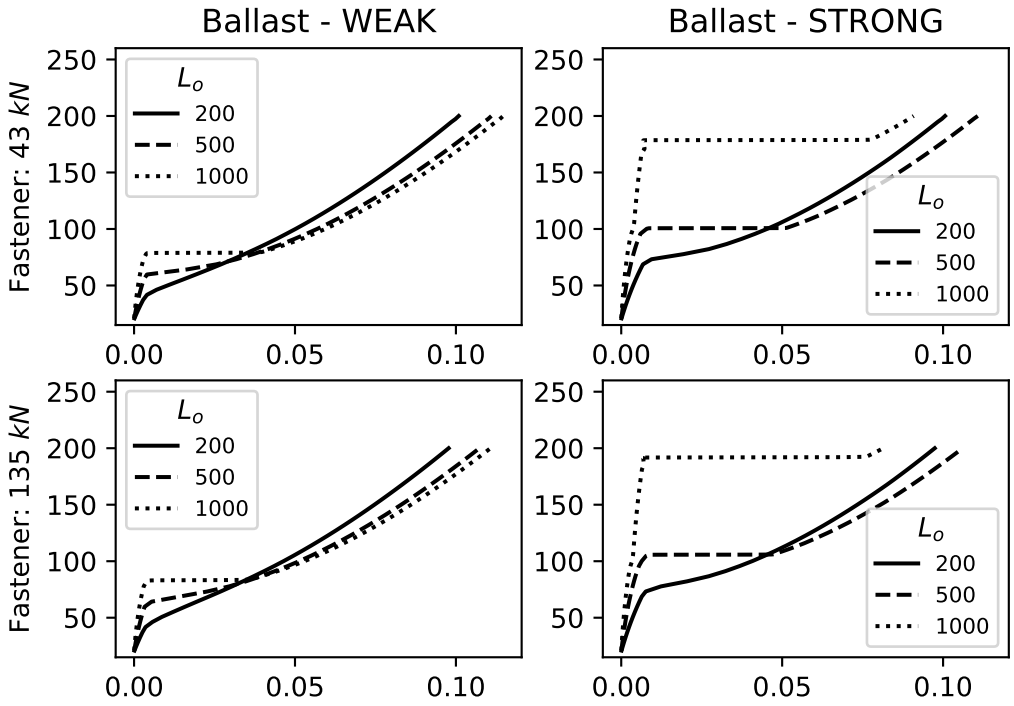

(b) 16.0 GPa sleeper

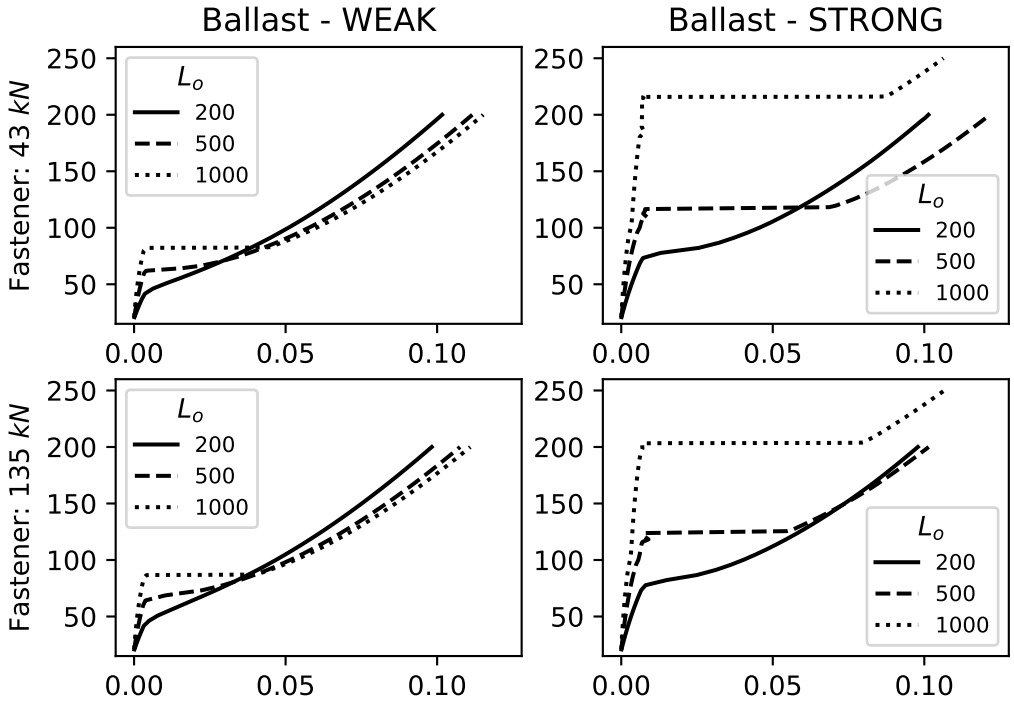

Figure D.5 – Displacement - UIC60 uic gauge

(a) 3.0 GPa sleeper

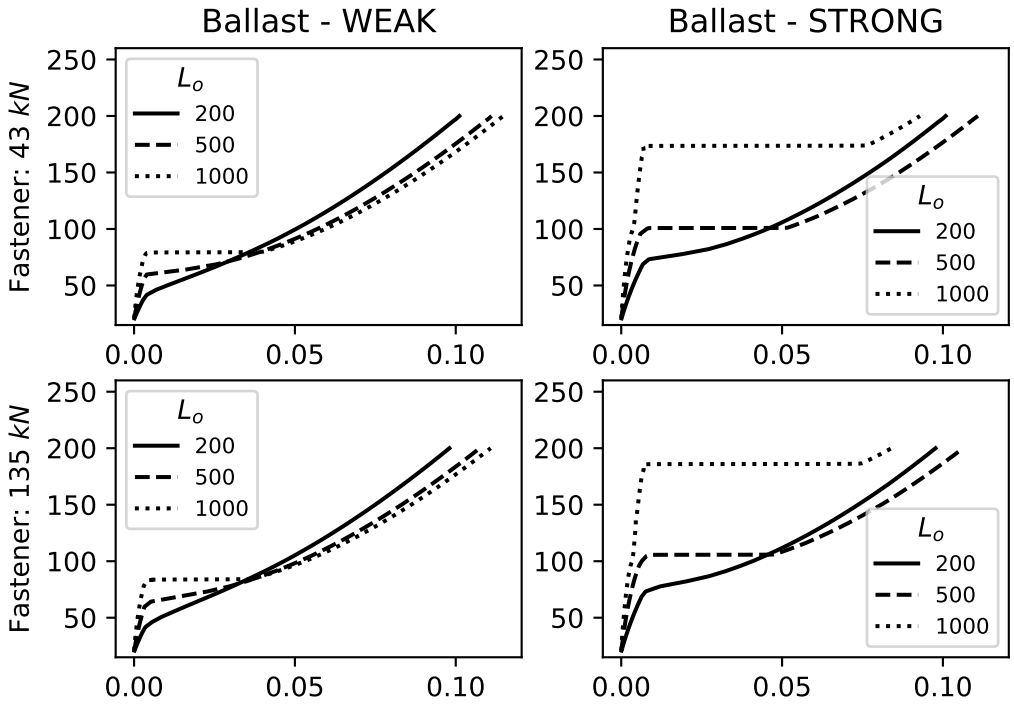

(b) 16.0 GPa sleeper

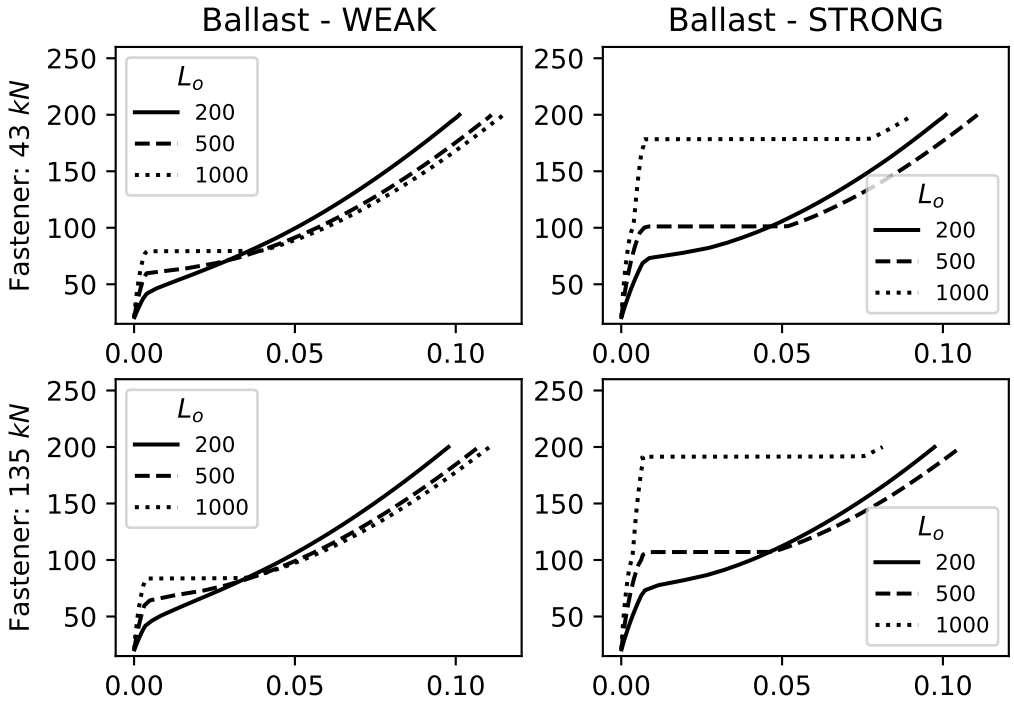

Figure D.6 – Displacement - UIC60 iberian gauge

(a) 3.0 GPa sleeper

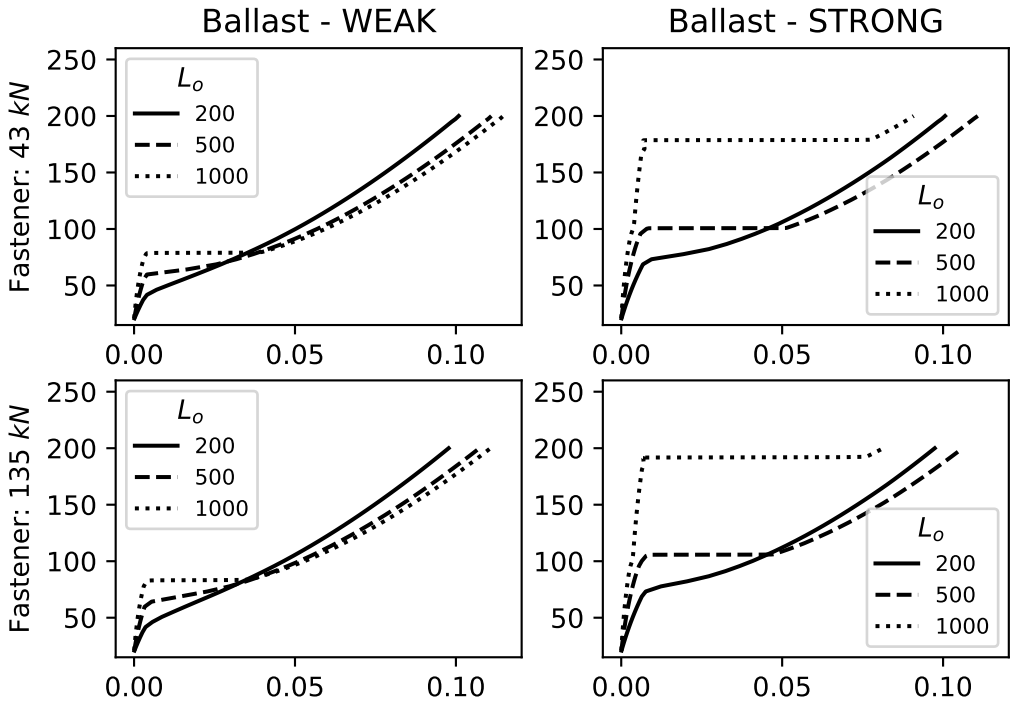

(b) 16.0 GPa sleeper

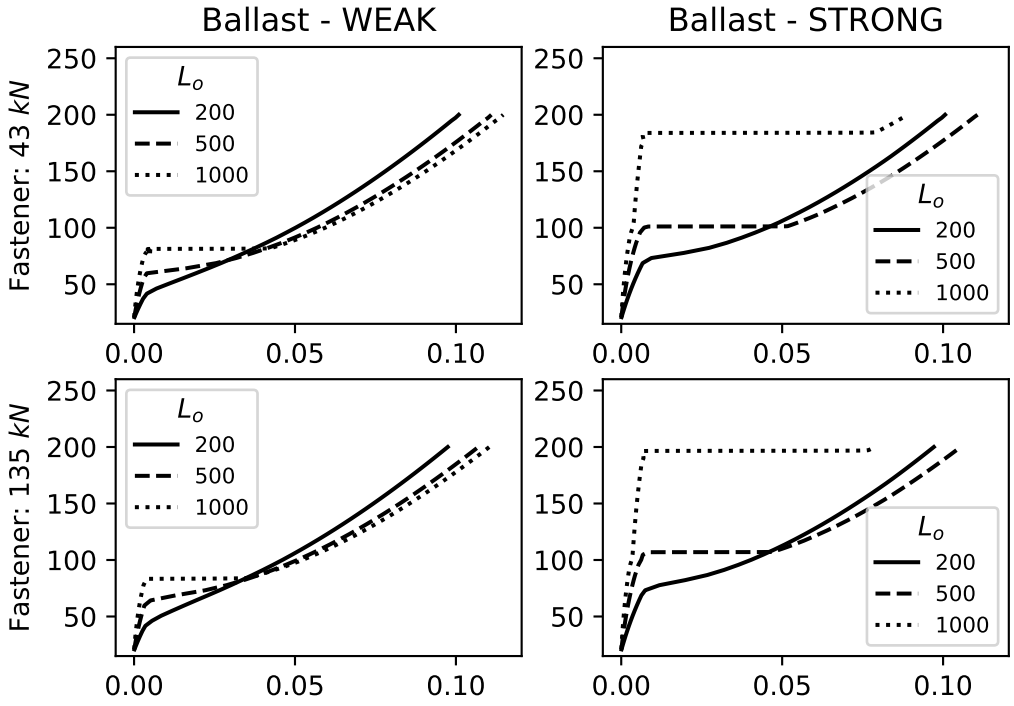

Figure D.7 – Displacement - UIC54 metric gauge

(a) 3.0 GPa sleeper

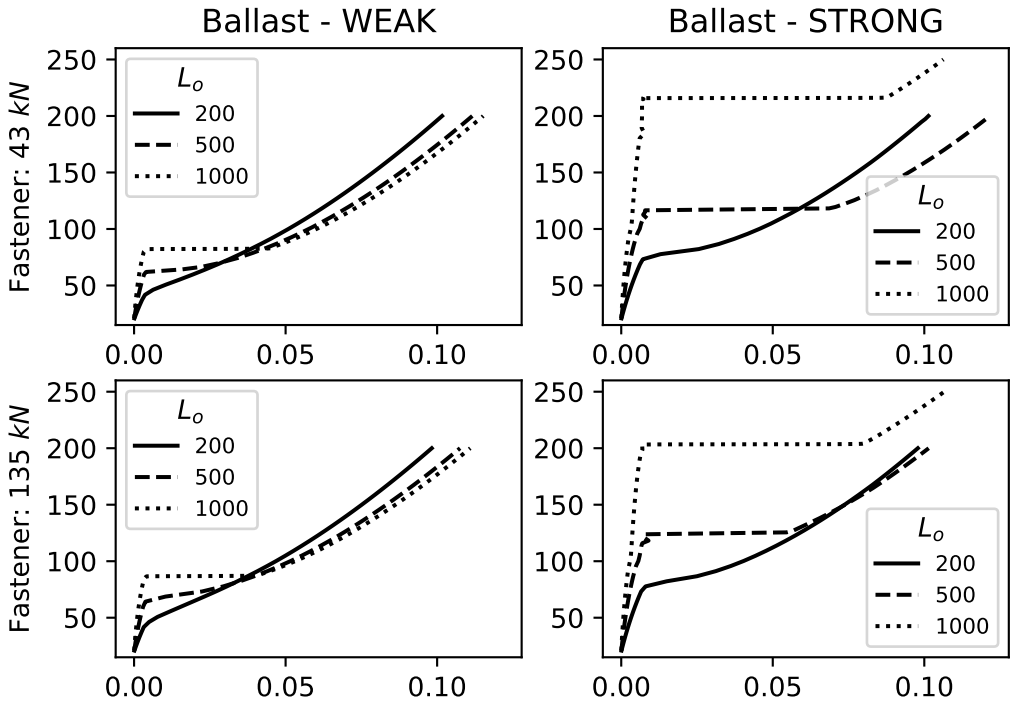

(b) 16.0 GPa sleeper

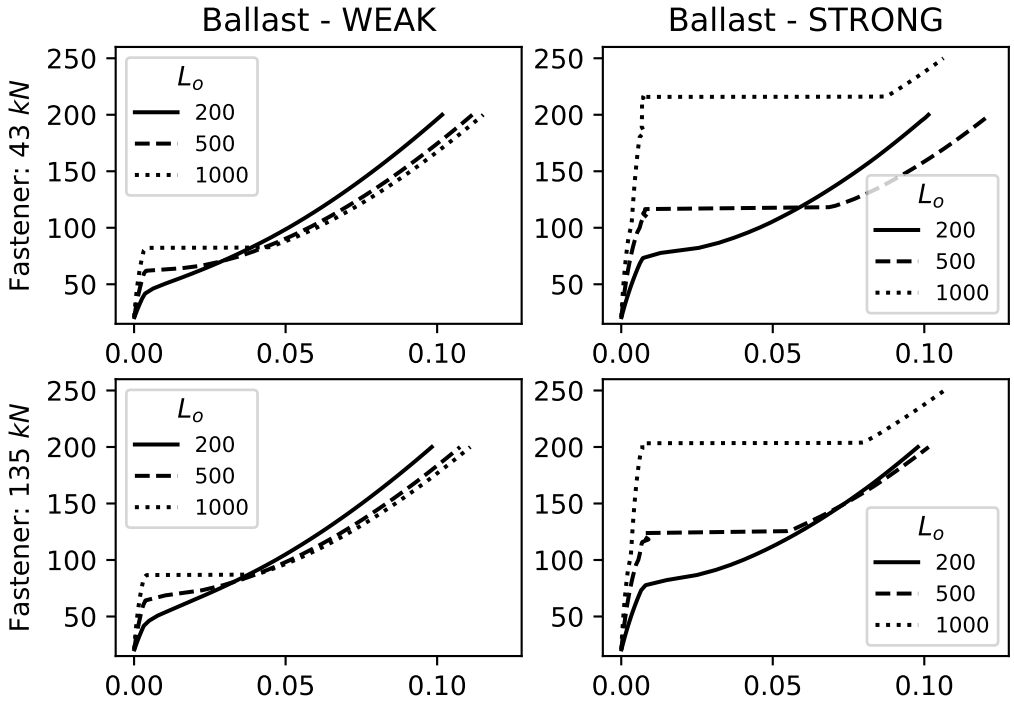

Figure D.8 – Displacement - UIC54 uic gauge

(a) 3.0 GPa sleeper

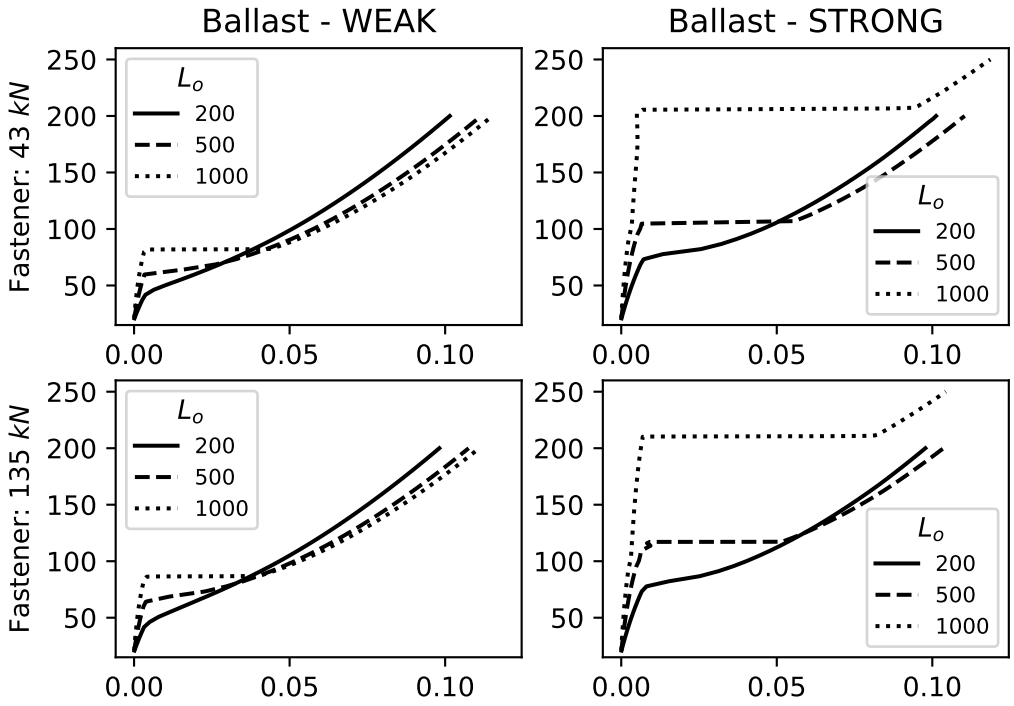

(b) 16.0 GPa sleeper

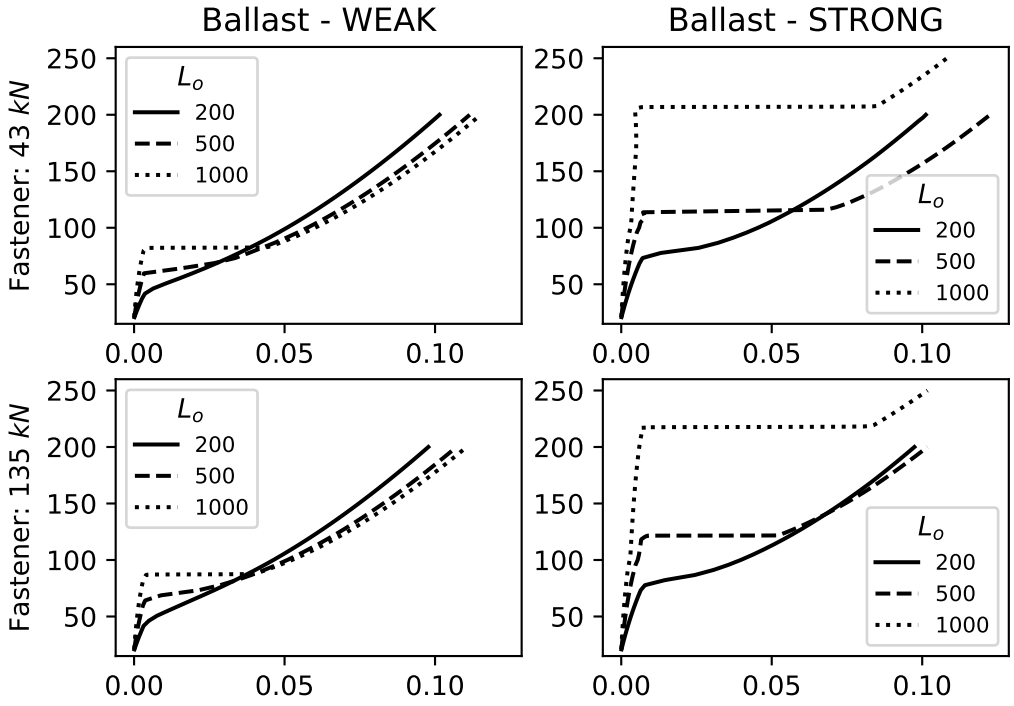

Figure D.9 – Rotation - UIC54 iberian gauge

(a) 3.0 GPa sleeper

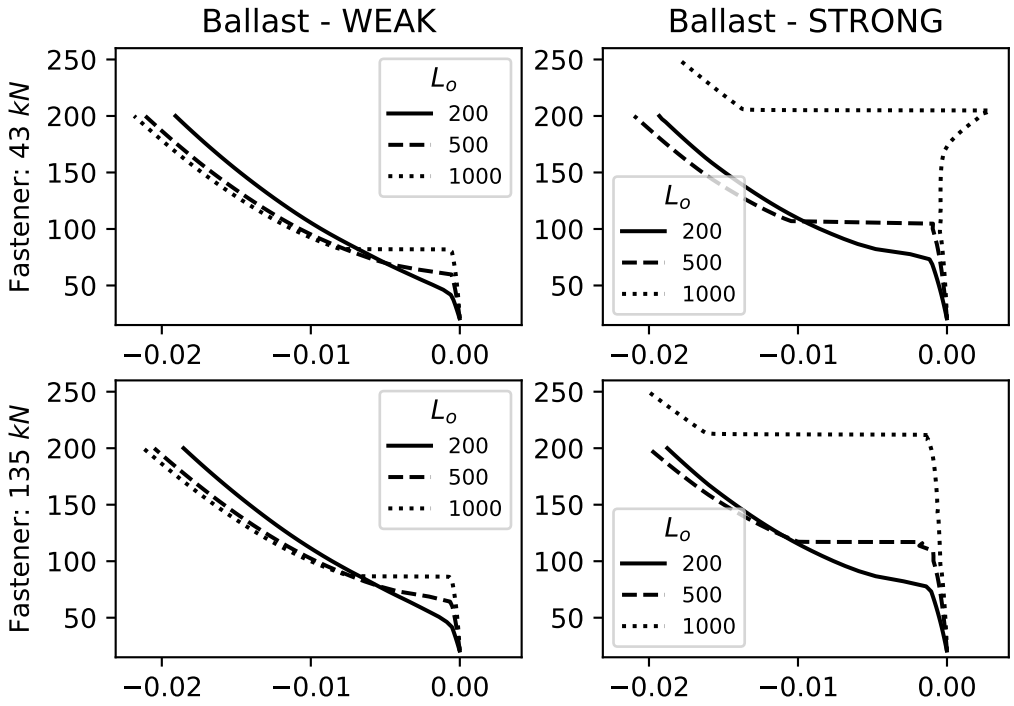

(b) 16.0 GPa sleeper

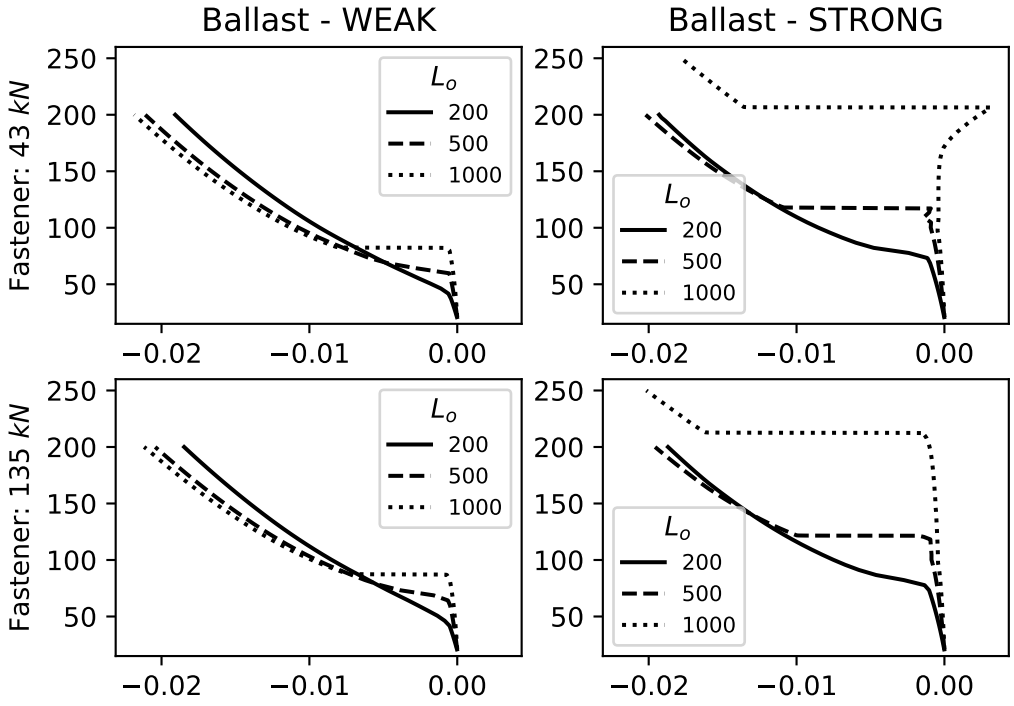

Figure D.10 – Rotation - UIC54 metric gauge

(a) 3.0 GPa sleeper

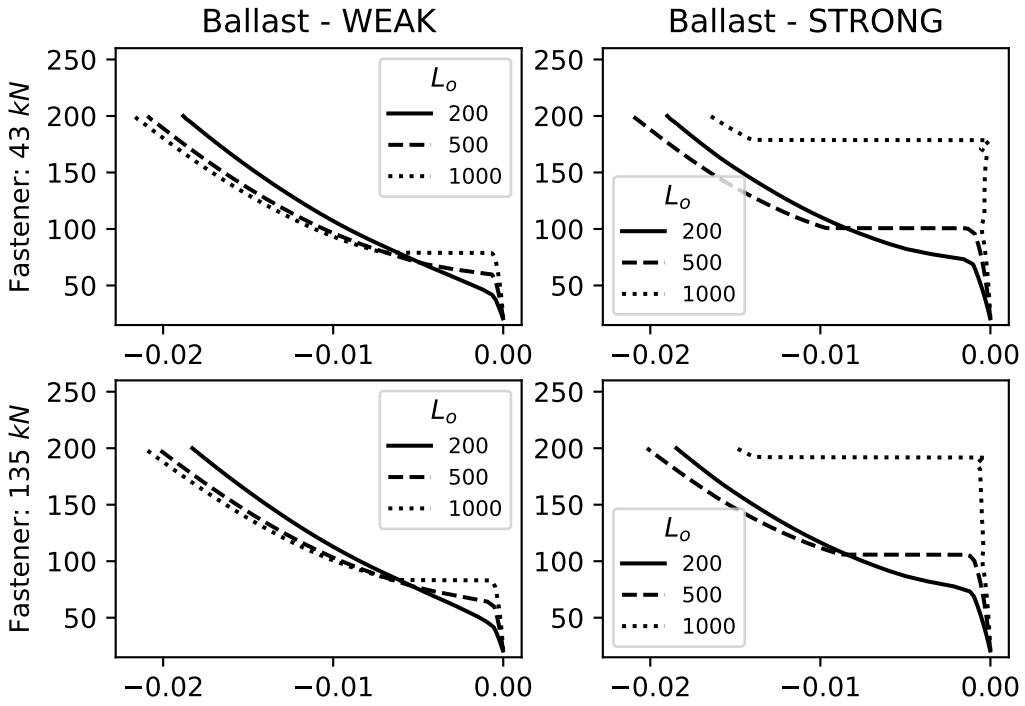

(b) 16.0 GPa sleeper

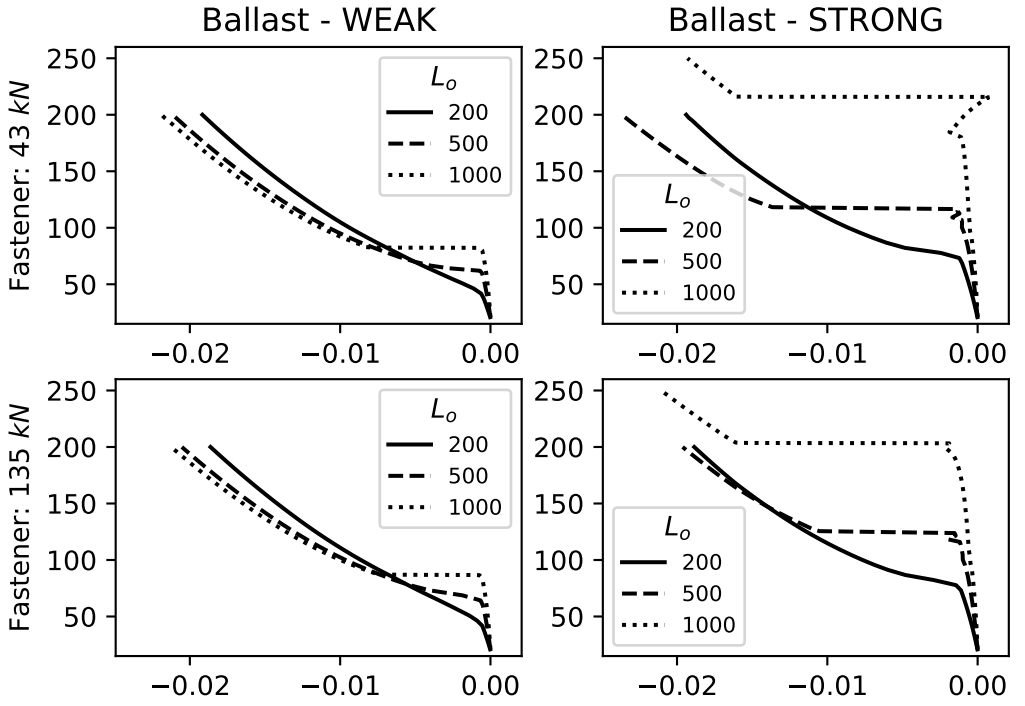

Figure D.11 – Rotation - UIC60 uic gauge

(a) 3.0 GPa sleeper

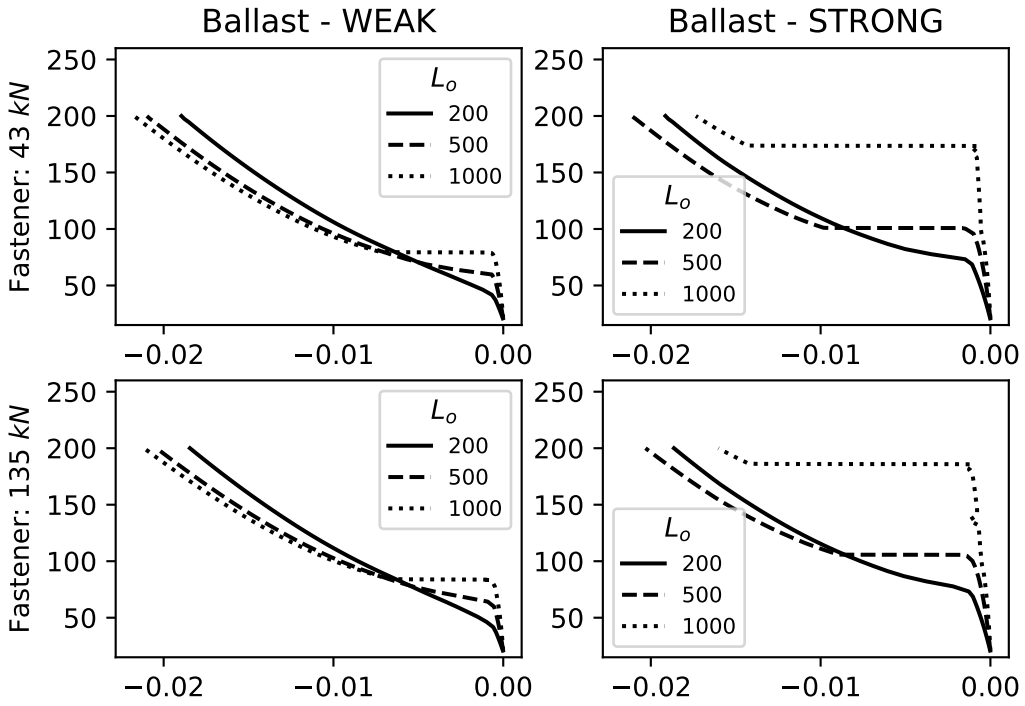

(b) 16.0 GPa sleeper

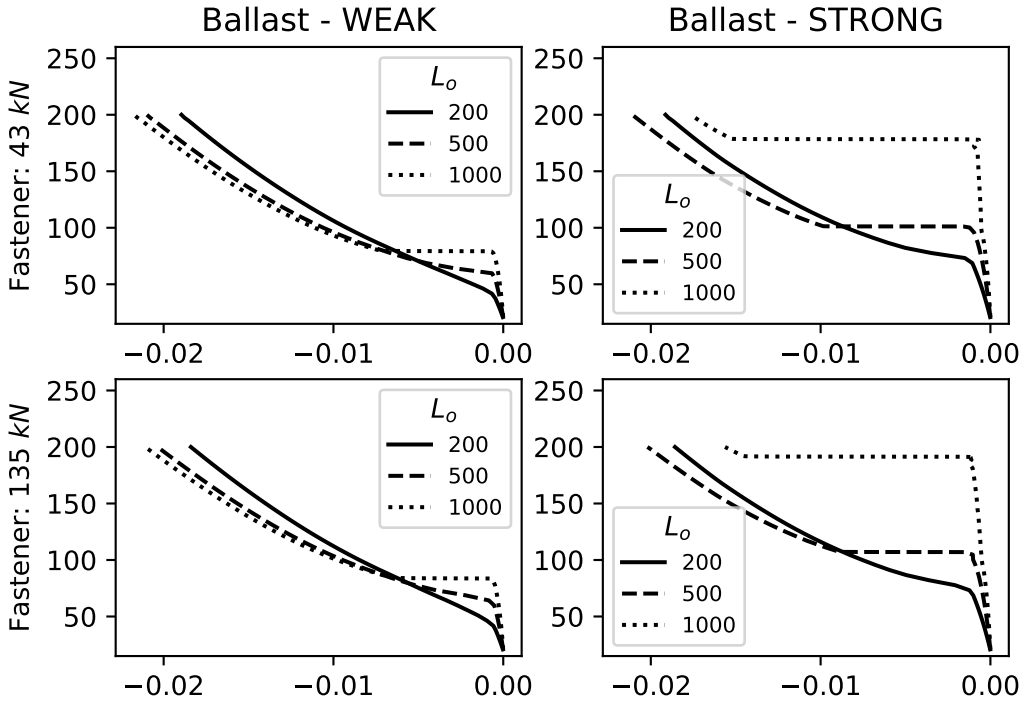

Figure D.12 – Rotation - UIC60 iberian gauge

(a) 3.0 GPa sleeper

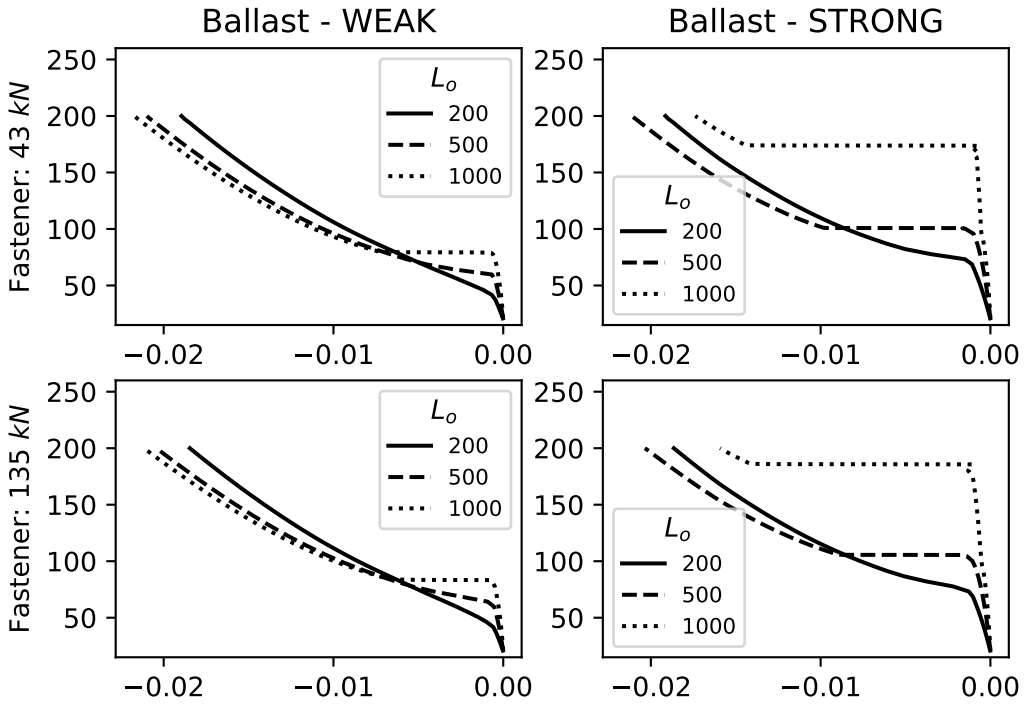

(b) 16.0 GPa sleeper

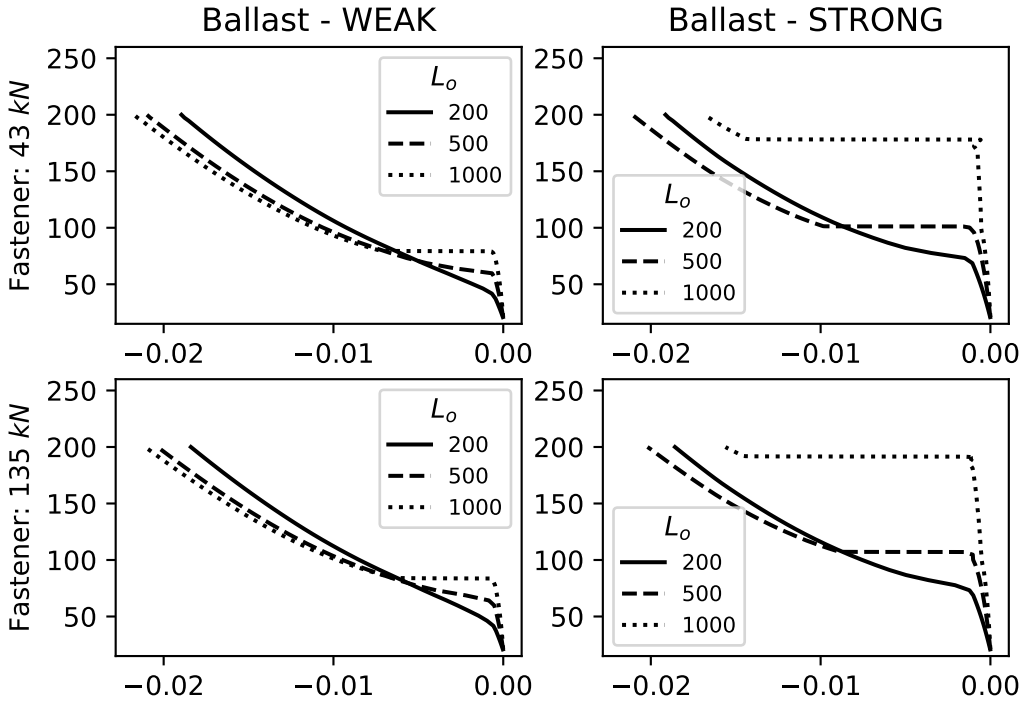

Annex

ANNEX E – PROPERTIES OF RAIL PROFILES

The information given on this section is based on EN 13674-1.

Figure E.1 – UIC54 drawing.

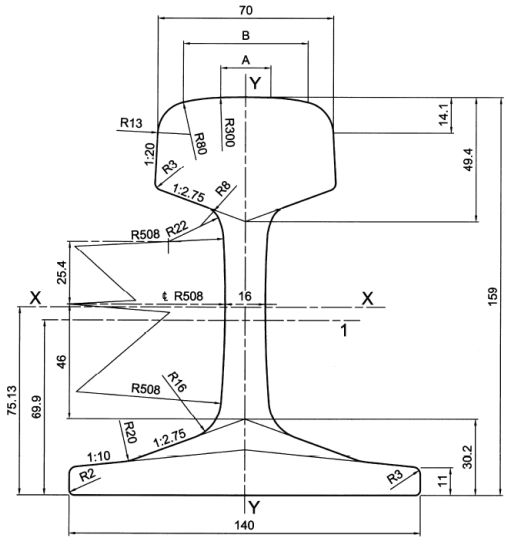

Table E.1 – UIC54 geometric properties.

Parameter	Value
Section Area (cm^2)	69.77
Mass ($kg\,m^{-1}$)	54.77
Moment of Inertia x-x (cm^4)	2337.9
Moment of Inertia y-y (cm^4)	59.9
A (mm)	20.024
B (mm)	49.727

Figure E.2 – UIC60 drawing.

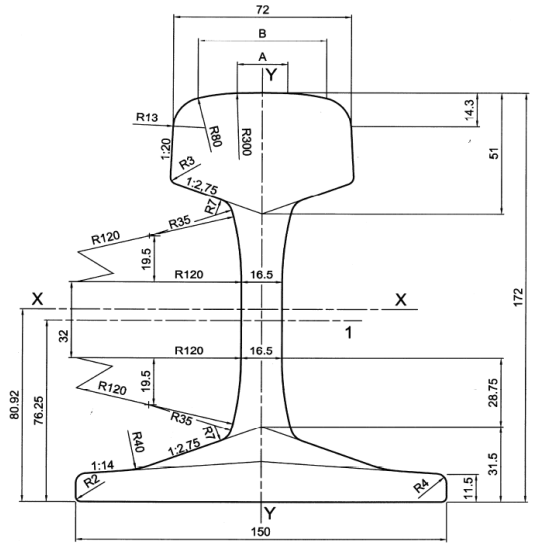

Table E.2 – UIC60 geometric properties.

Parameter	Value
Section Area (cm^2)	76.70
Mass ($kg\,m^{-1}$)	60.21
Moment of Inertia x-x (cm^4)	3038.3
Moment of Inertia y-y (cm^4)	68.3
A (mm)	20.456
B (mm)	52.053